Hannu Karema

Numerical treatment of inter-phase coupling and phasic pressures in multi-fluid modelling

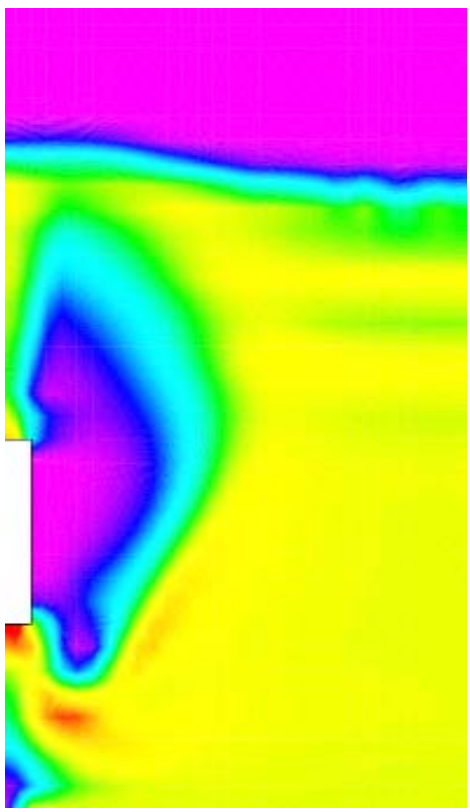

TECHNICAL RESEARCH CENTRE OF FINLAND ESPOO 2002

VTT PUBLICATIONS 458

Numerical treatment of inter-phase coupling and phasic pressures in multi-fluid modelling

Hannu Karema

VTT Processes

Thesis for the degree of Doctor of Technology to be presented with due permission for public examination and criticism in Auditorium K1702 at Tampere University of Technology on the 1st of March, 2002, at 12 o'clock noon.

TECHNICAL RESEARCH CENTRE OF FINLAND
ESPOO 2002

ISBN 951–38–5969–X (soft back ed.)
ISSN 1235–0621 (soft back ed.)

ISBN 951–38–5970–3 (URL:http://www.inf.vtt.fi/pdf/)
ISSN 1455–0849 (URL:http://www.inf.vtt.fi/pdf/)

JULKAISIJA – UTGIVARE – PUBLISHER

Valtion teknillinen tutkimuskeskus (VTT), Vuorimiehentie 5, PL 2000, 02044 VTT
puh. vaihde (09) 4561, faksi (09) 456 4374

Statens tekniska forskningscentral (VTT), Bergsmansvägen 5, PB 2000, 02044 VTT
tel. växel (09) 4561, fax (09) 456 4374

Technical Research Centre of Finland (VTT), Vuorimiehentie 5, P.O.Box 2000, FIN–02044 VTT, Finland
phone internat. + 358 9 4561, fax + 358 9 456 4374

VTT Prosessit, Metsäteollisuus, Koivurannantie 1, PL 1603, 40101 JYVÄSKYLÄ
puh. vaihde (014) 672 611, faksi (014) 672 597

VTT Processer, Skogsindustri, Koivurannantie 1, PL 1603, 40101 JYVÄSKYLÄ
tel. växel (014) 672 611, faksi (014) 672 597

VTT Processes, Pulp and Paper Industry, Koivurannantie 1, PL 1603, FIN–40101 JYVÄSKYLÄ, Finland
phone internat. + 358 14 672 611, fax + 358 14 672 597

Otamedia Oy, Espoo 2002

Karema, Hannu. Numerical treatment of inter-phase coupling and phasic pressures in multi-fluid modelling. Espoo 2002. Technical Research Centre of Finland, VTT Publications 458. 62 p. + app. 51 p.

Keywords multi-phase flow, multi-fluid modelling, inter-phase coupling, phasic pressures, numerical methods, Control Volume Method, Body Fitted Coordinates, fluidized beds, chemical reactors

Abstract

This thesis work concentrates on the area of dispersed multi-phase flows and, especially, to the problems encountered while solving their governing equations numerically with a collocated Control Volume Method (CVM). To allow flexible description of geometry all treatment is expressed in a form suitable for local Body Fitted Coordinates (BFC) in a multi-block structure. All work is related to conditions found in a simplified fluidized bed reactor. The problems covered are the treatment and efficiency of inter-phase coupling terms in sequential solution, the exceeding of the bounds of validity of the shared pressure concept in cases of high dispersed phase pressure and the conservation of mass in momentum interpolation for rapidly changing source terms.

The efficiency of different inter-phase coupling algorithms is studied in typical fluidized bed conditions, where the coupling of momentum equations is moderate in most sections of the bed and where several alternatives of different complexity exist. The interphase coupling algorithms studied are the partially implicit treatment, the Partial Elimination Algorithm (PEA) and the SImultaneous solution of Non-linearly Coupled Equations (SINCE). In addition to these special treatments of linearized coupling terms, the fundamental ideas of the SINCE are applied also to the SIMPLE(C) type pressure correction equation in the framework of the Inter- Phase Slip Algorithm (IPSA). The resulting solution algorithm referred to as the InterPhase Slip Algorithm – Coupled (IPSA–C) then incorporates interface couplings also into the mass balancing shared pressure correction step of the solution.

It is shown that these advanced methods to treat interphase coupling terms result in a faster convergence of momentum equations despite of the increased number of computational operations required by the algorithms. When solving the entire equation set, however, this improved solution efficiency is mostly lost due to the poorly performing pressure correction step in which volume fractions are assumed constant and the global mass balancing is based on shared pressure. Improved pressure correction algorithms utilizing separate fluid and dispersed phase pressures, the Fluid Pressure in Source term (FPS) and the Equivalent Approximation of Pressures (EAP), are then introduced. Further, an expanded Rhie-Chow momentum interpolation scheme is derived which allows equal treatment for all pressures. All the computations are carried out in the context of a collocated multi-block control volume solver CFDS-FLOW3D.

Preface

Most of this work was carried out at the Institute of Energy and Process Engineering at Tampere University of Technology while the author had a position of junior research fellow in the Academy of Finland. Research possibilities obtained by this position are gratefully acknowledged. The work was later completed at VTT Energy in the field of Forest Industry under the favourable attitude of Seppo Viinikainen, the Research Manager.

To my thesis supervisor Professor Reijo Karvinen I owe deep gratitude for the research opportunity and facilities he provided. My sincere thanks belong to AEA Technology for the help and co-operation they offered. In particular, my co-author Dr. Simon Lo faithfully and kindly provided all available time.

I express my thanks to my colleagues at the Institute of Energy and Process Engineering as well as at VTT Energy for their encouraging attitude towards my work.

Finally, I warmly thank my wife Marianne for her patience through all the late evenings spent and for her endless encouragement to complete the work.

Tampere, January 2002

Hannu Karema

LIST OF PUBLICATIONS

This thesis work contains as an essential part the following manuscript located in Appendix E:

Karema, H. and Lo, S. Efficiency of interphase coupling algorithms in fluidized bed conditions. *Computers & Fluids*, 1999. Vol. 28, pp. 323–360.

CONTENTS

Appendix E of this publication is not included in the PDF version.
Please order the printed version to get the complete publication
(http://otatrip.hut.fi/vtt/jure/index.html)

SYMBOLS

$\boldsymbol{A}^{(i)}$	adjugate Jacobian matrix, area vector of cell face	m^2
A_C	cell face area in computational space	m^2
$a_{U_\alpha^k}$, a_{Φ_α}	cell centre coefficients of discretized equations	
$B_{\alpha\beta}$	interface transfer coefficient of momentum	kg/m^3s
C^i	convection coefficient	kg/s
D^{ij}	diffusion tensor	kgm/s
$\boldsymbol{e}_{(i)}$	covariant basis vectors	
$\boldsymbol{F}^D$	interfacial force density	kg/m^2s^2
$\boldsymbol{F}^I$	interfacial source of momentum	kg/m^2s^2
$\boldsymbol{F}_T^I$	total force per unit volume due to interface	kg/m^2s^2
$\boldsymbol{F}^S$	momentum source other than gravity	kg/m^2s^2
$\boldsymbol{F}^T$	total source term (used to collect contributions)	kg/m^2s^2
G^{ij}	geometric diffusion tensor	m
$\boldsymbol{g}$	gravitational vector	m/s^2
$H_{\alpha k}^i$, h_α^k	pressure correction coefficients	
$\hat{I}_{m_\alpha}^i$	the total normal phasic mass flux	kg/s
$\hat{I}_{U_\alpha^k}^i$	the total normal phasic momentum flux	kgm/s^2
$\lvert\boldsymbol{J}\rvert$	Jacobian determinant	
$\boldsymbol{M}^I$	interfacial source of mass	kg/m^3s
M_α	source term in extended Rhie-Chow method	
$\dot{m}_{\beta\alpha}$	interfacial mass transfer from phase β to α	kg/m^3s
N_P	number of phases	
N_d	number of dispersed phases	
N_α	coefficient in extended Rhie-Chow method	
$\boldsymbol{n}$	normal vector of surface	
P	pressure	N/m^2
P^{a}	$\varepsilon P^{\mathrm{e}}$, apparent pressure	N/m^2
P^{e}	modified and effective pressure	N/m^2
P^I	interfacial mean pressure	N/m^2
$R_{m\alpha}$	mass residual term	kg/s
S	source term in discretized equation	

S^D	source term from deferred correction	
$s^R_{U^k_\alpha}$	(residual) source term	*kgm/s*
$\boldsymbol{T}$	stress tensor	N/m^2
$\bar{\boldsymbol{T}}_d^{\,\mathrm{c}}$	collision/contact stress of dispersed phase	N/m^2
$\bar{\boldsymbol{T}}_d^{\,\mathrm{k}}$	kinetic stress of dispersed phase	N/m^2
$\bar{\boldsymbol{T}}_d^{\,\mathrm{p}}$	particle-presence stress	N/m^2
$\bar{\boldsymbol{T}}_f^{\,\mathrm{t}}$	turbulent momentum transfer (Reynolds stresses)	N/m^2
$\bar{\boldsymbol{T}}_f^{\,\mathrm{v}}$	viscous stresses of fluid	N/m^2
t	time	*s*
$\boldsymbol{U}$	velocity vector	*m/s*
$\boldsymbol{U}_I$	interfacial velocity	*m/s*
V_C	cell volume in computational space	m^3
$W_{\boldsymbol{c}}$	weight factor for cell face interpolation	
$W_{\boldsymbol{H}}$	arc weight factor for cell centre gradients	
W_{pc}	weight factor for pressure correction method	
X	phase function	
$\boldsymbol{x}$	special coordinate	*m*
x, y, z	*i, j* and *k* coordinates in physical space	*m*
Γ	diffusivity of a scalar property	*kg/ms*
Γ^{ij}	diffusivity tensor of a scalar property	*kgm/s*
ε	volume fraction	
η	material viscosity	*kg/ms*
η^t	eddy viscosity	*kg/ms*
κ	average mean curvature of interfaces	*m*
ρ	density	kg/m^3
σ	surface tension coefficient	*N/m*
τ	shear stress	N/m^2
Φ	general dependent variable	
ξ, ς, ζ	*i, j* and *k* coordinates in computational space	*m*
$\langle\ \rangle$	generic integration operator	
$\bullet$	scalar product of vectors	
$\times$	vector product	
$\otimes$	dyadic product	

$[\hat{F}]_{\boldsymbol{d}}^{\boldsymbol{u}}$	$\hat{F}\big\|_{\boldsymbol{u}} - \hat{F}\big\|_{\boldsymbol{d}}$, difference of operand at specified locations
$[F]_{\boldsymbol{t}}^{\boldsymbol{t}+\boldsymbol{\Delta t}}$	difference of cell-based averages at respective times
$\{F\}_{\boldsymbol{t}}$	cell-based average at time *t*
$\{\ \|_H\}_C^P$	weighted linear interpolation to H between P and C
$\cap\, \boldsymbol{HP}$	arc lengths between cell centres H and P *m*
$\boldsymbol{u''}$	deviations from mass-weighted phase average
u'	contravariant component of a vector
${}^0\boldsymbol{F}$	constant part of a linear model for variable $\boldsymbol{F}$
${}^1\boldsymbol{F}$	first order coefficient of a linear model for variable $\boldsymbol{F}$
$(\boldsymbol{F})^T$	transpose of matrix $\boldsymbol{F}$
η^{eff}	macroscopic ‘effective’ constitutive property
${}^*\Phi$	value of dependent variable from previous outer iteration
Φ^*	intermediate value at current iteration
Φ^{**}	new value at current iteration

subscripts

I	interface of phases
f	fluid phase
d	dispersed phase
α, β	phase indexes

superscripts

–	phase average
~	mass-weighted phase average
^	normal flux component

1 INTRODUCTION

1.1 PROBLEM CONSIDERED

The field of multi-phase flow problems is a very wide field from stratified flows to highly dispersed flows such as systems of aerosols. This diverseness quite often requires modelling and solution approaches exploiting the special characteristics of each sub-type. This thesis work concentrates on the area of dispersed flows and, especially, to the problems encountered while solving them numerically with a collocated Control Volume Method (CVM). A requirement set from the beginning was that all treatment is expressed in a form suitable for flexible description of geometry. Thereby, an approach was selected based on multi-block structure with Body Fitted Coordinates (BFC) at each block. A simplified fluidized bed was set as the special application to concentrate on. Although having this sub-type of multi-phase flow problems in mind from the beginning, the selected method to derive the conservation equations and the numerical method studied are general methods in nature and they are also available to other types of multi-phase flow problems.

When considering the multi-fluid equations two properties of them are striking and typical of multi-phase problems. The first is the large number of dependent variables and the second is the inter-phase transfer of mass, momentum and energy between the phases. It is just the latter property that actually makes multi-phase problems more difficult to solve than single-phase problems. If the inter-phase transfer is negligible the multi-phase problem reduces almost to solving many conservation equations of the same type than in single-phase flow. Therefore, it was natural to start the work from the study of inter-phase coupling algorithms. The target application, a fluidized bed, is especially interesting in this aspect as most sections of both gas-particle and liquid-particle beds normally operate in conditions where the inter-phase coupling can be stated to be ‘moderate’. However, there usually exist at least small spots in the bed area where the coupling is tight. Currently, there is no information available on the required implicitness of inter-phase coupling algorithms or what benefits in overall solution efficiency could be achieved by a proper selection of them.

Deficiencies related to the customary solution algorithm applied in sequential CVM methods for multi-fluid problems were also expected. A principal subject here is the mass balancing pressure correction step of the interphase slip algorithm (IPSA) in which the volume fraction is held constant and the mass balancing is based on the adjustment of global mass by shared pressure gradient. In fluidized beds the average of the normal component stresses of the dispersed phase, i.e., the dispersed phase pressure, e.g., in connection of compaction of the bed at start-up, corners of the bed and at heat transfer surfaces, is strongly dependent on the volume fraction and, consequently, this dependency should be taken into account in the pressure correction step. The rising dispersed phase pressure also means that the performance of a pressure correction algorithm based on shared pressure concept will be poor if sufficient at all. Simple methods to reduce these problems, the Fluid Pressure in Source term (FPS) and the Equivalent Approximation of Pressures (EAP), are therefore presented.

In addition, the selected geometric description for the CVM method, the collo-

cated local body fitted coordinate (BFC) system with multi-block capability, requires some interpolation scheme to mimic a staggered grid arrangement. The customary solution for collocated methods is to utilize the Rhie-Chow momentum interpolation scheme. For rapid changes in source terms this interpolation method fails to conserve mass, a severe deficiency for a CVM method utilizing iterative solution. An improved Rhie-Chow interpolation method is therefore presented as well as an extension to multiple pressures which is applicable both for the Rhie-Chow interpolation method and its improved version.

1.2 BACKGROUND

Numerous different approaches to formulate conservation equations for dispersed multi-phase flows exist. Only the most recent method in the field, the lattice-Boltzmann method ([2], [3]), avoids this complication by having its foundation in the description at the molecular level and in the mutual interaction of these entities. In other approaches, some kind of averaging is required. Reeks ([47], [48]) applied kinetic theory in the phase space while most of the others have utilized regular space-time coordinates. The first derivation with volume averaging was presented by Drew [19]. Another corner stone in the field, introducing time averaging, is the more general publication of Ishii [31]. After first approaches ([11], [12]), the application of ensemble averaging has gained wide popularity ([20], [29], [30], [33]). This is in part a consequence of applying the kinetic theory of dense gases [15] to derive the constitutive equations of the dispersed phases ([17], [6]). Especially in the context of fluidized beds, the special volume averaging applied by Anderson & Jackson [4] has functioned as a basis for several flow models, e.g, [45, 50]. The equations in this work are most closely related to the mathematically formal treatment based on generalized functions by Drew [20].

Although the conservation equations can be derived by integrating the local conservation equations of mass, momentum and energy together with their associated interface conservation equations, i.e., jump conditions, over representative dimensions of either space, time or realizations of the system, all these methods produce conservation equations of the same structure. The main difference is found in the interpretation of the terms and in the content of the constitutive relations. By a rigorous mathematical treatment these averaged equations, customarily known as *the multi-fluid equations*, are an exact representation of the system. In reality, the multi-fluid equations include several terms that depend on the microscopic local variables or on the integrals over the inter-phase boundaries. These terms, e.g., stresses, diffusional fluxes, inter-phase transfers and pseudo-turbulent stresses, are called constitutive terms and they have to be replaced by models which depend only on averaged dynamic quantities or their derivatives. Discussions of general constitutive requirements can be found, e.g., from [31] and [21]. It is just these constitutive terms which bring in the typical problems related to solving the multi-fluid equation set. As no generally valid constitutive models exist and as most of them are quite crude approximations of reality, a multitude of different forms to write multi-fluid equations have evolved.

Two fundamentally different approaches to solve dispersed multi-phase flows have evolved in the past. Their conceptual difference lies in the treatment of the dispersed phases, where one is based on Lagrangian tracking of computational par-

ticles ([25], [23], [56]) and the other is based on the idea of interpenetrating continua and the Eulerian frame of reference, i.e., *multi-fluid model* ([19], [54], [31], [12], [20]). The former is naturally suited to dilute flows and the latter meets its theoretical justification better in denser flows [16]. However, numerous exceptions to this simple classification can be found, e.g., the PALAS concept [8], the application of kinetic theory in the phase space ([47], [48]) and the lattice Boltzmann method ([2], [3]). Efforts to combine the advantages of both approaches have also appeared [5]. Further, a variety of methods exist for the solution of the carrier phase balance equations and, in the case of the multi-fluid approach, for the dispersed phase balance equations as well. Methods based on unstructured grids, i.e., FEM [28] and CVFEM [40], usually exploit the simultaneous solution of all balance equations. This is a consequence of the unstructured mesh which results in a sparse coefficient matrix and, consequently, prevents the use of efficient iterative solvers tailored for band matrixes. This approach avoids the difficulties related to the numerical implementation of the inter-phase transfer terms but requires a huge amount of run time computer memory. In contrast, Control Volume Methods (CVM) built on structured grids use the sequential solution of balance equations in combination with iterative solvers, which results in large savings in memory requirement. The major disadvantage, as far as the multi-fluid approach is concerned, is the difficulty to implicitly consider the couplings of balance equations.

The easiest and most natural way to treat the interphase coupling term corresponds to considering it a linear source term, where the coefficient times the current phase variable forms the first-order term and the coefficient times the other phase variable acts as a constant term [55]. This method to treat the inter-phase coupling terms corresponds to an implicit scheme for the first-order term and an explicit scheme for the constant term, and it is referred as an partially implicit treatment. A fully explicit scheme would exploit an existing value also for the current phase variable. To enhance convergence in conditions of tight coupling more implicit methods are needed [42]. In this work, the fully implicit Partial Elimination Algorithm (PEA) [52] and the semi-implicit Simultaneus solution of non-linearly coupled equations (SINCE) [37, 38], described in detail, are meant to cover this requirement.

Two well-known sequential iterative solution algorithms for CVM approach in multi-fluid conditions exist, i.e., the Interphase Slip Algorithm (IPSA) [51–53] and the Implicit Multifield (IMF) method [26]. As having more implicit nature, the IPSA method has been selected as the basis of the solution algorithm in this work. The distinctive features of the IPSA are related to the mass balancing pressure correction step of the algorithm, in which the volume fractions are held constant and the mass balancing is based on the adjustment of global mass by shared pressure gradient. The average of the normal component stresses of the dispersed phase, i.e., the dispersed phase pressure, is sometimes strongly dependent on the volume fraction and, consequently, this dependency should be taken into a count in the pressure correction step. The special case here in mind is the compaction of a fluidized bed below the state of minimum fluidization. As the porosity of the fluidized bed reduces, the dispersed phase pressure steeply rises with the volume fraction and it is insufficient to use only the shared pressure for mass balancing. Two new methods to reduce these problems, the compressible and incompressible variants of the Fluid Pressure in Source term (FPS) and the Equivalent Approximation of Pressures (EAP), are introduced in this work.

Because the constant parts of the linearized interphase coupling terms are customarily treated as source terms, their information in a SIMPLE(C) type pressure correction equation [18], a part of the IPSA method, is lost. To improve this solution step, a solution algorithm, referred to as the Interphase Slip Algorithm-Coupled (IPSA-C), is given in this work. This method utilizes the same kind of formalism as the SINCE to include the interphase coupling terms semi-implicitly in the pressure correction equation.

In order to achieve adequate geometric flexibility in constructing the mesh, the CVM used is based on collocated local body fitted coordinate (BFC) system with multi-block capability. The essential feature of collocated methods is that the same mesh is used for all dependent variables. As the staggered arrangement of mesh for momentum equations is abandoned, some other means to avoid the decoupling of pressure and velocity fields has to be used. The customary solution for collocated methods is to utilize the Rhie-Chow momentum interpolation scheme [49] that actually mimics the staggered grid arrangement. For rapid changes in the source terms this interpolation method fails to conserve mass. A better behaving scheme has been described in Appendix D. In addition, if the shared pressure concept is abandoned and a proper treatment is given for the dispersed phase pressure the Rhie-Chow interpolation method has to be expanded. An approach available independently or with the improved Rhie-Chow scheme is given in this thesis work.

1.3 OUTLINE OF THIS WORK

By following the theme of the work, the material presented has been divided in three conceptual parts: the theoretical and the mathematical basis, the inter-phase coupling algorithms and further improvements of the solution method in order to gain better overall efficiency.

The first part comprises chapter 2 in which the mathematically exact multi-fluid equations are given in together with the related interfacial jump conditions. This is made to lay out solid basis for the later discussions of the numerics. In addition, the generalized form of multi-fluid equations for numerical solution are given and, finally, discretized for collocated CVM solver. All the treatment in this part, as well as in the other two parts, are carried out in a form applicable for local BFC grids. This may complicate the following of the general idea but reveals better the requirements and complications related to this geometric description.

The subject of the second part, the inter-phase coupling algorithms, are covered in chapter 3 and in the related publication attached to Appendix E. The chapter 3 itself is only a short summary of the material discussed in the publication, which includes a detailed description of the inter-phase coupling algorithms, i.e., the explicit treatment, the partially implicit treatment, the semi-implicit SINCE algorithm and the fully implicit PEA algorithm. Their efficiency were tested in a typical conditions found in gas-particle and liquid-particle fluidized beds. In addition, the IPSA-C solution method is introduced. This solution method includes the interphase coupling terms also into the pressure correction step in a semi-implicit manner, and consequently, enhances the accuracy of the traditional IPSA solution method.

The third part, i.e., chapter 4 and chapter 5, include improvements to the customary IPSA solution method in order to achieve better overall solution efficiency

and to avoid numerical problems typical for collocated CVM in fluidized bed conditions. In chapter 4 the new multi-pressure algorithms, i.e., the Fluid Pressure in Source term (FPS) and the Equivalent Approximation of Pressures (EAP), are explained. The relation of these methods to the multi-fluid equations and to the model equation for discretization is given in chapter 2 in context of the multi-fluid balance equations and constitutive models. Finally, chapter 5 describes how the multi-pressure concept can be included in the momentum interpolation in a way which is consistent with the requirement of second-order accuracy for approximation of pressure gradient.

2 MULTI-FLUID MODEL

The governing equations of the multi-fluid model are derived by integrating local conservation equations of mass, momentum and energy, valid in each phase separately, together with their associated interface conservation equations, i.e., the jump conditions, over representative dimensions of space [19, 54], time [31] or realizations of the system [12]. Each of these averaging methods produce governing equations of the same structure though the interpretation of the terms and the operations required for the interfacial source terms are unique. A mathematically formal treatment based on the generalized functions has been given by Drew [20]. This approach, followed below, has its origin in ensemble averaging.

Utilizing the notion $\langle\ \rangle$ for a generic integration process the phase average and the mass-weighted phase average of a variable Φ can be defined as

$$\overline{\Phi}_\alpha = \frac{\langle X_\alpha \Phi \rangle}{\varepsilon_\alpha} \quad \text{and} \quad \tilde{\Phi}_\alpha = \frac{\langle X_\alpha \rho \Phi \rangle}{\varepsilon_\alpha \bar{\rho}_\alpha}. \tag{1}$$

In equation (1) ρ and Φ are the detailed piece-wise continuous functions of material density and general dependent variable, whereas X_α is the phase function indicating the phase present at a specified location and time. Thus, the definition of X_α is

$$X_\alpha(\boldsymbol{x}, t) = \begin{cases} 1 & \text{if } \boldsymbol{x} \text{ is in phase } \alpha \text{ at time } t \\ 0 & \text{otherwise.} \end{cases} \tag{2}$$

It follows, that the average of phase function itself is the volume fraction of the phase in question

$$\varepsilon_\alpha = \langle X_\alpha \rangle . \tag{3}$$

Based on these definitions, the governing equations of mass and momentum can be written in the form:

$$\frac{\partial}{\partial t}(\varepsilon_\alpha \bar{\rho}_\alpha) + \nabla \bullet (\varepsilon_\alpha \bar{\rho}_\alpha \tilde{\boldsymbol{U}}_\alpha) = \langle [\rho(\boldsymbol{U} - \boldsymbol{U}_I)]_\alpha \bullet \nabla X_\alpha \rangle , \tag{4}$$

$$\begin{aligned} \frac{\partial}{\partial t}(\varepsilon_\alpha \bar{\rho}_\alpha \tilde{\boldsymbol{U}}_\alpha) + \nabla \bullet (\varepsilon_\alpha \bar{\rho}_\alpha \tilde{\boldsymbol{U}}_\alpha \otimes \tilde{\boldsymbol{U}}_\alpha) &= \nabla \bullet \varepsilon_\alpha \bar{\boldsymbol{T}}_\alpha + \varepsilon_\alpha \bar{\rho}_\alpha \boldsymbol{g} + \boldsymbol{F}_\alpha^S \\ &+ \langle [\rho \boldsymbol{U}(\boldsymbol{U} - \boldsymbol{U}_I) - \boldsymbol{T}]_\alpha \bullet \nabla X_\alpha \rangle . \end{aligned} \tag{5}$$

On the right side of equation (5), $\boldsymbol{F}_\alpha^S$ stands for the momentum source caused by other body forces than gravity. The two terms inside the angle brackets represent the interfacial source terms of mass and momentum denoted by

$$M_\alpha^I = \langle [\rho(\boldsymbol{U} - \boldsymbol{U}_I)]_\alpha \bullet \nabla X_\alpha \rangle \quad \text{and} \tag{6}$$

$$\boldsymbol{F}_\alpha^I = \langle [\rho \boldsymbol{U}(\boldsymbol{U} - \boldsymbol{U}_I) - \boldsymbol{T}]_\alpha \bullet \nabla X_\alpha \rangle . \tag{7}$$

The square brackets in these equations are used to express the limit process where the interface is approached from the side of phase α

$$[\Phi]_\alpha = \lim_{\boldsymbol{x}_\alpha \to \boldsymbol{x}_I} \Phi(\boldsymbol{x}_\alpha, t) . \tag{8}$$

In addition, the interfacial sources M_α^I and $\boldsymbol{F}_\alpha^I$ have to fulfil the interfacial jump conditions of mass and momentum

$$\sum_{\alpha = 1}^{N_P} M_\alpha^I = 0 \quad \text{and} \tag{9}$$

$$\sum_{\alpha = 1}^{N_P} \boldsymbol{F}_\alpha^I = \boldsymbol{F}_T^I . \tag{10}$$

In equation (10), $\boldsymbol{F}_T^I$ is the contribution to the total force per unit volume on the mixture due to the interface, mainly originating from the spatial changes in the surface tension, and N_P stands for the number of phases present. Without M_α^I and $\boldsymbol{F}_\alpha^I$, the equations (4) and (5) closely resemble the balance equations of single phase flow.

2.1 CONSTITUTIVE EQUATIONS

A large number of studies and intuitive speculations about the constitutive models of the stress tensor $\bar{\boldsymbol{T}}_\alpha$ and about the interfacial sources M_α^I and $\boldsymbol{F}_\alpha^I$ have been conducted, e.g., [7, 11, 19, 20, 21, 29, 30, 31, 46]. In the following discussion, in addition of the conventional treatments of Ishii [31] and Drew [20], the results of the two consistent and mathematically rigorous control volume/control surface approaches are referred, namely the volume averaging method of Prosperetti & Jones [46] and the micromechanical ensemble averaging method of Hwang & Shen [29, 30].

2.1.1 Stress tensor

In analogy with fluids, the stress tensor of each phase is normally divided into isotropic and deviatoric components

$$\bar{\boldsymbol{T}}_\alpha = -\bar{P}_\alpha \boldsymbol{I} + \bar{\tau}_\alpha , \tag{11}$$

where the isotropic part $\bar{P}_\alpha$, defined to be the mean of the trace of deformation rate, is called the pressure. The stress tensor $\bar{\boldsymbol{T}}_\alpha$ itself includes contributions from several different mechanisms. For the fluid phase two contributions are realised, $\bar{\boldsymbol{T}}_f^{\,\mathrm{v}}$ and $\bar{\boldsymbol{T}}_f^{\,\mathrm{t}}$, corresponding to the viscous stresses and to the turbulent momentum transfer (analogous to Reynolds stresses). For the dispersed phase, contributions arise by the hydrodynamic forces at the control volume surface cutting dispersed entities, the particle-presence stress $\bar{\boldsymbol{T}}_d^{\,\mathrm{p}}$ [7, 29], by the random motion of the dispersed phase, the kinetic stress $\bar{\boldsymbol{T}}_d^{\,\mathrm{k}}$ (analogous to Reynolds stresses), and by the collisions and contacts between the dispersed entities, the collision/contact stress $\bar{\boldsymbol{T}}_d^{\,\mathrm{c}}$ [32, 39]. These contributions are noted in short as

$$\bar{\boldsymbol{T}}_f = \bar{\boldsymbol{T}}_f^{\,\mathrm{v}} + \bar{\boldsymbol{T}}_f^{\,\mathrm{t}} \quad \text{and} \tag{12}$$

$$\bar{\boldsymbol{T}}_d = \bar{\boldsymbol{T}}_d^{\,\mathrm{p}} + \bar{\boldsymbol{T}}_d^{\,\mathrm{k}} + \bar{\boldsymbol{T}}_d^{\,\mathrm{c}}. \tag{13}$$

2.1.2 Interfacial momentum source

The interfacial source of momentum $\boldsymbol{F}_\alpha^I$, represented by equation (7), includes two different participating mechanisms, namely the momentum transfer produced by the phase change process and the force resulting from the existing stress on the interfaces. It is customary to describe the former mechanism by defining the macroscopic interfacial velocity $\boldsymbol{U}_\alpha^I$ as [20, 31]

$$M_\alpha^I \boldsymbol{U}_\alpha^I = \langle [\rho \boldsymbol{U}(\boldsymbol{U} - \boldsymbol{U}_I)]_\alpha \bullet \nabla X_\alpha \rangle . \tag{14}$$

Commonly, the latter portion of the interfacial momentum source $\boldsymbol{F}_\alpha^I$ is expressed as [20, 31, 34]

$$\langle -[\boldsymbol{T}^{\,\mathrm{v}}]_\alpha \bullet \nabla X_\alpha \rangle = P_\alpha^I \nabla \varepsilon_\alpha + \boldsymbol{F}_\alpha^D, \tag{15}$$

where P_α^I is the macroscopic interfacial mean pressure [1, 31] defined by

$$P_\alpha^I \nabla \varepsilon_\alpha = \langle -[P]_\alpha \nabla X_\alpha \rangle , \tag{16}$$

and $\boldsymbol{F}_\alpha^D$ denotes the interfacial force density

$$\boldsymbol{F}_\alpha^D = \langle [P - P_\alpha^I]_\alpha \nabla X_\alpha - [\tau_f^{\mathrm{v}}]_\alpha \bullet \nabla X_\alpha \rangle . \tag{17}$$

Equation (15) corresponds to the ‘current engineering practice’ as stated by Prosperetti & Jones [46]. Most of the published treatments and numerical simulations are based on this definition which is referred as the *Interfacial Mean Pressure model*, IMP, in this text.

As stated by Prosperetti & Jones [46], the definition of the interfacial mean pressure P_α^I given in equation (16) is restrictive in a way that the term $P_\alpha^I \nabla \varepsilon_\alpha$ van-

ishes in the case of a non-existent volume fraction gradient even for a varying pressure distribution on the interfaces. This inconsistency in the phasic momentum balance may lead to non-physical results in cases where P_α^I is important. In the mathematically rigorous treatments of Prosperetti & Jones [46] and Hwang & Shen [29, 30], the definition (16) is avoided. Although using different averaging methods and notions, both of these treatments come to parallel results, which are here referenced with a common name *Direct Interfacial Force model*, DIF.

According to DIF, the latter mechanism of the interfacial momentum source can be expressed as

$$\langle -[\boldsymbol{T}^{\mathrm{v}}]_\alpha \bullet \nabla X_\alpha \rangle \;=\; \varepsilon_\alpha \nabla \bullet \bar{\boldsymbol{T}}_f^{\mathrm{v}} + \boldsymbol{F}_\alpha^D - \nabla \bullet (\varepsilon_\alpha \bar{\boldsymbol{T}}_\alpha^{\mathrm{p}}) \,. \tag{18}$$

In equation (18), the first term on the right side originates from a linear approximation of the continuous phase stress components in the scale of the dispersed phase. The existence of this term is supported by the equation of motion for small rigid particles derived by Maxey & Riley [41]. In their treatment this term arises from the contribution of the undisturbed fluid flow. The second term in equation (18) is the interfacial force density $\boldsymbol{F}_\alpha^D$, a consequence of the disturbance to the fluid flow caused by the particle, including the contributions from the hydrodynamic drag force, the apparent mass force and the Basset history force. The last term results from the stress field on locations of the control surface where it intersects the dispersed phase. A mathematically rigorous definition of the particle-presence stress $\bar{\boldsymbol{T}}_\alpha^{\mathrm{p}}$ can be found from Batchelor [7] and Hwang & Shen [29].

2.2 MOMENTUM BALANCES

The momentum balances of the continuous and dispersed phases for the two treatments of the interfacial transfer term are now obtained by inserting the definitions (12)–(15) and (12)–(14), (18) in equation (5), respectively. Since a typical dispersed multi-phase flow problem involves one continuous phase and several dispersed phases, these balance equations are written in a corresponding form. This is achieved simply by including the phase interaction terms from all participating phases. Details of the rearrangement and simplification of the stress terms are given in Appendix A. Thus, the momentum balances for fluid f and for dispersed phases d, for the two different treatments, can be written as:

Interfacial Mean Pressure model, IMP;

$$\begin{aligned} \frac{\partial}{\partial t}(\varepsilon_f \bar{\rho}_f \tilde{\boldsymbol{U}}_f) + \nabla \bullet (\varepsilon_f \bar{\rho}_f \tilde{\boldsymbol{U}}_f \otimes \tilde{\boldsymbol{U}}_f) \;=\; & -\varepsilon_f \nabla \bar{P}_f + \nabla \bullet (\varepsilon_f \bar{\tau}_f^{\mathrm{v}}) + \nabla \bullet (\varepsilon_f \bar{\boldsymbol{T}}_f^{\mathrm{t}}) \\ & + (P_f^I - \bar{P}_f) \nabla \varepsilon_f + M_f^I \boldsymbol{U}_f^I + \boldsymbol{F}_T^I - \sum_{\beta=1}^{N_d} \boldsymbol{F}_\beta^D + \boldsymbol{F}_f^S + \varepsilon_f \bar{\rho}_f \boldsymbol{g} \quad \text{and} \end{aligned} \tag{19}$$

$$\frac{\partial}{\partial t}(\varepsilon_d \bar{\rho}_d \tilde{\boldsymbol{U}}_d) + \nabla \bullet (\varepsilon_d \bar{\rho}_d \tilde{\boldsymbol{U}}_d \otimes \tilde{\boldsymbol{U}}_d) = -\varepsilon_d \nabla \bar{P}_d + \nabla \bullet (\varepsilon_d \bar{\tau}_d^{\mathrm{p}}) + \nabla \bullet (\varepsilon_d (\bar{\boldsymbol{T}}_d^{\mathrm{k}} + \bar{\boldsymbol{T}}_d^{\mathrm{c}})) + (P_d^I - \bar{P}_d)\nabla \varepsilon_d + M_d^I \boldsymbol{U}_d^I + \boldsymbol{F}_d^D + \boldsymbol{F}_d^S + \varepsilon_d \bar{\rho}_d \boldsymbol{g} \quad , \tag{20}$$

Direct Interfacial Force model, DIF;

$$\frac{\partial}{\partial t}(\varepsilon_f \bar{\rho}_f \tilde{\boldsymbol{U}}_f) + \nabla \bullet (\varepsilon_f \bar{\rho}_f \tilde{\boldsymbol{U}}_f \otimes \tilde{\boldsymbol{U}}_f) = \varepsilon_f \nabla \bullet \bar{\boldsymbol{T}}_f^{\mathrm{v}} + \nabla \bullet (\varepsilon_f \bar{\boldsymbol{T}}_f^{\mathrm{t}}) + M_f^I \boldsymbol{U}_f^I + \boldsymbol{F}_T^I - \sum_{\beta=1}^{N_d} (\boldsymbol{F}_\beta^D - \nabla \bullet (\varepsilon_\beta (\bar{\boldsymbol{T}}_\beta^{\mathrm{p}} - \bar{\boldsymbol{T}}_f^{\mathrm{v}}))) + \boldsymbol{F}_f^S + \varepsilon_f \bar{\rho}_f \boldsymbol{g} \quad \text{and} \tag{21}$$

$$\frac{\partial}{\partial t}(\varepsilon_d \bar{\rho}_d \tilde{\boldsymbol{U}}_d) + \nabla \bullet (\varepsilon_d \bar{\rho}_d \tilde{\boldsymbol{U}}_d \otimes \tilde{\boldsymbol{U}}_d) = \varepsilon_d \nabla \bullet \bar{\boldsymbol{T}}_f^{\mathrm{v}} + \nabla \bullet (\varepsilon_d (\bar{\boldsymbol{T}}_d^{\mathrm{k}} + \bar{\boldsymbol{T}}_d^{\mathrm{c}})) + M_d^I \boldsymbol{U}_d^I + \boldsymbol{F}_d^D + \boldsymbol{F}_d^S + \varepsilon_d \bar{\rho}_d \boldsymbol{g} \quad . \tag{22}$$

If the relative velocities between the phases are not high, and if there exists no appreciable dispersed phase expansion/contraction, it can be assumed that the phasic pressures $\bar{P}_\alpha$ and interfacial mean pressures P_α^I in equations (19) and (20) are equal in each phase [46]. Also, in the absence of surface tension the phasic pressures $\bar{P}_f$ and $\bar{P}_d$ are almost equal [22]. These simplifications lead to the concept of shared pressure, i.e., the pressure force realized in balance equation of each phase is the fluid pressure multiplied by the volume fraction of the respective phase.

By reverting to the treatments of Prosperetti & Jones [46] and Hwang & Shen [29], it is realised that the term

$$\nabla \bullet (\varepsilon_\beta (\bar{\boldsymbol{T}}_\beta^{\mathrm{p}} - \bar{\boldsymbol{T}}_f^{\mathrm{v}})) \tag{23}$$

represents the forces created by the difference of the mean interfacial stress and the mean fluid stress on those parts of the control surface intersecting the dispersed phase. Accordingly, with the same limitations as when considering $P_\alpha^I \approx \bar{P}_\alpha$ above, the term (23) can be neglected. The same is true also for the approximation $\bar{P}_f \approx \bar{P}_d$.

Under these limitations the only difference between the IMP and DIF models is found in the viscous stress terms. On the other hand, in turbulent particulate flows the contribution from the turbulent momentum transfer is often much larger than from the viscous stresses $\bar{\boldsymbol{T}}_f^{\mathrm{t}} \gg \bar{\boldsymbol{T}}_f^{\mathrm{v}}$ and thus the difference between the models becomes immaterial.

2.3 GENERALIZED FORMS

For numerical treatment, the balance equations (4), (19)–(22) are represented in a generalized form in which all problem specific models are adapted. In this gener-

alized form, the interfacial source terms are customarily linearized as [14, 24, 35]

$$M_\alpha^I = \sum_{\beta=1}^{N_P} (\dot{m}_{\beta\alpha} - \dot{m}_{\alpha\beta}) \quad \text{and} \tag{24}$$

$$\boldsymbol{F}_\alpha^I = \sum_{\beta=1}^{N_P} (\dot{m}_{\beta\alpha}\tilde{\boldsymbol{U}}_\beta - \dot{m}_{\alpha\beta}\tilde{\boldsymbol{U}}_\alpha) + \boldsymbol{F}_\alpha^D, \text{ where} \tag{25}$$

$$\boldsymbol{F}_\alpha^D = \sum_{\beta=1}^{N_P} B_{\alpha\beta}(\tilde{\boldsymbol{U}}_\beta - \tilde{\boldsymbol{U}}_\alpha) + {}^0\boldsymbol{F}_\alpha^D. \tag{26}$$

In equation (26) ${}^0\boldsymbol{F}_\alpha^D$ is used to denote the constant term of the linearized interfacial force density and N_P stands for the total number of phases. Consequently, the multi-fluid balance equations of mass and momentum for a turbulent particulate flow are often expressed as a straightforward extension of their single phase counterparts as

$$\frac{\partial}{\partial t}(\varepsilon_\alpha\bar{\rho}_\alpha) + \nabla\bullet(\varepsilon_\alpha\bar{\rho}_\alpha\tilde{\boldsymbol{U}}_\alpha) = \sum_{\beta=1}^{N_P} (\dot{m}_{\beta\alpha} - \dot{m}_{\alpha\beta}) \text{ and} \tag{27}$$

$$\begin{aligned}
&\frac{\partial}{\partial t}(\varepsilon_\alpha\bar{\rho}_\alpha\tilde{\boldsymbol{U}}_\alpha) + \nabla\bullet(\varepsilon_\alpha(\bar{\rho}_\alpha\tilde{\boldsymbol{U}}_\alpha\otimes\tilde{\boldsymbol{U}}_\alpha - \eta_\alpha^{\text{eff}}\nabla\tilde{\boldsymbol{U}}_\alpha)) \\
&\quad = -\varepsilon_\alpha\nabla\bar{P}_f + \nabla\bullet(\varepsilon_\alpha\eta_\alpha^{\text{eff}}(\nabla\tilde{\boldsymbol{U}}_\alpha)^T) + \varepsilon_\alpha\bar{\rho}_\alpha\boldsymbol{g} \\
&+ \sum_{\beta=1}^{N_P} (\dot{m}_{\beta\alpha}\tilde{\boldsymbol{U}}_\beta - \dot{m}_{\alpha\beta}\tilde{\boldsymbol{U}}_\alpha) + \sum_{\beta=1}^{N_P} B_{\alpha\beta}(\tilde{\boldsymbol{U}}_\beta - \tilde{\boldsymbol{U}}_\alpha) + \boldsymbol{F}_\alpha^T,
\end{aligned} \tag{28}$$

where the source term $\boldsymbol{F}_\alpha^T$ is used to collect different terms of that character

$$\boldsymbol{F}_\alpha^T = \boldsymbol{F}_\alpha^S + {}^0\boldsymbol{F}_\alpha^D. \tag{29}$$

Here, the treatment of viscous stresses in the momentum equation (28) follows the IMP-model as usual.

The generalized momentum balance has been written on the basis of a general linear viscous fluid model, which is expressed as

$$\bar{\boldsymbol{T}}_\alpha = \eta_\alpha(\nabla\tilde{\boldsymbol{U}}_\alpha + (\nabla\tilde{\boldsymbol{U}}_\alpha)^T) - \bar{P}_\alpha\boldsymbol{I} + \left(\eta_\alpha^b - \frac{2}{3}\eta_\alpha\right)\nabla\bullet\tilde{\boldsymbol{U}}_\alpha\boldsymbol{I}. \tag{30}$$

In single phase flows, the constitutive model (30) is easily adapted to the generalized form of the momentum balance by defining the modified pressure

$$\bar{P}_\alpha^{\,\mathrm{e}} \;=\; \bar{P}_\alpha \;-\left(\eta_\alpha^{\mathrm{b}} - \frac{2}{3}\eta_\alpha\right)\nabla \bullet \tilde{\boldsymbol{U}}_\alpha\,, \tag{31}$$

which is used in place of $\bar{P}_\alpha$. This is in contrast with multi-phase flows, where the appearance of the hydrodynamic pressure terms and other stress contributions differ from each other. In this case, the definition (31) provides no valid simplification of the balance equations with either of the approaches, the IMP or the DIF. Thus, a more suitable template for the momentum balance (28) is provided by

$$\begin{aligned}
&\frac{\partial}{\partial t}(\varepsilon_\alpha \bar{\rho}_\alpha \tilde{\boldsymbol{U}}_\alpha) + \nabla \bullet (\varepsilon_\alpha(\bar{\rho}_\alpha \tilde{\boldsymbol{U}}_\alpha \otimes \tilde{\boldsymbol{U}}_\alpha - \eta_\alpha^{\mathrm{eff}} \nabla \tilde{\boldsymbol{U}}_\alpha)) \\
&= -\varepsilon_\alpha \nabla \bar{P}_f + \nabla \bullet (\varepsilon_\alpha \eta_\alpha^{\mathrm{eff}} (\nabla \tilde{\boldsymbol{U}}_\alpha)^T) - \nabla(\varepsilon_\alpha \bar{P}_\alpha^{\,\mathrm{e}}) + \varepsilon_\alpha \bar{\rho}_\alpha \boldsymbol{g} \\
&+ \sum_{\beta=1}^{N_{\mathrm{P}}} (\dot{m}_{\beta\alpha} \tilde{\boldsymbol{U}}_\beta - \dot{m}_{\alpha\beta} \tilde{\boldsymbol{U}}_\alpha) + \sum_{\beta=1}^{N_{\mathrm{P}}} B_{\alpha\beta}(\tilde{\boldsymbol{U}}_\beta - \tilde{\boldsymbol{U}}_\alpha) + \boldsymbol{F}_\alpha^T\,,
\end{aligned} \tag{32}$$

where the phasic pressure $\bar{P}_\alpha$ in the definition of the modified pressure (31) is associated with the other pressure like contributions than the mean fluid pressure $\bar{P}_f$. For the fluid phase, this modified pressure arises from the last term of the equation (31) and from the eddy viscosity hypothesis

$$\begin{aligned}
\varepsilon_f \bar{\boldsymbol{T}}_f^{\,\mathrm{t}} \;&=\; \langle X_\alpha \rho\, \boldsymbol{u}_\alpha'' \otimes \boldsymbol{u}_\alpha'' \rangle\big|_{\alpha = f} \\
&=\; \varepsilon_f \left(\eta_f^{\mathrm{t}} (\nabla \tilde{\boldsymbol{U}}_f + (\nabla \tilde{\boldsymbol{U}}_f)^T) - \frac{2}{3}\bar{\rho}_f \tilde{k}_f \boldsymbol{I} - \frac{2}{3}\eta_f^{\mathrm{t}} \nabla \bullet \tilde{\boldsymbol{U}}_f \boldsymbol{I}\right)\,,
\end{aligned} \tag{33}$$

where $\boldsymbol{u}_\alpha''$ represents the deviations from the mass-weighted phase averages, η_f^{t} denotes the eddy viscosity and $\tilde{k}_f$ stands for the kinetic energy of the turbulent fluctuations, respectively. The ‘turbulent pressure’ is identified as the second term on the right side.

In the same way, additional ‘pressure’ contributions arise from the constitutive equations for the kinetic and collisional momentum transfer of the dispersed phases [27, 32, 39]. Since these contributions become considerable in some applications, e.g., in fluidized beds [13], they can not generally be neglected.

In numerical solution the momentum balance (32) is treated like three scalar variables, each representing one Cartesian component of momentum, by adapting it to the corresponding balance equation of a generic dependent scalar variable $\tilde{\Phi}_\alpha$

$$\begin{aligned}
&\frac{\partial}{\partial t}(\varepsilon_\alpha \bar{\rho}_\alpha \tilde{\Phi}_\alpha) + \nabla \bullet (\varepsilon_\alpha(\bar{\rho}_\alpha \tilde{\boldsymbol{U}}_\alpha \tilde{\Phi}_\alpha - \Gamma_\alpha \nabla \tilde{\Phi}_\alpha)) \\
&= \sum_{\beta=1}^{N_{\mathrm{P}}} (\dot{m}_{\beta\alpha} \tilde{\Phi}_\beta - \dot{m}_{\alpha\beta} \tilde{\Phi}_\alpha) + \sum_{\beta=1}^{N_{\mathrm{P}}} B_{\alpha\beta}^I (\tilde{\Phi}_\beta - \tilde{\Phi}_\alpha) + S_\alpha\,.
\end{aligned} \tag{34}$$

2.4 DISCRETIZED EQUATIONS

In order to facilitate the numerical solution of the macroscopic balance equations (27), (32) and (34) in a general 3D geometry using Body-Fitted Coordinates (BFC) combined with the multi-block method, these equations are expressed in the covariant tensor form [14, 36]. The coordinate system used in this context is the local non-orthogonal coordinate system (ξ, ς, ζ), referred to as the computational space, obtained from the Cartesian coordinate system (x, y, z), i.e., the physical space, by the numerical curvilinear coordinate transformation $\xi^i(x^j)$. Details of the derivation are given in Appendix B.

Because there is no danger of confusion, the phase and mass-weighted phase average notations above the dependent variables, e.g., Φ_α and Φ_α, have been omitted in the subsequent treatment in order to enhance the readability of the equations. Thus, the transformed balance equations in the computational space are

$$\frac{\partial}{\partial t}(|\boldsymbol{J}|\,\varepsilon_\alpha\rho_\alpha) + \frac{\partial}{\partial \xi^i}(\hat{I}^i_{m_\alpha}) = \sum_{\beta=1}^{N_P} |\boldsymbol{J}|(\dot{m}_{\beta\alpha} - \dot{m}_{\alpha\beta}), \tag{35}$$

$$\begin{aligned}\frac{\partial}{\partial t}(|\boldsymbol{J}|\varepsilon_\alpha\rho_\alpha U^k_\alpha) + \frac{\partial}{\partial \xi^i}(\hat{I}^i_{U^k_\alpha}) &= -\varepsilon_\alpha A^i_k \frac{\partial P_f}{\partial \xi^i} + \frac{\partial}{\partial \xi^i}\left(\varepsilon_\alpha \eta^{\mathrm{eff}}_\alpha \frac{A^i_m A^j_k}{|\boldsymbol{J}|}\frac{\partial U^m_\alpha}{\partial \xi^j}\right) \\ &\quad - A^i_k \frac{\partial}{\partial \xi^i}(\varepsilon_\alpha P^e_\alpha) + |\boldsymbol{J}|\,\varepsilon_\alpha\rho_\alpha \boldsymbol{g} \\ &\quad + \sum_{\beta=1}^{N_P} |\boldsymbol{J}|(\dot{m}_{\beta\alpha}U^k_\beta - \dot{m}_{\alpha\beta}U^k_\alpha) + \sum_{\beta=1}^{N_P} |\boldsymbol{J}|\,B_{\alpha\beta}(U^k_\beta - U^k_\alpha) + |\boldsymbol{J}|\boldsymbol{F}^T_\alpha \quad \text{and}\end{aligned} \tag{36}$$

$$\begin{aligned}&\frac{\partial}{\partial t}(|\boldsymbol{J}|\varepsilon_\alpha\rho_\alpha\Phi_\alpha) + \frac{\partial}{\partial \xi^i}(\hat{I}^i_{\Phi_\alpha}) \\ &= \sum_{\beta=1}^{N_P} |\boldsymbol{J}|(\dot{m}_{\beta\alpha}\Phi_\beta - \dot{m}_{\alpha\beta}\Phi_\alpha) + \sum_{\beta=1}^{N_P} |\boldsymbol{J}|\,B^I_{\alpha\beta}(\Phi_\beta - \Phi_\alpha) + |\boldsymbol{J}|S_\alpha .\end{aligned} \tag{37}$$

where $|\boldsymbol{J}|$ is the Jacobian determinant (B3), $A^i_m = \boldsymbol{A}^{(i)}$ (Figure 1(a)) represents the adjugate Jacobian matrix (B4), $\hat{U}^i_\alpha$ stands for the normal flux velocity component (B21), and the total normal phasic fluxes $\hat{I}^i_{m_\alpha}$, $\hat{I}^i_{U^k_\alpha}$ and $\hat{I}^i_{\Phi_\alpha}$ are defined as specified in Appendix B.

In the process of the coordinate transformation, all the derivatives of the macroscopic balance equations (27), (32) and (34) in the physical space have been expressed with the corresponding terms in the computational space, where the transformed macroscopic balance equations (35), (36) and (37) are discretized. This is done following the conservative finite-volume approach with collocated dependent variables.

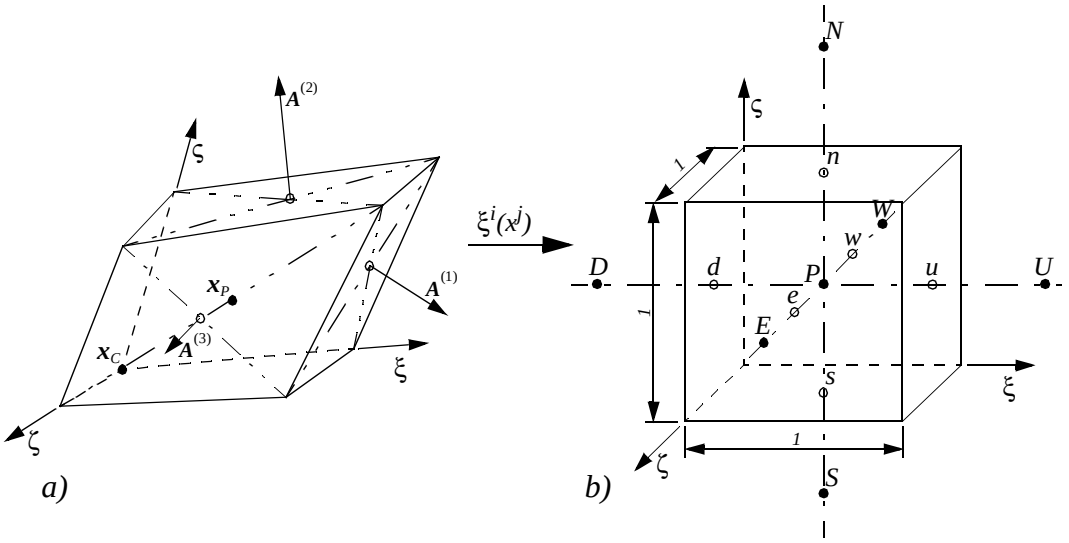

Figure 1. (a) Area vectors on the faces of the finite-volume cell in the physical space. (b) The notion of the neighbouring cell centres and cell faces in the computational space.

Integrating the generic balance equation (37) over a single finite-volume cell (Figure 1(b)) in the computational space with the help of the Gauss law results in

$$\int_{V_C} \frac{\partial}{\partial t}(|\boldsymbol{J}|\varepsilon_\alpha \rho_\alpha \Phi_\alpha) dV_C + \int_{A_C} \hat{I}^i_{\Phi_\alpha} \bullet \boldsymbol{n}\, dA_C$$

$$= \int_{V_C} \sum_{\beta=1}^{N_P} |\boldsymbol{J}|(\dot{m}_{\beta\alpha}\Phi_\beta - \dot{m}_{\alpha\beta}\Phi_\alpha) dV_C + \int_{V_C} \sum_{\beta=1}^{N_P} |\boldsymbol{J}|\, B^I_{\alpha\beta}(\Phi_\beta - \Phi_\alpha) dV_C \qquad (38)$$

$$+ \int_V |\boldsymbol{J}| S_\alpha dV_C \ ,$$

where V_C is the volume of the finite-volume cell in the computational space and A_C is the surface of this cell. Up to the second-order accuracy, the edges of a rectangular volume V_C in the computational space are transformed into the physical space as

$$(\delta\xi, \delta\varsigma, \delta\zeta) \rightarrow (\delta\xi\, \boldsymbol{e}_{(1)}, \delta\varsigma\, \boldsymbol{e}_{(2)}, \delta\zeta\, \boldsymbol{e}_{(3)}), \qquad (39)$$

where $\boldsymbol{e}_{(i)}$ are the covariant basis vectors (Appendix B). Accordingly, the computational space volumes and cell face areas are related to the physical space volumes V_P and areas as

$$V_C = \delta\xi\delta\varsigma\delta\zeta \rightarrow |\boldsymbol{J}|\delta\xi\delta\varsigma\delta\zeta = V_P\, \delta\xi\delta\varsigma\delta\zeta \ , \qquad (40)$$

$$\delta\varsigma\delta\zeta \rightarrow \boldsymbol{A}^{(1)}\delta\varsigma\delta\zeta\,, \quad \delta\xi\delta\zeta \rightarrow \boldsymbol{A}^{(2)}\delta\xi\delta\zeta \quad \text{and} \quad \delta\xi\delta\varsigma \rightarrow \boldsymbol{A}^{(3)}\delta\xi\delta\varsigma\,. \qquad (41)$$

Setting the lengths of the finite-volume cell edges in the computational space to be unity $\delta\xi = \delta\varsigma = \delta\zeta = 1$, all the cells in the physical space are transformed into cubes of unit volume and unit face areas in the computational space.

Based on the same type of integral balances as equation (38) and on relations (40) and (41), the discretization of the macroscopic balance equations (35), (36) and (37) can be formally represented as

$$\left[\frac{\{|\boldsymbol{J}|\,\varepsilon_\alpha \rho_\alpha\}}{\Delta t}\right]_{\boldsymbol{t}}^{\boldsymbol{t+\Delta t}} + [\hat{I}^1_{m_\alpha}]^{\boldsymbol{u}}_{\boldsymbol{d}} + [\hat{I}^2_{m_\alpha}]^{\boldsymbol{n}}_{\boldsymbol{s}} + [\hat{I}^3_{m_\alpha}]^{\boldsymbol{e}}_{\boldsymbol{w}} = \sum_{\beta=1}^{N_P} \{|\boldsymbol{J}|(\dot{m}_{\beta\alpha} - \dot{m}_{\alpha\beta})\}\ , \tag{42}$$

$$\begin{aligned}\left[\frac{\{|\boldsymbol{J}|\varepsilon_\alpha \rho_\alpha U^k_\alpha\}}{\Delta t}\right]_{\boldsymbol{t}}^{\boldsymbol{t+\Delta t}} + [\hat{I}^1_{U^k_\alpha}]^{\boldsymbol{u}}_{\boldsymbol{d}} + [\hat{I}^2_{U^k_\alpha}]^{\boldsymbol{n}}_{\boldsymbol{s}} + [\hat{I}^3_{U^k_\alpha}]^{\boldsymbol{e}}_{\boldsymbol{w}} &= -\left\{\varepsilon_\alpha A^i_k \frac{\partial P_\alpha}{\partial \xi^i}\right\} \\ + \left[\varepsilon_\alpha \eta_\alpha \frac{A^1_m A^j_k}{|\boldsymbol{J}|}\frac{\partial U^m_\alpha}{\partial \xi^j}\right]^{\boldsymbol{u}}_{\boldsymbol{d}} + \left[\varepsilon_\alpha \eta_\alpha \frac{A^2_m A^j_k}{|\boldsymbol{J}|}\frac{\partial U^m_\alpha}{\partial \xi^j}\right]^{\boldsymbol{n}}_{\boldsymbol{s}} + \left[\varepsilon_\alpha \eta_\alpha \frac{A^3_m A^j_k}{|\boldsymbol{J}|}\frac{\partial U^m_\alpha}{\partial \xi^j}\right]^{\boldsymbol{e}}_{\boldsymbol{w}} &\\ - \left\{A^i_k \frac{\partial}{\partial \xi^i}(\varepsilon_\alpha P^e_\alpha)\right\} + \{|\boldsymbol{J}|\,\varepsilon_\alpha \rho_\alpha \boldsymbol{g}\} + \{|\boldsymbol{J}|\boldsymbol{F}^T_\alpha\} &\\ + \sum_{\beta=1}^{N_P} \{|\boldsymbol{J}|(\dot{m}_{\beta\alpha} U^k_\beta - \dot{m}_{\alpha\beta} U^k_\alpha)\} + \sum_{\beta=1}^{N_P} \{|\boldsymbol{J}|\,B_{\alpha\beta}(U^k_\beta - U^k_\alpha)\} \text{ and} &\end{aligned} \tag{43}$$

$$\begin{aligned}\left[\frac{\{|\boldsymbol{J}|\varepsilon_\alpha \rho_\alpha \Phi_\alpha\}}{\Delta t}\right]_{\boldsymbol{t}}^{\boldsymbol{t+\Delta t}} + [\hat{I}^1_{\Phi_\alpha}]^{\boldsymbol{u}}_{\boldsymbol{d}} + [\hat{I}^2_{\Phi_\alpha}]^{\boldsymbol{n}}_{\boldsymbol{s}} + [\hat{I}^3_{\Phi_\alpha}]^{\boldsymbol{e}}_{\boldsymbol{w}} &\\ = \sum_{\beta=1}^{N_P} \{|\boldsymbol{J}|(\dot{m}_{\beta\alpha}\Phi_\beta - \dot{m}_{\alpha\beta}\Phi_\alpha)\} + \sum_{\beta=1}^{N_P} \{|\boldsymbol{J}|\,B^I_{\alpha\beta}(\Phi_\beta - \Phi_\alpha)\} + \{|\boldsymbol{J}|S_\alpha\}\ .&\end{aligned} \tag{44}$$

In equations (42), (43) and (44), the notation $\{\ \}$ indicates that the operand is integrated over the volume of the finite-volume cell in question. Because the computational space cells are all of unit volume, the resulting mean value is directly expressed on the unit-volume basis. Further, the notation $[\ ]^{\boldsymbol{u,\,n,\,e}}_{\boldsymbol{d,\,s,\,w}}$ expresses a difference between the values of the operand at specified locations (Figure 1(b)), e.g.,

$$[\hat{I}^1_{\Phi_\alpha}]^{\boldsymbol{u}}_{\boldsymbol{d}} = \hat{I}^1_{\Phi_\alpha}\Big|_{\boldsymbol{u}} - \hat{I}^1_{\Phi_\alpha}\Big|_{\boldsymbol{d}}. \tag{45}$$

The right-hand side notation implies that the operand is integrated over the respective face of the finite-volume cell. The result of this integration is directly on the

unit-area basis. For the time derivative term, the corresponding notation $[\ ]_{\boldsymbol{t}}^{\boldsymbol{t+\Delta t}}$ expresses the difference of cell-based volume averages at respective times

$$[S_\alpha]_{\boldsymbol{t}}^{\boldsymbol{t+\Delta t}} = \{S_\alpha\}_{\boldsymbol{t+\Delta t}} - \{S_\alpha\}_{\boldsymbol{t}}. \tag{46}$$

Thus, the total normal phasic fluxes $\hat{I}^i_{m_\alpha}$, $\hat{I}^i_{U^k_\alpha}$ and $\hat{I}^i_{\Phi_\alpha}$ are represented as

$$[\hat{I}^i_{m_\alpha}]_{\boldsymbol{l}}^{\boldsymbol{h}} = C^i_\alpha\big|_{\boldsymbol{h}} - C^i_\alpha\big|_{\boldsymbol{l}}, \tag{47}$$

$$[\hat{I}^i_{U^k_\alpha}]_{\boldsymbol{l}}^{\boldsymbol{h}} = C^i_\alpha\big|_{\boldsymbol{h}} U^k_\alpha\big|_{\boldsymbol{h}} - C^i_\alpha\big|_{\boldsymbol{l}} U^k_\alpha\big|_{\boldsymbol{l}} - D^{ij}_\alpha\big|_{\boldsymbol{h}} \left.\frac{\partial U^k_\alpha}{\partial \xi^j}\right|_{\boldsymbol{h}} + D^{ij}_\alpha\big|_{\boldsymbol{l}} \left.\frac{\partial U^k_\alpha}{\partial \xi^j}\right|_{\boldsymbol{l}}, \tag{48}$$

$$[\hat{I}^i_{\Phi_\alpha}]_{\boldsymbol{l}}^{\boldsymbol{h}} = C^i_\alpha\big|_{\boldsymbol{h}} \Phi_\alpha\big|_{\boldsymbol{h}} - C^i_\alpha\big|_{\boldsymbol{l}} \Phi_\alpha\big|_{\boldsymbol{l}} - D^{ij}_{\Phi_\alpha}\big|_{\boldsymbol{h}} \left.\frac{\partial \Phi_\alpha}{\partial \xi^j}\right|_{\boldsymbol{h}} + D^{ij}_{\Phi_\alpha}\big|_{\boldsymbol{l}} \left.\frac{\partial \Phi_\alpha}{\partial \xi^j}\right|_{\boldsymbol{l}}, \tag{49}$$

$$\text{where} \quad i = \begin{cases} 1\ ;\ \boldsymbol{h} = \boldsymbol{u}, \boldsymbol{l} = \boldsymbol{d} \\ 2\ ;\ \boldsymbol{h} = \boldsymbol{n}, \boldsymbol{l} = \boldsymbol{s} \\ 3\ ;\ \boldsymbol{h} = \boldsymbol{e}, \boldsymbol{l} = \boldsymbol{w} \end{cases}$$

indicates the pair of faces in question. Comparison between equations (B19) and (47), (48) and (49) reveals that the phasic convection and diffusion coefficients C^i_α, D^{ij}_α and $D^{ij}_{\Phi_\alpha}$ are specified by the relations

$$C^i_\alpha\big|_{\boldsymbol{c}} = \varepsilon_\alpha\big|_{\boldsymbol{c}} \rho_\alpha\big|_{\boldsymbol{c}} \boldsymbol{A}^{(i)} \bullet \boldsymbol{U}_\alpha\big|_{\boldsymbol{c}} = \varepsilon_\alpha\big|_{\boldsymbol{c}} \rho_\alpha\big|_{\boldsymbol{c}} \hat{U}^i_\alpha\big|_{\boldsymbol{c}}, \tag{50}$$

$$D^{ij}_\alpha\big|_{\boldsymbol{c}} = \varepsilon_\alpha\big|_{\boldsymbol{c}} \eta_\alpha\big|_{\boldsymbol{c}} \left.\frac{A^i_m A^j_m}{|\boldsymbol{J}|}\right|_{\boldsymbol{c}} = \varepsilon_\alpha\big|_{\boldsymbol{c}} \eta_\alpha\big|_{\boldsymbol{c}} G^{ij}\big|_{\boldsymbol{c}}, \tag{51}$$

$$D^{ij}_{\Phi_\alpha}\big|_{\boldsymbol{c}} = \varepsilon_\alpha\big|_{\boldsymbol{c}} \Gamma_\alpha\big|_{\boldsymbol{c}} \left.\frac{A^i_m A^j_m}{|\boldsymbol{J}|}\right|_{\boldsymbol{c}} = \varepsilon_\alpha\big|_{\boldsymbol{c}} \Gamma_\alpha\big|_{\boldsymbol{c}} G^{ij}\big|_{\boldsymbol{c}}, \tag{52}$$

$$\text{where} \quad i = \begin{cases} 1\ ;\ \boldsymbol{c} = \boldsymbol{u}, \boldsymbol{d} \\ 2\ ;\ \boldsymbol{c} = \boldsymbol{n}, \boldsymbol{s} \\ 3\ ;\ \boldsymbol{c} = \boldsymbol{e}, \boldsymbol{w} \end{cases}.$$

2.4.1 Profile assumptions

Because the discretization is done in the computational space, integrating an operand over the finite-volume cell with a constant value results in

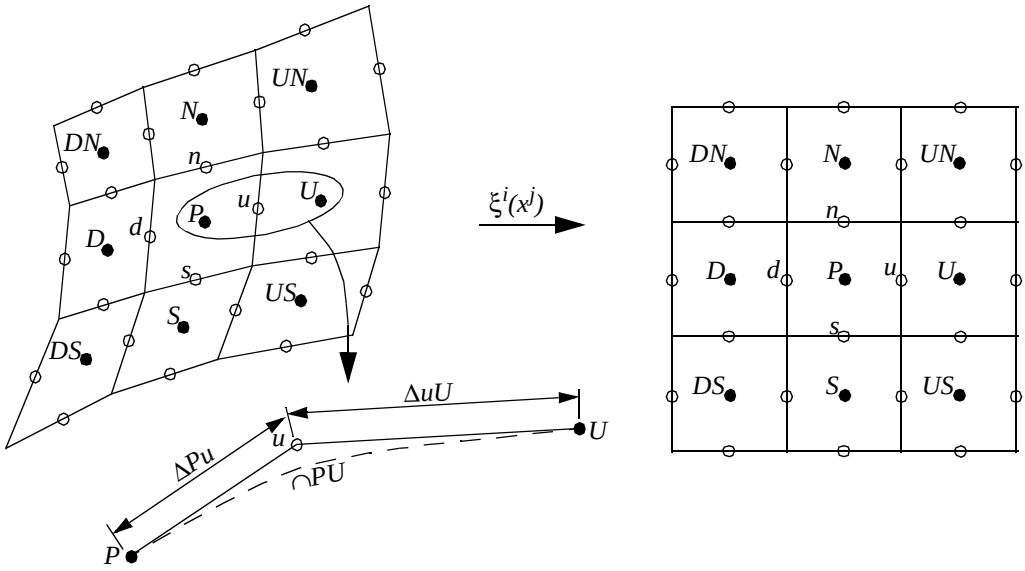

Figure 2. Notations used in the context of discretization approximations. The inset of the physical space reveals the weight factors.

$$\{\Phi\} \approx \Phi|_{\boldsymbol{P}} V_C = \Phi|_{\boldsymbol{P}} = \Phi_{\boldsymbol{P}} , \tag{53}$$

where $\Phi|_{\boldsymbol{P}}$ is the value of the operand at the centre of the cell.

Since the rest of the terms in equations (42), (43) and (44) express the flux of the operand through the faces of the finite-volume cell, they are calculated as the difference of the average value of the operand at the opposite faces of the cell as indicated by equation (45). For the averaging, the real profile of the operand over the face is approximated with a constant value located at the centre of the face. This approximation is already reflected in the chosen form of the notation. Accordingly, integration over the face leads to

$$\int_{A_C^i} \Phi dA_C^i \approx \Phi|_{\boldsymbol{c}} A_C^i = \Phi|_{\boldsymbol{c}} = \Phi_{\boldsymbol{c}} , \tag{54}$$

where $\Phi|_{\boldsymbol{c}}$ is the value of the operand at the centre of the cell face.

2.4.2 Values on cell faces

To calculate the flux terms $[\Phi]_{\boldsymbol{d}}^{\boldsymbol{u}}$, the material properties and the values of the dependent variables at the centres of the cell faces are needed. These values are found by a weighted linear interpolation scheme from the cell centre values. The weight factors used in this context are based on the distances between cell centres and the corresponding cell faces in the physical space (Figure 2). The value on the cell face is then given by

$$\Phi|_{\boldsymbol{c}} = \Phi_{\boldsymbol{c}} = (1 - W_{\boldsymbol{c}})\Phi_{\boldsymbol{P}} + W_{\boldsymbol{c}}\Phi_{\boldsymbol{C}}\,, \quad W_{\boldsymbol{c}} = \frac{\Delta \boldsymbol{Pc}}{\Delta \boldsymbol{Pc} + \Delta \boldsymbol{Cc}} \tag{55}$$

where $\boldsymbol{c} = (\boldsymbol{u}, \boldsymbol{d}, \boldsymbol{n}, \boldsymbol{s}, \boldsymbol{e}, \boldsymbol{w})$ and $\boldsymbol{C} = (\boldsymbol{U}, \boldsymbol{D}, \boldsymbol{N}, \boldsymbol{S}, \boldsymbol{E}, \boldsymbol{W})$.

This scheme is second-order accurate in rectangular non-uniform meshes.

2.4.3 Gradients at cell centres

The source terms include the pressure gradients calculated at cell centres. In a general case, other source terms involving gradients of dependent variables, e.g., the model used in the test case of this article, may also exist. These gradients are approximated by the same type of weighted interpolation scheme as the one for values on cell faces, but to enhance accuracy, the weight factors in this case are based on arc lengths between the cell centres (Figure 2). Although calculating the arc lengths is computationally expensive, the Rhie-Chow interpolation method [49], used to provide the normal flux velocity components $\hat{U}_{\alpha}^{i}$ on the cell faces, necessitates the second-order accuracy also on the non-uniform curvilinear meshes. Thus, by defining two weight factors, one on the positive side and the other on the negative side of the cell centre in consideration, the gradient at the cell centre is calculated as

$$\left.\frac{\partial \Phi}{\partial x^{i}}\right|_{\boldsymbol{P}} = W_{\boldsymbol{L}}\,\Phi_{\boldsymbol{H}} + (W_{\boldsymbol{H}} - W_{\boldsymbol{L}})\Phi_{\boldsymbol{P}} - W_{\boldsymbol{H}}\,\Phi_{\boldsymbol{L}}\,, \tag{56}$$

in which the weight factors are defined to be

$$W_{\boldsymbol{H}} = \frac{1}{\cap \boldsymbol{HP} + \cap \boldsymbol{PL}} \frac{\cap \boldsymbol{HP}}{\cap \boldsymbol{PL}},$$

$$W_{\boldsymbol{L}} = \frac{1}{\cap \boldsymbol{HP} + \cap \boldsymbol{PL}} \frac{\cap \boldsymbol{PL}}{\cap \boldsymbol{HP}}.$$

Accordingly, the pressure gradient source term in the discretized momentum equation (43) is not calculated on the computational space but directly from the physical space gradient, as specified by equation (56). The relation between these two forms of the pressure gradient source term is given in Appendix B by equation (B25).

2.4.4 Gradients on cell faces

The total normal phasic fluxes (48) and (49) include gradients of the dependent variable on the cell faces in their terms involved with diffusion fluxes. Furthermore, in the discretized momentum balance (43) those terms of the deformation rate tensor not analogous with the viscous diffusion are classified as source terms and also involve gradients of this type. These gradients are all discretized using

central differences in the computational space. For the gradients normal to the cell faces, the central difference method is applied as

$$\left.\frac{\partial \Phi}{\partial \xi^i}\right|_{\boldsymbol{c}} = \Phi_{\boldsymbol{C}} - \Phi_{\boldsymbol{P}} \quad \text{with} \quad i = \begin{cases} 1\ ;\ \boldsymbol{C} = \boldsymbol{U}, \boldsymbol{c} = \boldsymbol{u} \\ 2\ ;\ \boldsymbol{C} = \boldsymbol{N}, \boldsymbol{c} = \boldsymbol{n} \\ 3\ ;\ \boldsymbol{C} = \boldsymbol{E}, \boldsymbol{c} = \boldsymbol{e} \end{cases} . \tag{57}$$

In the case of cross-derivatives, i.e., derivatives on the plane of the cell face, the gradients are approximated as the mean of the two central differences calculated at the cell centres on both sides of the face in question. As an example, the cross-derivatives on the cell face $\boldsymbol{u}$ are (Figure 2)

$$\left.\frac{\partial \Phi}{\partial \zeta}\right|_{\boldsymbol{u}} = \frac{1}{4}(\Phi_{\boldsymbol{N}} - \Phi_{\boldsymbol{S}} + \Phi_{\boldsymbol{UN}} - \Phi_{\boldsymbol{US}}), \tag{58}$$

$$\left.\frac{\partial \Phi}{\partial \zeta}\right|_{\boldsymbol{u}} = \frac{1}{4}(\Phi_{\boldsymbol{E}} - \Phi_{\boldsymbol{W}} + \Phi_{\boldsymbol{UE}} - \Phi_{\boldsymbol{UW}}). \tag{59}$$

The other ten cross-derivatives on the remaining five faces are defined in an analogous way.

The approximation of the cross-derivatives as in equations (58) and (59) connects 18 neighbouring cells to the treatment of every finite-volume cell. To allow the use of the standard linear equation system solvers, the treatment is reduced back to the usual one involving only the eight neighbouring cells sharing a cell face with the cell under consideration by the deferred correction approach, i.e., treating the cross-derivatives as source terms by using values from the previous iteration for the dependent variables in question. Thus, in addition to the terms related to the gradients normal to the cell faces (the diagonal terms of the diffusion tensor), the deferred correction approach results in the following additional source terms expressing the effect of non-orthogonality

$$\begin{aligned} S_{\Phi_\alpha}^{D} = &\left[D_{\Phi_\alpha}^{12} \frac{\partial\, {}^{*}\Phi_\alpha}{\partial \zeta} + D_{\Phi_\alpha}^{13} \frac{\partial\, {}^{*}\Phi_\alpha}{\partial \zeta} \right]_{\boldsymbol{d}}^{\boldsymbol{u}} + \left[D_{\Phi_\alpha}^{21} \frac{\partial\, {}^{*}\Phi_\alpha}{\partial \xi} + D_{\Phi_\alpha}^{23} \frac{\partial\, {}^{*}\Phi_\alpha}{\partial \zeta} \right]_{\boldsymbol{s}}^{\boldsymbol{n}} \\ &+ \left[D_{\Phi_\alpha}^{31} \frac{\partial\, {}^{*}\Phi_\alpha}{\partial \xi} + D_{\Phi_\alpha}^{32} \frac{\partial\, {}^{*}\Phi_\alpha}{\partial \zeta} \right]_{\boldsymbol{w}}^{\boldsymbol{e}}, \end{aligned} \tag{60}$$

where ${}^{*}\Phi_\alpha$ denotes the value of the dependent variable from the previous iteration.

Following the details given above, the formally discretized macroscopic balance equations (42), (43) and (44) can now be written in their final form. To enhance the readability and to keep more physical nature in the discretized equations, they are next given in a partly discretized form retaining most of the terms in their previous

form. This practice should also aid in transferring the presented methods to approaches using different discretization schemes. Thus the macroscopic balance equations of the phasic mass, momentum and generic dependent scalar variables are

$$C_\alpha\big|_{\boldsymbol{u}} - C_\alpha\big|_{\boldsymbol{d}} + C_\alpha\big|_{\boldsymbol{n}} - C_\alpha\big|_{\boldsymbol{s}} + C_\alpha\big|_{\boldsymbol{e}} - C_\alpha\big|_{\boldsymbol{w}} = M_\alpha^I\big|_{\boldsymbol{P}} V_P - \left[\frac{\varepsilon_\alpha\big|_{\boldsymbol{P}}\rho_\alpha\big|_{\boldsymbol{P}} V_P}{\Delta t}\right]_{\boldsymbol{t}}^{\boldsymbol{t+\Delta t}}, \tag{61}$$

$$\begin{aligned}
&\sum_{\boldsymbol{c}}^{\boldsymbol{u,d,n,s,e,w}} a_{U_\alpha^k}\big|_{\boldsymbol{c}} \; U_\alpha^k\big|_{\boldsymbol{P}} = \sum_{\boldsymbol{C}}^{\boldsymbol{u,d,n,s,e,w}} a_{U_\alpha^k}\big|_{\boldsymbol{c}} \, U_\alpha^k\big|_{\boldsymbol{C}} \\
&- \varepsilon_\alpha\big|_{\boldsymbol{P}} A_k^i\big|_{\boldsymbol{P}} \frac{\partial P_f}{\partial \xi^i}\bigg|_{\boldsymbol{P}} - A_k^i\big|_{\boldsymbol{P}} \frac{\partial}{\partial \xi^i}(\varepsilon_\alpha P_\alpha^{\mathrm{e}})\bigg|_P + \varepsilon_\alpha\big|_{\boldsymbol{P}}\rho_\alpha\big|_{\boldsymbol{P}} \boldsymbol{g}\, V_P \\
&+ \left[\varepsilon_\alpha \eta_\alpha^{\mathrm{eff}} \frac{A_m^1 A_k^j}{|\boldsymbol{J}|}\frac{\partial U_\alpha^m}{\partial \xi^j}\right]_{\boldsymbol{d}}^{\boldsymbol{u}} + \left[\varepsilon_\alpha \eta_\alpha^{\mathrm{eff}} \frac{A_m^2 A_k^j}{|\boldsymbol{J}|}\frac{\partial U_\alpha^m}{\partial \xi^j}\right]_{\boldsymbol{s}}^{\boldsymbol{n}} + \left[\varepsilon_\alpha \eta_\alpha^{\mathrm{eff}} \frac{A_m^3 A_k^j}{|\boldsymbol{J}|}\frac{\partial U_\alpha^m}{\partial \xi^j}\right]_{\boldsymbol{w}}^{\boldsymbol{e}} \\
&+ \sum_{\beta=1}^{N_{\mathrm{P}}} \left(\dot{m}_{\beta\alpha}\big|_{\boldsymbol{P}} U_\beta^k\big|_{\boldsymbol{P}} - \dot{m}_{\alpha\beta}\big|_{\boldsymbol{P}} U_\alpha^k\big|_{\boldsymbol{P}}\right) V_P + \sum_{\beta=1}^{N_{\mathrm{P}}} B_{\alpha\beta}\big|_{\boldsymbol{P}} \left(U_\beta^k\big|_{\boldsymbol{P}} - U_\alpha^k\big|_{\boldsymbol{P}}\right) V_P \\
&+ {}^1\boldsymbol{F}_\alpha^T\big|_{\boldsymbol{P}} U_\alpha^k\big|_{\boldsymbol{P}} V_P + {}^0\boldsymbol{F}_\alpha^T\big|_{\boldsymbol{P}} V_P + S_{U_\alpha^k}^D - \left[\varepsilon_\alpha\big|_{\boldsymbol{P}}\rho_\alpha\big|_{\boldsymbol{P}} U_\alpha^k\big|_{\boldsymbol{P}} V_P\right]_{\boldsymbol{t}}^{\boldsymbol{t+\Delta t}} \text{ and}
\end{aligned} \tag{62}$$

$$\begin{aligned}
&\sum_{\boldsymbol{c}}^{\boldsymbol{u,d,n,s,e,w}} a_{\Phi_\alpha}\big|_{\boldsymbol{c}} \; \Phi_\alpha\big|_{\boldsymbol{P}} = \sum_{\boldsymbol{C}}^{\boldsymbol{u,d,n,s,e,w}} a_{\Phi_\alpha}\big|_{\boldsymbol{c}} \, \Phi_\alpha\big|_{\boldsymbol{C}} \\
&+ \sum_{\beta=1}^{N_{\mathrm{P}}} (\dot{m}_{\beta\alpha}\big|_{\boldsymbol{P}} \Phi_\beta\big|_{\boldsymbol{P}} - \dot{m}_{\alpha\beta}\big|_{\boldsymbol{P}} \Phi_\alpha\big|_{\boldsymbol{P}}) V_P + \sum_{\beta=1}^{N_{\mathrm{P}}} B_{\alpha\beta}^I\big|_{\boldsymbol{P}} (\Phi_\beta\big|_{\boldsymbol{P}} - \Phi_\alpha\big|_{\boldsymbol{P}})\, V_P \\
&+ {}^1S_\alpha\big|_{\boldsymbol{P}} \Phi_\alpha\big|_{\boldsymbol{P}} V_P + {}^0S_\alpha\big|_{\boldsymbol{P}} V_P + S_{\Phi_\alpha}^D - \left[\frac{\varepsilon_\alpha\big|_{\boldsymbol{P}}\rho_\alpha\big|_{\boldsymbol{P}} \Phi_\alpha\big|_{\boldsymbol{P}} V_P}{\Delta t}\right]_{\boldsymbol{t}}^{\boldsymbol{t+\Delta t}}.
\end{aligned} \tag{63}$$

In equations (62) and (63), ${}^1\boldsymbol{F}_\alpha^T$, ${}^1S_\alpha$ are the coefficient part and ${}^0\boldsymbol{F}_\alpha^T$, ${}^0S_\alpha$ the constant part of the linearized total source term (29). Furthermore, the advection terms have been treated using the hybrid differencing scheme, in which the central differencing is utilized when the cell Peclet number ($\mathrm{Pe}_\alpha = C_\alpha / D_{\Phi_\alpha}$) is below

two and the upwind differencing, ignoring diffusion, is performed when the Pe_α is greater than two. This scheme together with the deferred correction approach associated with the gradients on the cell faces (60) guarantees the diagonal dominance of the resulting coefficient matrix. For that reason hybrid differencing scheme serves as the base method for which other more accurate schemes can be built upon by the deferred correction approach [14, 36]. With hybrid differencing the matrix coefficients can be written as

$$a_{\Phi_\alpha}\big|_{\boldsymbol{h}} = \max\left(\frac{1}{2}\left| C_\alpha\big|_{\boldsymbol{h}}\right|, D^{ii}_{\Phi_\alpha}\big|_{\boldsymbol{h}}\right) - \frac{1}{2}\, C_\alpha\big|_{\boldsymbol{h}}\,, \quad i = \begin{cases} 1\ ;\ \boldsymbol{h} = \boldsymbol{u} \\ 2\ ;\ \boldsymbol{h} = \boldsymbol{n} \\ 3\ ;\ \boldsymbol{h} = \boldsymbol{e} \end{cases} \text{ and } \tag{64}$$

$$a_{\Phi_\alpha}\big|_{\boldsymbol{l}} = \max\left(\frac{1}{2}\left| C_\alpha\big|_{\boldsymbol{l}}\right|, D^{ii}_{\Phi_\alpha}\big|_{\boldsymbol{l}}\right) + \frac{1}{2}\, C_\alpha\big|_{\boldsymbol{l}}\,, \quad i = \begin{cases} 1\ ;\ \boldsymbol{l} = \boldsymbol{d} \\ 2\ ;\ \boldsymbol{l} = \boldsymbol{s} \\ 3\ ;\ \boldsymbol{l} = \boldsymbol{w} \end{cases} . \tag{65}$$

To save some space, the summations over the cells and the neighbouring cells are simplified as

$$\sum_{\boldsymbol{c}}^{\boldsymbol{u},\boldsymbol{d},\boldsymbol{n},\boldsymbol{s},\boldsymbol{e},\boldsymbol{w}} a_{\Phi_\alpha}\big|_{\boldsymbol{c}} \quad \rightarrow \quad \sum_{\boldsymbol{c}} a_{\Phi_\alpha}\big|_{\boldsymbol{c}} \qquad \text{and} \tag{66}$$

$$\sum_{\substack{\boldsymbol{c} \\ \boldsymbol{C}}}^{\substack{\boldsymbol{u},\boldsymbol{d},\boldsymbol{n},\boldsymbol{s},\boldsymbol{e},\boldsymbol{w} \\ \boldsymbol{U},\boldsymbol{D},\boldsymbol{N},\boldsymbol{S},\boldsymbol{E},\boldsymbol{W}}} a_{\Phi_\alpha}\big|_{\boldsymbol{c}}\, \Phi_\alpha\big|_{\boldsymbol{C}} \quad \rightarrow \quad \sum_{\boldsymbol{c},\boldsymbol{C}} a_{\Phi_\alpha}\big|_{\boldsymbol{c}}\, \Phi_\alpha\big|_{\boldsymbol{C}} \tag{67}$$

in the following treatment. The latter notation should be understood as a summation of a product term with two simultaneously changing indices.

3 INTER-PHASE COUPLING ALGORITHMS

The characteristic feature of multi-fluid model equations is that the phasic balance equations (4) and (5) are coupled to the phasic balance equations of other phases through the interfacial source terms of mass M_α^I and momentum $\boldsymbol{F}_\alpha^I$. For numerical treatment, these terms are customarily linearized as given by equations (24)–(26) and, correspondingly, appear in the discretized balance equations (61), (62) and (63) in that form. As the coupling of phases becomes tighter, the importance of these interfacial sources grows and, accordingly, the time scale associated with the interfacial transport decreases. Then, in sequential iterative solution methods, the treatment of the inter-phase coupling terms in the solution algorithm becomes critical for both the efficiency and stability of the solver.

Four different possibilities exist to handle the linearized inter-phase coupling terms, namely,

the explicit treatment

$$\sum_{\beta=1}^{N_P} B_{\alpha\beta}(\Phi_\beta - \Phi_\alpha) \rightarrow \sum_{\beta=1}^{N_P} B_{\alpha\beta}({}^{*}\Phi_\beta - {}^{*}\Phi_\alpha), \tag{68}$$

the partially implicit treatment

$$\sum_{\beta=1}^{N_P} B_{\alpha\beta}(\Phi_\beta - \Phi_\alpha) \rightarrow \sum_{\beta=1}^{N_P} B_{\alpha\beta}({}^{*}\Phi_\beta - \Phi_\alpha^{**}), \tag{69}$$

the semi-implicit treatment

$$\sum_{\beta=1}^{N_P} B_{\alpha\beta}(\Phi_\beta - \Phi_\alpha) \rightarrow \sum_{\beta=1}^{N_P} B_{\alpha\beta}(\Phi_\beta^{*} - \Phi_\alpha^{*}) \quad \text{and} \tag{70}$$

the fully implicit treatment

$$\sum_{\beta=1}^{N_P} B_{\alpha\beta}(\Phi_\beta - \Phi_\alpha) \rightarrow \sum_{\beta=1}^{N_P} B_{\alpha\beta}(\Phi_\beta^{**} - \Phi_\alpha^{**}). \tag{71}$$

In equations (68)–(71) the notations ${}^{*}\Phi_\alpha$, Φ_α^{*} and Φ_α^{**} denote the current estimate, an intermediate estimate during an inner iteration and the new estimate of a dependent variable of the phase α. However, it should be remembered that the fully implicit treatment can never be fully attained in sequential solvers, but the term is understood as meaning a treatment where all information of a phasic balance equation, except source terms, is taken at the level of a new estimate. A true fully implicit treatment would be approached by calculating new source terms at every inner iteration cycle. Inter-phase coupling algorithms intended to mimic the classification (68)–(71) have been studied by Karema & Lo [34], presented in the Appendix E of this publication.

Customarily, the sequential iterative control volume solvers are based on the SIMPLE (Semi-Implicit Method for Pressure-Linked Equations) type [44] solution algorithm utilizing a pressure correction step to conserve mass on cell basis at

every outer iteration. An extension of the SIMPLE method to multi-phase flows, called the IPSA (InterPhase Slip Algorithm) algorithm [51, 52, 53], was used by Karema & Lo [34] in their study of inter-phase coupling algorithms. As the IPSA algorithm neglects inter-phase coupling terms in its formulation, in order to achieve a more accurate pressure correction step, an improved IPSA based solution method, called the IPSA–C (InterPhase Slip Algorithm – Coupled) algorithm [10], was also studied. With this solution algorithm, a semi-implicit treatment of inter-phase coupling terms can be included into the solver.

The test cases, the gas-particle bed (A) and the liquid-particle bed (B), were selected to represent typical but simplified problems in the area of fluidized bed hydrodynamics and the constitutive models for inter-phase momentum transfer and dispersed phase stresses were set as given by Bouillard *et al.* [9]. There, to prevent the dispersed phase from compacting to unreasonably high volume fractions, the normal component of the dispersed phase stress is retained and modelled with a simple Coulombic approach (see Eq. 69 in Appendix E). When the porosity of the bed decreases below the state of minimum fluidization ε_{mf} this model produces a strong repulsive force to prevent bed compaction. In hydrodynamic terms this reflects a condition in which the collision time scale reduces below the aerodynamic time scale related to momentum transfer by phase interaction. Naturally, the repulsive force $\overline{T}_d^n$ is a strong function of fluid volume fraction ε_f. All tests documented in Appendix E were based on the customary representation of multi-fluid equations (27) and (28) and they were solved by IPSA or IPSA–C solution methods. Accordingly, the dispersed phase normal stress was implemented as a source term with a zero first order term.

In both flow configurations A and B the semi-implicit SINCE method resulted in about 5% and the fully implicit PEA method about 35% higher convergence rate of phasic momentum equations, respectively. The most important reason for the improvement can be found in the correctness of the few first approximates when a new time step is entered. The effect of including interphase coupling terms into the pressure correction scheme, the essence of the IPSA–C, is limited to the first few time steps, and there is practically no improvement of the overall convergence rate.

When the time step of simulation is kept below the characteristic time scale of interfacial transfer processes, the partially implicit treatment of coupling terms in combination with the IPSA solution algorithm provides the most efficient approach. This result is totally based on the smaller number of computational operations required by these simpler schemes. When a longer time step is required or there is a spot in the solution domain involved with very small characteristic time scales of interfacial coupling, the semi-implicit or fully implicit treatment of coupling terms becomes necessary. Then the PEA method provides the best efficiency for two-phase flows, providing a considerably better convergence with momentum equations but being only slightly more laborious computationally than the partially implicit treatment. In multi-phase flows the SINCE method provides the only option for the partially implicit treatment. Its convergence rate with momentum equations is only slightly better than with the partially implicit method though it is computationally more involved. The IPSA–C is arguably the preferred solution method for conditions where the interfacial coupling is tighter than in the flow configurations studied, e.g., in bubbly air-water flows.

Studying mass residuals reveals that in practice the improvement in computational speed attained with implicit-like algorithms in solving momentum equations

is almost completely lost in the pressure correction step of the solution. This would have been acceptable for the IPSA solution method as it neglects inter-phase coupling terms in correcting the pressures but the existence of this problem also with the IPSA–C method indicate that the convergence rate of solution is limited by other factors. In addition, this problem is much more pronounced in gas-particle bed than in liquid-particle bed and in both test cases it becames worse after some initial period of integration time starting from the initial field. All these aspects point towards a poorly performing pressure correction algorithm. After analysis it was realized that the limiting factor in predicting the total mass balance and especially the mass balance of the dispersed phase was threefold. First, in cells where the bed compaction was high, i.e., the porosity of the bed below the minimum fluidisation porosity ε_{mf}, the shared pressure, for which the mass balancing pressure correction step is based on, is not adequate to prevent the bed compacting to an unreasonably low porosity. Second, the characteristic feature of the IPSA solution method to keep the volume fractions constant during pressure correction step hinders the too high compaction to be realized and prevented. Third, as in the IPSA the volume fractions are solved after momentum equations and pressure correction equation, the large value of static pressure compared to dynamic pressure in fluidized beds is not effectively countered, i.e., as long as cell-based imbalances are governed by the velocity field, the enhanced convergence rate of momentum equations enters the mass balances. Apparently, the pressure correction step of the multi-fluid solution method should be further improved by incorporating also the pressure-like contributions of the dispersed phases, in addition to the shared pressure, and by including a mechanism to take into account the strong dependency of the solid pressure on volume fractions. Further, in the momentum equations the pressure-like contributions should be treated equivalently with the shared pressure gradient. These topics are covered in detail in chapter 4. In Figure 3 the problematic areas of the gas-particle bed are seen to be located beneath and above the obstacle at the centre line and below the bubble. Evidently, the flow field in the vicinity of the obstacle has a dramatic effect on the development of the bubble and its accurate prediction is necessary. In liquid-particle bed the problem of unphysically high compaction does not exist (Figure 4) and the main problem is in the third item, namely considering volume fractions as constant during the pressure correction step.

Another type of difficulty present in the gas-particle bed but non-existent in the liquid-particle bed, still related to mass balancing, is originating from the large discrepancy of the source terms across sharp interfaces between the fluid and particles in circumstances when the particle density is several orders of magnitude higher than the fluid density. Then, the weighted linear interpolation applied to source terms while carrying out the Rhie-Chow momentum interpolation is not accurate enough resulting in mass imbalance in adjacent cells of the interface. This is realised as the small wrinkles around the interface with finer mesh in Figure 3, i.e., sharper interface, and will ultimately lead to divergence of a control volume based solver. For the liquid-particle bed the customary Rhie-Chow interpolation is still adequate. A geometric interpolation procedure [43] for source terms in this instance could have been used but as it does not necessarily conserve mass in non-uniform curvilinear meshes a so-called *improved* Rhie-Chow momentum interpolation [14] was utilized. This method is briefly described in Appendix D. If the customary representation of multi-fluid equations (27) and (28), where the apparent

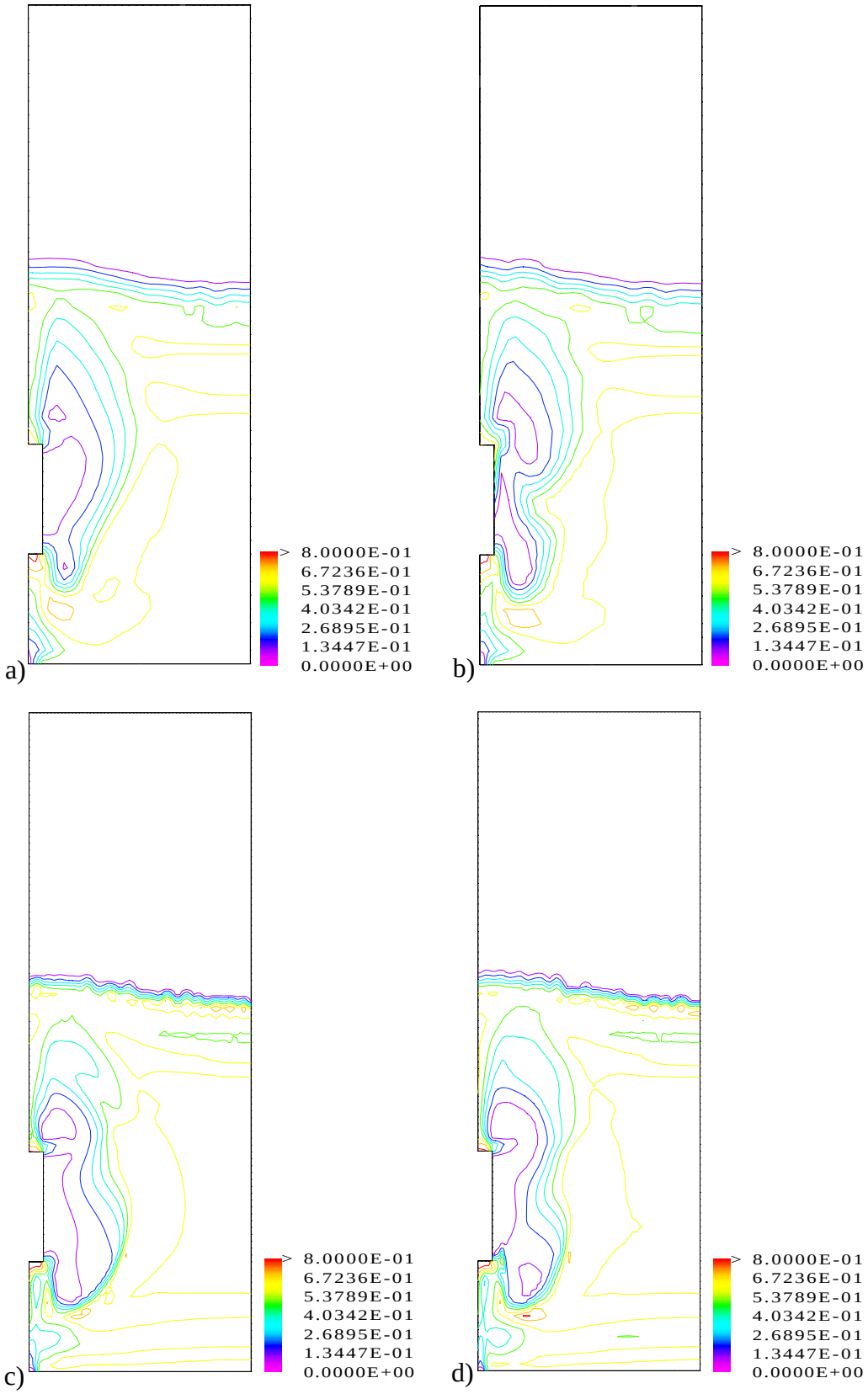

Figure 3. Volume fraction field of particles ε_d *in test case A with different representations of geometry: (a) multi-block rectangular* 31×48 *mesh, (b) multi-block* 31×48 *BFC-mesh, (c) multi-block* 62×96 *rectangular mesh and (d) multi-block* 62×96 *BFC-mesh.*

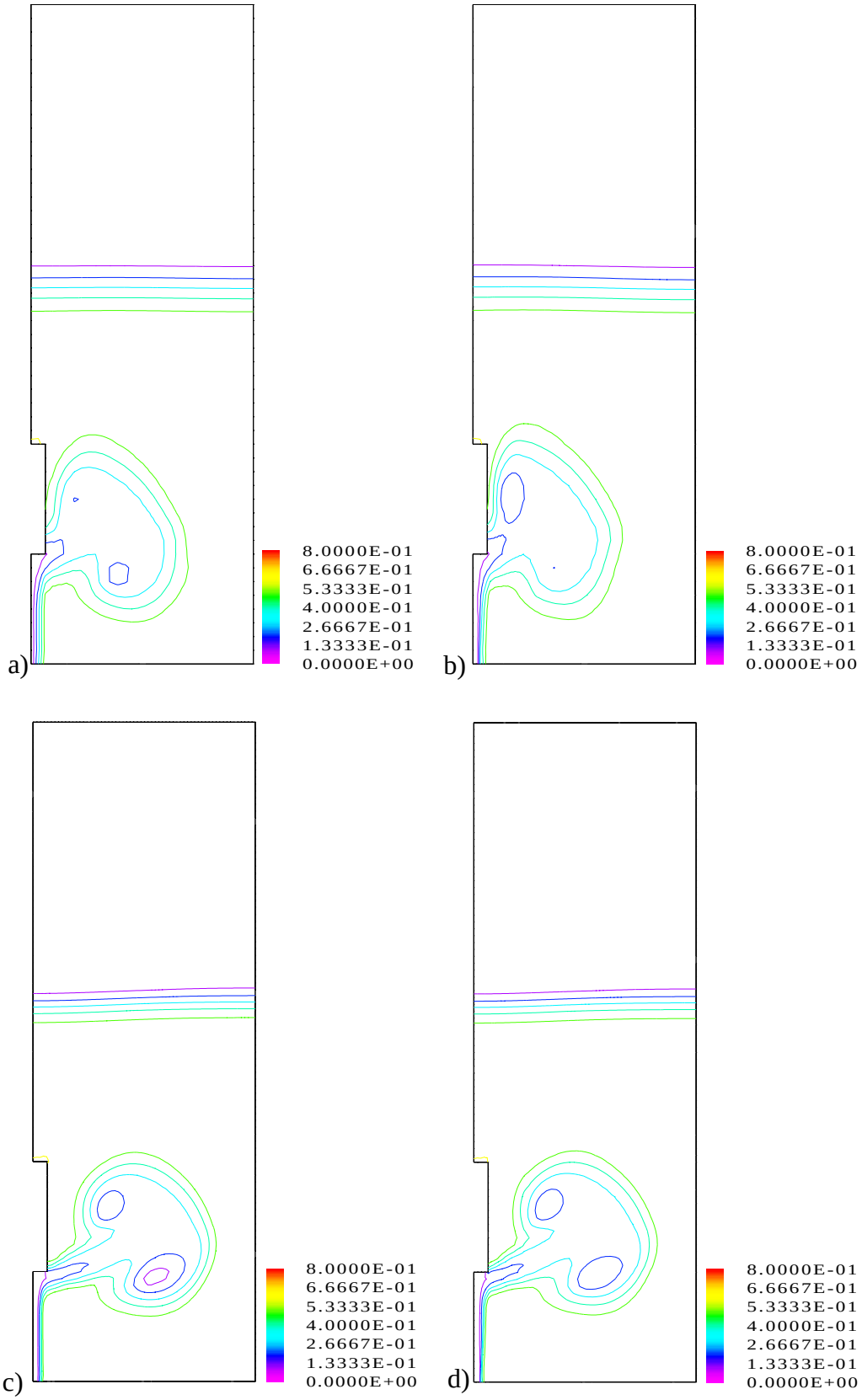

Figure 4. Volume fraction field of particles ε_d *in test case B with different representations of geometry: (a) multi-block rectangular* 31×48 *mesh, (b) multi-block* 31×48 *BFC-mesh, (c) multi-block* 62×96 *rectangular mesh and (d) multi-block* 62×96 *BFC-mesh.*

pressure term of the dispersed phase is modelled as a source term, is applied, this method should also enhance stability of the solver in areas of high bed compaction. In order to reach an equal order of approximation for the apparent pressure terms as for the shared pressure, the *extended* Rhie-Chow momentum interpolation derived in section 5 can be used instead of or in combination with the *improved* Rhie-Chow interpolation.

4 MULTI-PRESSURE ALGORITHMS

In section 2.2 it was shown that the momentum balances of both the IMP and DIF approaches simplify to the same form under certain restrictions. These restrictions necessitate that the dispersed phase entities are small compared to the length scales of the mean fluid flow field, that the interfacial mean pressure can be approximated with the phasic mean pressure $P_\alpha^I = \bar{P}_\alpha$ and that the fluid phase turbulent stresses exceed considerably the viscous stresses. The resulting approximate momentum balance was shown to be conveniently represented for numerical treatment as the generalized form (32). The associated formally discretized momentum balance was then given by equation (62), as discussed in sections 2.3 and 2.4, respectively. Since in the equation (62), there are two pressure terms, one related with the mean fluid pressure P_f and the other with the pressure like contributions $\underline{P}_\alpha^e$ originating from the other constitutive equations, in the frame of sequential control volume methods (CVM) some extended pressure correction scheme is required in order to solve this kind of equation set. These extended schemes are next studied in the context of two different sequential solution strategies, called the phase-sequential and the equation-sequential solution methods, respectively.

The main features of the treatment in this chapter follow closely the IPSA method [51, 52, 53] and its implementation to the collocated multi-block control volume solver, described by Karema & Lo [34]. The two distinctive features of this method are related to the pressure correction step. The first neglects the contribution of the volumetric changes to the pressure, i.e., the phasic volume fractions are held constant during this step. The second feature relates to the use of the shared pressure concept in performing the pressure correction. While only one pressure is defined, it is adjusted in a way which fulfils the total mass balance on element basis at every outer iteration. Though allowing simple pressure correction algorithm and control over the fulfilment of global mass conservation, the IPSA type algorithms become inefficient when the pressure like contributions $\underline{P}_\alpha^e$ grow in importance or when they become strongly dependent on the phasic volume fractions.

In the subsequent treatment, these two distinctive features are partly abandoned. For the fluid phase and for the incompressible treatment of the dispersed phases, the first feature is still retained, but in the compressible treatment of the dispersed phases, the contributions of the volume fractions on the pressure are not neglected. Because the balance equations (62) involve multiple pressures, the second feature can not be applied, and the pressure corrections are then based on the phasic mass balances. In this context, it is important to notice that the naming convention for the treatments of the dispersed phases originates from the analogous treatment of single phase flows. Thus, the compressible treatment here implies that the material densities are independent of pressure but the volume fractions are not.

There are two solution methods referred in this chapter, i.e., the *phase-sequential* and the *equation-sequential* solution methods, which represent two alternative approaches to construct a sequential CVM solver. Two versions of the extended pressure correction scheme are explained, Fluid Pressure in Source term (FPS) and Equivalent Approximation of Pressures (EAP). Both of these pressure correction schemes can be applied in either of the solution methods. However, as the FPS is naturally suited to the phase-sequential solution method and the EAP to the equa-

tion-sequential solution method, they are discussed in connection with these solution methods.

4.1 PHASE-SEQUENTIAL SOLUTION METHOD AND FPS

The key feature of the phase-sequential solution method is found from the order of balance equations solved. As seen from Figure 5, the solution proceeds dominantly from phase to phase. This approach represents a natural extension of general solvers originally designed for single phase flows. The major disadvantage of this simple structure lies in the difficulty to implement efficient inter-phase coupling algorithms, e.g., such as the PEA, the SINCE and the IPSA–C [34].

4.1.1 Treatment of fluid phase

The treatment starts from the discretized phasic momentum balance (62) written for the fluid phase

$$a_{U_f^k}\Big|_{\boldsymbol{P}} U_f^k\Big|_{\boldsymbol{P}} = \sum_{\boldsymbol{c},\,\boldsymbol{C}} a_{U_f^k}\Big|_{\boldsymbol{c}} U_f^k\Big|_{\boldsymbol{C}} - \varepsilon_f\Big|_{\boldsymbol{P}} A_k^i\Big|_{\boldsymbol{P}} \frac{\partial P_f}{\partial \xi^i}\Big|_{\boldsymbol{P}} + s_{U_f^k}^R \text{, where} \tag{72}$$

$$a_{U_f^k}\Big|_{\boldsymbol{P}} = \sum_{\boldsymbol{c}} a_{U_f^k}\Big|_{\boldsymbol{c}} + \sum_{\beta\,=\,1}^{N_\mathrm{P}} \dot{m}_{f\beta}\Big|_{\boldsymbol{P}} V_P + \sum_{\beta\,=\,1}^{N_\mathrm{P}} B_{f\beta}\Big|_{\boldsymbol{P}} V_P - {}^1\boldsymbol{F}_f^T\Big|_{\boldsymbol{P}} V_P + \frac{\varepsilon_f\Big|_{\boldsymbol{P}} \rho_f\Big|_{\boldsymbol{P}} V_P}{\Delta t} \quad \text{and} \tag{73}$$

$$s_{U_f^k}^R = -A_k^i\Big|_{\boldsymbol{P}} \frac{\partial}{\partial \xi^i}(\varepsilon_f P_f^\mathrm{e})\Big|_{\boldsymbol{P}} + \left[\varepsilon_f \eta_f^\mathrm{eff} \frac{A_m^1 A_k^j}{|\boldsymbol{J}|} \frac{\partial U_f^m}{\partial \xi^j}\right]_{\boldsymbol{d}} + \left[\varepsilon_f \eta_f^\mathrm{eff} \frac{A_m^2 A_k^j}{|\boldsymbol{J}|} \frac{\partial U_f^m}{\partial \xi^j}\right]_{\boldsymbol{s}} + \left[\varepsilon_f \eta_f^\mathrm{eff} \frac{A_m^3 A_k^j}{|\boldsymbol{J}|} \frac{\partial U_f^m}{\partial \xi^j}\right]_{\boldsymbol{e}} + \varepsilon_f\Big|_{\boldsymbol{P}} \rho_f\Big|_{\boldsymbol{P}} \boldsymbol{g}\, V_P + \sum_{\beta\,=\,1}^{N_\mathrm{P}} \dot{m}_{\beta f}\Big|_{\boldsymbol{P}} U_\beta^k\Big|_{\boldsymbol{P}} V_P + \sum_{\beta\,=\,1}^{N_\mathrm{P}} B_{f\beta}\Big|_{\boldsymbol{P}} U_\beta^k\Big|_{\boldsymbol{P}} V_P + {}^0\boldsymbol{F}_f^T\Big|_{\boldsymbol{P}} V_P + S_{U_f^k}^D + \frac{\left(\varepsilon_f\Big|_{\boldsymbol{P}} \rho_f\Big|_{\boldsymbol{P}} U_f^k\Big|_{\boldsymbol{P}} V_P\right)}{\Delta t}\Bigg|_{\boldsymbol{t}} \tag{74}$$

In the spirit of the pressure correction algorithm, the term associated with the modified pressure of fluid P_f^e has been classified as part of the source term $s_{U_f^k}^R$. This is justified by considering the importance of this term to be small compared to the actual pressure gradient term in normal conditions. With this assumption, the treatment resembles the customary IPSA method.

As shown in Appendix C, the connection between the fluid pressure corrections,

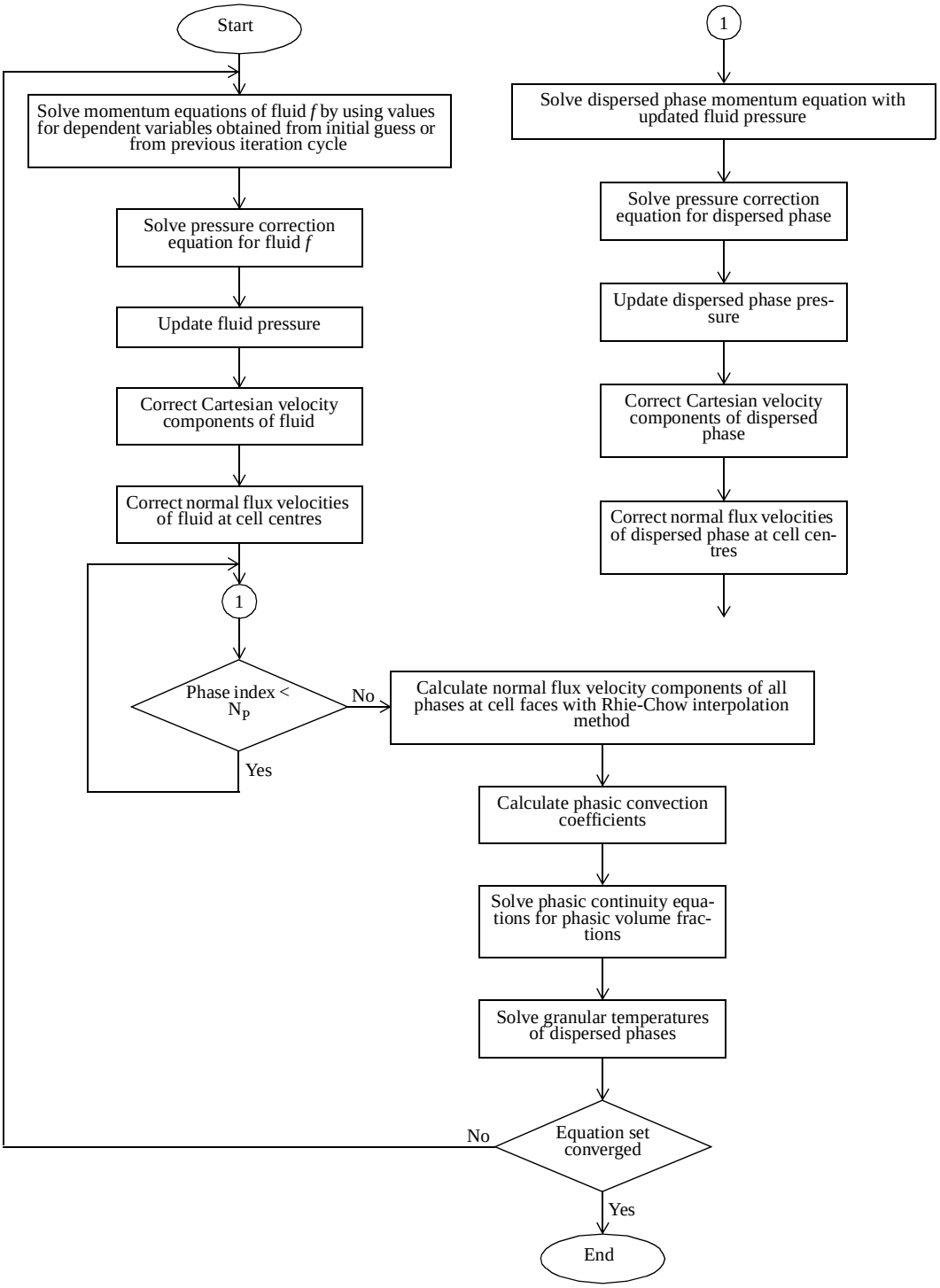

Figure 5. Computational flow chart of phase-sequential solution method.

which obey the mass balance of fluid (61), and the phasic Cartesian velocity components can be obtained on the basis of equation (72). The result can be written in a compact form as

$$\delta U_f^k\Big|_{\boldsymbol{P}} = -H_{fk}^i\Big|_{\boldsymbol{P}} \frac{\partial \delta P_f}{\partial \xi^i}\Bigg|_{\boldsymbol{P}}, \text{ where} \tag{75}$$

$$H_{fk}^i\Big|_{\boldsymbol{P}} = \frac{\varepsilon_f\big|_{\boldsymbol{P}} A_k^i\big|_{\boldsymbol{P}}}{V_P}\, h_f^k\Big|_{\boldsymbol{P}} \quad \text{and} \tag{76}$$

$$h_f^k\Big|_{\boldsymbol{P}} = \frac{V_P}{a_{U_f^k}\big|_{\boldsymbol{P}} - W_{pc}\sum\limits_{\boldsymbol{c},\,\boldsymbol{C}} a_{U_f^k}\big|_{\boldsymbol{c}}}. \tag{77}$$

The corresponding corrections to the phasic normal flux velocity components are then found directly from equation (75) by utilizing the associated definition

$$\delta \hat{U}_f^{\,i} = A_k^i \delta U_f^k. \tag{78}$$

This results in the following relation between the fluid pressure corrections and the phasic normal flux velocity components of fluid

$$\delta \hat{U}_f^{\,i}\Big|_{\boldsymbol{P}} = -\hat{H}_f^{\,ij}\Big|_{\boldsymbol{P}} \frac{\partial \delta P_f}{\partial \xi^j}\Bigg|_{\boldsymbol{P}}, \text{ where} \tag{79}$$

$$\hat{H}_f^{\,ij}\Big|_{\boldsymbol{P}} = A_k^i\Big|_{\boldsymbol{P}} H_{fk}^j\Big|_{\boldsymbol{P}} = \sum_{k\,=\,1}^{3} \frac{\varepsilon_f\big|_{\boldsymbol{P}} A_k^i\big|_{\boldsymbol{P}} A_k^j\big|_{\boldsymbol{P}}}{V_P}\, h_f^k\Big|_{\boldsymbol{P}}. \tag{80}$$

The corrections to the phasic normal flux velocity components produce also new estimates for the phasic convection coefficients of the fluid (50). These can be expressed as

$$C_f^i\Big|^* = C_f^i + \delta C_f^i = \varepsilon_f \rho_f \hat{U}_f^{\,i} + \varepsilon_f \rho_f \delta \hat{U}_f^{\,i}. \tag{81}$$

By inserting equation (81) to the mass balance of the fluid (61) the following balance equation for the corrections is obtained

$$\delta C_f^1\Big|_{\boldsymbol{u}} - \delta C_f^1\Big|_{\boldsymbol{d}} + \delta C_f^2\Big|_{\boldsymbol{n}} - \delta C_f^2\Big|_{\boldsymbol{s}} + \delta C_f^3\Big|_{\boldsymbol{e}} - \delta C_f^3\Big|_{\boldsymbol{w}} + R_{m_f} = 0, \text{ where} \tag{82}$$

$$R_{m_f} = \frac{[\varepsilon_f\big|_{\boldsymbol{P}} \rho_f\big|_{\boldsymbol{P}} V_P]_{\boldsymbol{t}}^{\boldsymbol{t}+\boldsymbol{\Delta t}}}{\Delta t} + C_f^1\Big|_{\boldsymbol{u}} - C_f^1\Big|_{\boldsymbol{d}} + C_f^2\Big|_{\boldsymbol{n}} - C_f^2\Big|_{\boldsymbol{s}} + C_f^3\Big|_{\boldsymbol{e}} - C_f^3\Big|_{\boldsymbol{w}} - M_f^I\Big|_{\boldsymbol{P}} V_P. \tag{83}$$

The substitution of the relation (81) to the mass balance (82) results in the balance equation for the corrections of the phasic normal flux velocity components of fluid

$$\begin{aligned}\varepsilon_f\big|_{\boldsymbol{u}}\rho_f\big|_{\boldsymbol{u}}\delta\hat{U}_f^{\,1}\big|_{\boldsymbol{u}} - \varepsilon_f\big|_{\boldsymbol{d}}\rho_f\big|_{\boldsymbol{d}}\delta\hat{U}_f^{\,1}\big|_{\boldsymbol{d}} + \varepsilon_f\big|_{\boldsymbol{n}}\rho_f\big|_{\boldsymbol{n}}\delta\hat{U}_f^{\,2}\big|_{\boldsymbol{n}} - \varepsilon_f\big|_{\boldsymbol{s}}\rho_f\big|_{\boldsymbol{s}}\delta\hat{U}_f^{\,2}\big|_{\boldsymbol{s}} \\ + \varepsilon_f\big|_{\boldsymbol{e}}\rho_f\big|_{\boldsymbol{e}}\delta\hat{U}_f^{\,3}\big|_{\boldsymbol{e}} - \varepsilon_f\big|_{\boldsymbol{w}}\rho_f\big|_{\boldsymbol{w}}\delta\hat{U}_f^{\,3}\big|_{\boldsymbol{w}} + R_{m_f} = 0\ .\end{aligned} \tag{84}$$

In the equation (84) the corrections of the phasic normal flux velocity components are introduced on the cell faces necessitating the interpolation of these values from the cell centres where they are originally determined, as seen from equation (79). The adjugate Jacobian matrix A_k^i is naturally defined on the cell face but the coefficient h_f^k must be interpolated. If the pressure correction gradients on the cell faces are approximated with central differences on the computational space, equation (79) can be substituted to the fluid mass balance (84) to give corrections of the fluid pressure fulfilling continuity

$$a_{P_f}\big|_{\boldsymbol{P}}\delta P_f\big|_{\boldsymbol{P}} = \sum_{\boldsymbol{c},\,\boldsymbol{C}} a_{P_f}\big|_{\boldsymbol{c}}\delta P_f\big|_{\boldsymbol{C}} + S_{P_f}^{D} - R_{m_f}, \text{ where} \tag{85}$$

$$a_{P_f}\big|_{\boldsymbol{P}} = \sum_{\boldsymbol{c},\,\boldsymbol{C}} a_{P_f}\big|_{\boldsymbol{c}} \quad \text{and} \quad a_{P_f}\big|_{\boldsymbol{c}} = \varepsilon_f\big|_{\boldsymbol{c}}\rho_f\big|_{\boldsymbol{c}}\hat{H}_f^{\,ii}\big|_{\boldsymbol{c}}\,. \tag{86}$$

The term $S_{P_f}^{D}$ in equation (85) denotes the cross-derivatives of the fluid pressure corrections treated according to the deferred correction approach. With the formal discretization notion it can be written as

$$\begin{aligned}S_{P_f}^{D} = \left[E_{P_f}^{12}\frac{\partial\,{}^{*}\delta P_f}{\partial\zeta} + E_{P_f}^{13}\frac{\partial\,{}^{*}\delta P_f}{\partial\zeta}\right]_{\boldsymbol{d}}^{\boldsymbol{u}} + \left[E_{P_f}^{21}\frac{\partial\,{}^{*}\delta P_f}{\partial\xi} + E_{P_f}^{23}\frac{\partial\,{}^{*}\delta P_f}{\partial\zeta}\right]_{\boldsymbol{s}}^{\boldsymbol{n}} \\ + \left[E_{P_f}^{31}\frac{\partial\,{}^{*}\delta P_f}{\partial\xi} + E_{P_f}^{32}\frac{\partial\,{}^{*}\delta P_f}{\partial\zeta}\right]_{\boldsymbol{w}}^{\boldsymbol{e}}\ , \text{ where}\end{aligned} \tag{87}$$

$$E_{P_f}^{ij} = \varepsilon_f\big|_{\boldsymbol{c}}\rho_f\big|_{\boldsymbol{c}}\hat{H}_f^{\,ij}\big|_{\boldsymbol{c}}\,. \tag{88}$$

In equation (88) ${}^{*}\delta P_f$ denotes the value of pressure correction from the previous iteration.

4.1.2 Treatment of dispersed phases in FPS

In the phase-sequential solution scheme, the pressure correction of the fluid, and consequently the updated fluid pressure, is solved before the momentum equa-

tions of the dispersed phases are entered. By following the FPS treatment, the fluid pressure gradient term in the momentum equations of the dispersed phases is considered as a known source term. Thus, the momentum equations can be expressed as

$$a_{U_\alpha^k}\Big|_{\boldsymbol{P}} U_\alpha^k\Big|_{\boldsymbol{P}} = \sum_{\boldsymbol{c},\,\boldsymbol{C}} a_{U_\alpha^k}\Big|_{\boldsymbol{c}} U_\alpha^k\Big|_{\boldsymbol{C}} - A_k^i\Big|_{\boldsymbol{P}} \frac{\partial P_\alpha^{\mathrm{a}}}{\partial \xi^i}\Big|_{\boldsymbol{P}} + s_{U_\alpha^k}^R \text{, where} \tag{89}$$

$$a_{U_\alpha^k}\Big|_{\boldsymbol{P}} = \sum_{\boldsymbol{c}} a_{U_\alpha^k}\Big|_{\boldsymbol{c}} + \sum_{\beta=1}^{N_{\mathrm{P}}} \dot{m}_{\alpha\beta}\Big|_{\boldsymbol{P}} V_P + \sum_{\beta=1}^{N_{\mathrm{P}}} B_{\alpha\beta}\Big|_{\boldsymbol{P}} V_P - {}^1\boldsymbol{F}_\alpha^T\Big|_{\boldsymbol{P}} V_P + \frac{\varepsilon_\alpha\Big|_{\boldsymbol{P}} \rho_\alpha\Big|_{\boldsymbol{P}} V_P}{\Delta t} \text{ and} \tag{90}$$

$$\begin{aligned} s_{U_\alpha^k}^R = {} & - \varepsilon_\alpha\Big|_{\boldsymbol{P}} A_k^i\Big|_{\boldsymbol{P}} \frac{\partial P_f}{\partial \xi^i}\Big|_{\boldsymbol{P}}^{*} + \left[\varepsilon_\alpha \eta_\alpha^{\mathrm{eff}} \frac{A_m^1 A_k^j}{|\boldsymbol{J}|} \frac{\partial U_\alpha^m}{\partial \xi^j}\right]_{\boldsymbol{d}}^{\boldsymbol{u}} + \left[\varepsilon_\alpha \eta_\alpha^{\mathrm{eff}} \frac{A_m^2 A_k^j}{|\boldsymbol{J}|} \frac{\partial U_\alpha^m}{\partial \xi^j}\right]_{\boldsymbol{s}}^{\boldsymbol{n}} \\ & + \left[\varepsilon_\alpha \eta_\alpha^{\mathrm{eff}} \frac{A_m^3 A_k^j}{|\boldsymbol{J}|} \frac{\partial U_\alpha^m}{\partial \xi^j}\right]_{\boldsymbol{w}}^{\boldsymbol{e}} + \varepsilon_\alpha\Big|_{\boldsymbol{P}} \rho_\alpha\Big|_{\boldsymbol{P}} \boldsymbol{g}\, V_P + \sum_{\beta=1}^{N_{\mathrm{P}}} \dot{m}_{\beta\alpha}\Big|_{\boldsymbol{P}} U_\beta^k\Big|_{\boldsymbol{P}} V_P \\ & + \sum_{\beta=1}^{N_{\mathrm{P}}} B_{\alpha\beta}\Big|_{\boldsymbol{P}} U_\beta^k\Big|_{\boldsymbol{P}} V_P + {}^0\boldsymbol{F}_\alpha^T\Big|_{\boldsymbol{P}} V_P + S_{U_\alpha^k}^D + \frac{\left(\varepsilon_\alpha\Big|_{\boldsymbol{P}} \rho_\alpha\Big|_{\boldsymbol{P}} U_\alpha^k\Big|_{\boldsymbol{P}} V_P\right)}{\Delta t}\Bigg|_{\boldsymbol{t}} . \end{aligned} \tag{91}$$

In equation (91) the fluid pressure gradient term locater bar has been denoted with an asterisk superscript in order to emphasize that the fluid pressure is an updated value fulfilling the mass balance of the fluid phase (61). In addition, the modified pressure of the dispersed phase, defined in the equation (31), has been replaced with an apparent pressure

$$P_\alpha^{\mathrm{a}} = \varepsilon_\alpha P_\alpha^{\mathrm{e}} . \tag{92}$$

By proceeding as with the fluid phase in section 4.1.1, the details of which are given in Appendix C, the corrections to the phasic Cartesian velocity components of the dispersed phase can be expressed in the form

$$\delta U_\alpha^k\Big|_{\boldsymbol{P}} = -H_{\alpha k}^i\Big|_{\boldsymbol{P}} \frac{\partial\, \delta P_\alpha^{\mathrm{a}}}{\partial \xi^i}\Big|_{\boldsymbol{P}} \text{, where} \tag{93}$$

$$H_{\alpha k}^i\Big|_{\boldsymbol{P}} = \frac{A_k^i\Big|_{\boldsymbol{P}}}{V_P} h_\alpha^k\Big|_{\boldsymbol{P}} \quad \text{and} \tag{94}$$

$$h_\alpha^k\Big|_{\boldsymbol{P}} = \frac{V_P}{a_{U_\alpha^k}\Big|_{\boldsymbol{P}} - W_{pc}\sum_{\boldsymbol{c},\boldsymbol{C}} a_{U_\alpha^k}\Big|_{\boldsymbol{c}}}. \tag{95}$$

Again, by utilizing the associated definition (78), the corresponding corrections to the phasic normal flux velocity components can be written as

$$\delta\hat{U}_\alpha^i\Big|_{\boldsymbol{P}} = -\hat{H}_\alpha^{ij}\Big|_{\boldsymbol{P}} \frac{\partial\,\delta P_\alpha^{\mathrm{a}}}{\partial\xi^j}\Bigg|_{\boldsymbol{P}}, \text{ where} \tag{96}$$

$$\hat{H}_\alpha^{ij}\Big|_{\boldsymbol{P}} = A_k^i\Big|_{\boldsymbol{P}} H_{\alpha k}^j\Big|_{\boldsymbol{P}} = \sum_{k=1}^{3} \frac{A_k^i\Big|_{\boldsymbol{P}} A_k^j\Big|_{\boldsymbol{P}}}{V_P}\, h_\alpha^k\Big|_{\boldsymbol{P}}. \tag{97}$$

4.1.2.1 Incompressible model for dispersed phases

As the correction equations of the phasic Cartesian and normal flux velocities, (93) and (96), closely resemble to the corresponding equations of the fluid phase, (75) and (79), a fully analogous treatment for the dispersed phases apply. With the help of the dispersed phase mass balance and the correction equations (93) and (96), the pressure correction equation for the dispersed phases can be written as

$$a_{P_\alpha}\Big|_{\boldsymbol{P}} \delta P_\alpha^{\mathrm{a}}\Big|_{\boldsymbol{P}} = \sum_{\boldsymbol{c},\boldsymbol{C}} a_{P_\alpha}\Big|_{\boldsymbol{c}} \delta P_\alpha^{\mathrm{a}}\Big|_{\boldsymbol{C}} + S_{P_\alpha}^D - R_{m_\alpha}, \text{ where} \tag{98}$$

$$a_{P_\alpha}\Big|_{\boldsymbol{P}} = \sum_{\boldsymbol{c},\boldsymbol{C}} a_{P_\alpha}\Big|_{\boldsymbol{c}} \quad \text{and} \quad a_{P_\alpha}\Big|_{\boldsymbol{c}} = \varepsilon_\alpha\Big|_{\boldsymbol{c}} \rho_\alpha\Big|_{\boldsymbol{c}} \hat{H}_\alpha^{ii}\Big|_{\boldsymbol{c}}. \tag{99}$$

In equation (98) R_{m_α} denotes the mass residual of the phase α

$$\begin{aligned} R_{m_\alpha} = {} & \frac{[\varepsilon_\alpha\Big|_{\boldsymbol{P}} \rho_\alpha\Big|_{\boldsymbol{P}} V_P\,]_{\boldsymbol{t}}^{\boldsymbol{t}+\Delta\boldsymbol{t}}}{\Delta t} \\ & + C_\alpha^1\Big|_{\boldsymbol{u}} - C_\alpha^1\Big|_{\boldsymbol{d}} + C_\alpha^2\Big|_{\boldsymbol{n}} - C_\alpha^2\Big|_{\boldsymbol{s}} + C_\alpha^3\Big|_{\boldsymbol{e}} - C_\alpha^3\Big|_{\boldsymbol{w}} - M_\alpha^I\Big|_{\boldsymbol{P}} V_P \end{aligned} \tag{100}$$

and the term $S_{P_\alpha}^D$ is used to denote the cross-derivatives of the phasic apparent pressure corrections, treated as for the fluid phase, with the deferred correction approach

$$S_{P_\alpha}^{D} = \left[E_{P_\alpha}^{12} \frac{\partial\, {}^{*}\delta P_\alpha^{a}}{\partial \varsigma} + E_{P_\alpha}^{13} \frac{\partial\, {}^{*}\delta P_\alpha^{a}}{\partial \zeta} \right]_{\boldsymbol{d}}^{\boldsymbol{u}} + \left[E_{P_\alpha}^{21} \frac{\partial\, {}^{*}\delta P_\alpha^{a}}{\partial \xi} + E_{P_\alpha}^{23} \frac{\partial\, {}^{*}\delta P_\alpha^{a}}{\partial \zeta} \right]_{\boldsymbol{s}}^{\boldsymbol{n}} + \left[E_{P_\alpha}^{31} \frac{\partial\, {}^{*}\delta P_\alpha^{a}}{\partial \xi} + E_{P_\alpha}^{32} \frac{\partial\, {}^{*}\delta P_\alpha^{a}}{\partial \varsigma} \right]_{\boldsymbol{w}}^{\boldsymbol{e}} \quad \text{, where} \tag{101}$$

$$E_{P_\alpha}^{ij} = \varepsilon_\alpha \big|_{\boldsymbol{c}} \rho_\alpha \big|_{\boldsymbol{c}} \hat{H}_\alpha^{ij} \big|_{\boldsymbol{c}} . \tag{102}$$

4.1.2.2 Compressible model for dispersed phases

As stated at the beginning of chapter 4, the naming convention for the treatments of the dispersed phases originates from the analogous treatment found in single phase flows. Thus, the compressible treatment here implies that the material densities are independent on pressure but the volume fractions are not. This approach is desirable in conditions where the modified pressure depends strongly on the phasic volume fractions, in which case the IPSA-like treatment, called as the incompressible model here, would lead to poor performance of the solution algorithm.

Consequently, by treating the dispersed phase as a pseudo-compressible fluid, in which the $\varepsilon_\alpha(P_\alpha^{a})$ dependency is handled like the $\rho_f(P_f)$ dependency in compressible single phase flows, the corrections to the phasic normal flux velocity components (96), satisfying the phasic continuity equation, produce the following changes to the phasic convection coefficients (50)

$$\begin{aligned} C_\alpha^{i} \Big|^{*} &= (\varepsilon_\alpha + \delta\varepsilon_\alpha)\rho_\alpha(\hat{U}_\alpha^{i} + \delta\hat{U}_\alpha^{i}) \\ &= \varepsilon_\alpha\rho_\alpha\hat{U}_\alpha^{i} + \varepsilon_\alpha\rho_\alpha\delta\hat{U}_\alpha^{i} + \delta\varepsilon_\alpha\rho_\alpha\hat{U}_\alpha^{i} + \delta\varepsilon_\alpha\rho_\alpha\delta\hat{U}_\alpha^{i} \\ &\approx \varepsilon_\alpha\rho_\alpha\hat{U}_\alpha^{i} + \varepsilon_\alpha\rho_\alpha\delta\hat{U}_\alpha^{i} + \delta\varepsilon_\alpha\rho_\alpha\hat{U}_\alpha^{i} \quad . \end{aligned} \tag{103}$$

In equation (103), the second order term including changes to both variables has been neglected.

Substitution of equation (103) to the mass balance of the dispersed phase (61) results in the following balance equation

$$
\begin{aligned}
&(\varepsilon_\alpha \rho_\alpha \delta\hat{U}_\alpha^1 + \delta\varepsilon_\alpha \rho_\alpha \hat{U}_\alpha^1)\Big|_{\boldsymbol{u}} - (\varepsilon_\alpha \rho_\alpha \delta\hat{U}_\alpha^1 + \delta\varepsilon_\alpha \rho_\alpha \hat{U}_\alpha^1)\Big|_{\boldsymbol{d}} \\
&+ (\varepsilon_\alpha \rho_\alpha \delta\hat{U}_\alpha^2 + \delta\varepsilon_\alpha \rho_\alpha \hat{U}_\alpha^2)\Big|_{\boldsymbol{n}} - (\varepsilon_\alpha \rho_\alpha \delta\hat{U}_\alpha^2 + \delta\varepsilon_\alpha \rho_\alpha \hat{U}_\alpha^2)\Big|_{\boldsymbol{s}} \\
&+ (\varepsilon_\alpha \rho_\alpha \delta\hat{U}_\alpha^3 + \delta\varepsilon_\alpha \rho_\alpha \hat{U}_\alpha^3)\Big|_{\boldsymbol{e}} - (\varepsilon_\alpha \rho_\alpha \delta\hat{U}_\alpha^3 + \delta\varepsilon_\alpha \rho_\alpha \hat{U}_\alpha^3)\Big|_{\boldsymbol{w}} \\
&+ R_{m_\alpha} + \frac{(\delta\varepsilon_\alpha\big|_{\boldsymbol{P}} \rho_\alpha\big|_{\boldsymbol{P}} V_P)}{\Delta t}\Bigg|_{\boldsymbol{t+\Delta t}} = 0 \quad ,
\end{aligned}
\tag{104}
$$

where R_{m_α} is the phasic mass residual defined in equation (100). When writing equation (104), the time dependent term has been divided into two parts consisting of the time dependent pseudo-compressible term and the conventional time dependent term as

$$
\begin{aligned}
&\frac{[(\varepsilon_\alpha + \delta\varepsilon_\alpha)\big|_{\boldsymbol{P}} \rho_\alpha\big|_{\boldsymbol{P}} V_P]_{\boldsymbol{t}}^{\boldsymbol{t+\Delta t}}}{\Delta t} \\
&\qquad = \frac{(\delta\varepsilon_\alpha\big|_{\boldsymbol{P}} \rho_\alpha\big|_{\boldsymbol{P}} V_P)}{\Delta t}\Bigg|_{\boldsymbol{t+\Delta t}} + \frac{[\varepsilon_\alpha\big|_{\boldsymbol{P}} \rho_\alpha\big|_{\boldsymbol{P}} V_P]_{\boldsymbol{t}}^{\boldsymbol{t+\Delta t}}}{\Delta t} \quad .
\end{aligned}
\tag{105}
$$

By denoting the $\varepsilon_\alpha(P_\alpha^{\mathrm{a}})$ dependency as c_α, the correction of the phasic volume fraction $\delta\varepsilon_\alpha$ can be expressed as

$$
\delta\varepsilon_\alpha = \frac{\partial \varepsilon_\alpha}{\partial P_\alpha^{\mathrm{a}}} \delta P_\alpha^{\mathrm{a}} = c_\alpha \delta P_\alpha^{\mathrm{a}} \, . \tag{106}
$$

Substitution of the definition (106) and the corrections of the phasic normal flux velocity components (96) to the phasic mass balance (104) changes it into the form

$$
\begin{aligned}
&\frac{\left(c_\alpha\big|_{\boldsymbol{P}} \rho_\alpha\big|_{\boldsymbol{P}} V_P \, \delta P_\alpha^{\mathrm{a}}\big|_{\boldsymbol{P}}\right)}{\Delta t}\Bigg|_{\boldsymbol{t+\Delta t}} + \left[c_\alpha \rho_\alpha \hat{U}_\alpha^1 \delta P_\alpha^{\mathrm{a}} - \varepsilon_\alpha \rho_\alpha \hat{H}_\alpha^{1j} \frac{\partial \delta P_\alpha^{\mathrm{a}}}{\partial \xi^j}\right]_{\boldsymbol{d}}^{\boldsymbol{u}} \\
&\qquad + \left[c_\alpha \rho_\alpha \hat{U}_\alpha^2 \delta P_\alpha^{\mathrm{a}} - \varepsilon_\alpha \rho_\alpha \hat{H}_\alpha^{2j} \frac{\partial \delta P_\alpha^{\mathrm{a}}}{\partial \xi^j}\right]_{\boldsymbol{s}}^{\boldsymbol{n}} \\
&\qquad + \left[c_\alpha \rho_\alpha \hat{U}_\alpha^3 \delta P_\alpha^{\mathrm{a}} - \varepsilon_\alpha \rho_\alpha \hat{H}_\alpha^{3j} \frac{\partial \delta P_\alpha^{\mathrm{a}}}{\partial \xi^j}\right]_{\boldsymbol{w}}^{\boldsymbol{e}} + R_{m_\alpha} = 0 \quad .
\end{aligned}
\tag{107}
$$

If the coefficient terms of the apparent pressure corrections and their gradients are understood as the pseudo convection and diffusion coefficients,

$$C_{P_\alpha}^{i}\Big|_{\boldsymbol{c}} = c_\alpha\big|_{\boldsymbol{c}}\rho_\alpha\big|_{\boldsymbol{c}}\hat{U}_\alpha^{\,i}\Big|_{\boldsymbol{c}} \quad \text{and} \quad D_{P_\alpha}^{ij}\Big|_{\boldsymbol{c}} = \varepsilon_\alpha\big|_{\boldsymbol{c}}\rho_\alpha\big|_{\boldsymbol{c}}\hat{H}_\alpha^{\,ij}\Big|_{\boldsymbol{c}}, \tag{108}$$

respectively, the apparent pressure correction equation (107) resembles closely the form of the momentum equation (36) or, more accurately, the form of a generalized balance equation (B12) for single phase flow [14, 34]. Thus, with the definitions (108), the apparent pressure correction equation (107) can be written as

$$\begin{aligned}&\left.\frac{\left(c_\alpha\big|_{\boldsymbol{P}}\rho_\alpha\big|_{\boldsymbol{P}} V_P\,\delta P_\alpha^{\,\mathrm{a}}\big|_{\boldsymbol{P}}\right)}{\Delta t}\right|_{\boldsymbol{t}+\boldsymbol{\Delta t}} + \left[C_{P_\alpha}^{1}\delta P_\alpha^{\,\mathrm{a}} - D_{P_\alpha}^{1j}\frac{\partial\,\delta P_\alpha^{\,\mathrm{a}}}{\partial\xi^j}\right]_{\boldsymbol{u}}\\ &+\left[C_{P_\alpha}^{2}\delta P_\alpha^{\,\mathrm{a}} - D_{P_\alpha}^{2j}\frac{\partial\,\delta P_\alpha^{\,\mathrm{a}}}{\partial\xi^j}\right]_{\boldsymbol{n}} + \left[C_{P_\alpha}^{3}\delta P_\alpha^{\,\mathrm{a}} - D_{P_\alpha}^{3j}\frac{\partial\,\delta P_\alpha^{\,\mathrm{a}}}{\partial\xi^j}\right]_{\boldsymbol{w}} + R_{m_\alpha} = 0\ .\end{aligned} \tag{109}$$

In addition, the resulting phasic apparent pressure correction equation (109) is fully analogous with the pressure correction scheme used for high-speed compressible gas flows [14].

4.2 EQUATION-SEQUENTIAL SOLUTION METHOD AND EAP

A natural base for a solver originally designed for multi-phase problems is set by the equation-sequential method. As shown on Figure 6, the main loop of the solution proceeds in this case from one balance equation type to an other. For each of these balance equations there is an inner loop consisting of sequential treatment of the phases. This structure allows easy implementation of many inter-phase coupling algorithms [34].

With the assumptions mentioned in section 4.1.1, the treatment of the fluid pressure correction equation for the equation-sequential solution method is equivalent with the treatment of the phase-sequential solution method derived there. Consequently, only the treatment of dispersed phases is shown in this section.

4.2.1 Treatment of dispersed phases in EAP

By comparing Figures 5 and 6 it is clear that in both of the solution methods, because of the sequential structure, the fluid pressure correction equation is solved before the pressure corrections of the dispersed phases. Despite of being a known term in the momentum balances of the dispersed phases, the fluid pressure gradient term in the EAP approach is treated equivalently with the apparent pressure gradient term. Thus, the dispersed phase momentum equation in the EAP approach is written as

$$a_{U_\alpha^k}\Big|_{\boldsymbol{P}} U_\alpha^k\Big|_{\boldsymbol{P}} = \sum_{\boldsymbol{c},\,\boldsymbol{C}} a_{U_\alpha^k}\Big|_{\boldsymbol{c}} U_\alpha^k\Big|_{\boldsymbol{C}} - A_k^i\Big|_{\boldsymbol{P}}\frac{\partial P_\alpha^{\,\mathrm{a}}}{\partial\xi^i}\Big|_{\boldsymbol{P}} - \varepsilon_\alpha\big|_{\boldsymbol{P}} A_k^i\Big|_{\boldsymbol{P}}\frac{\partial P_f}{\partial\xi^i}\Big|_{\boldsymbol{P}} + s_{U_\alpha^k}^{R}, \tag{110}$$

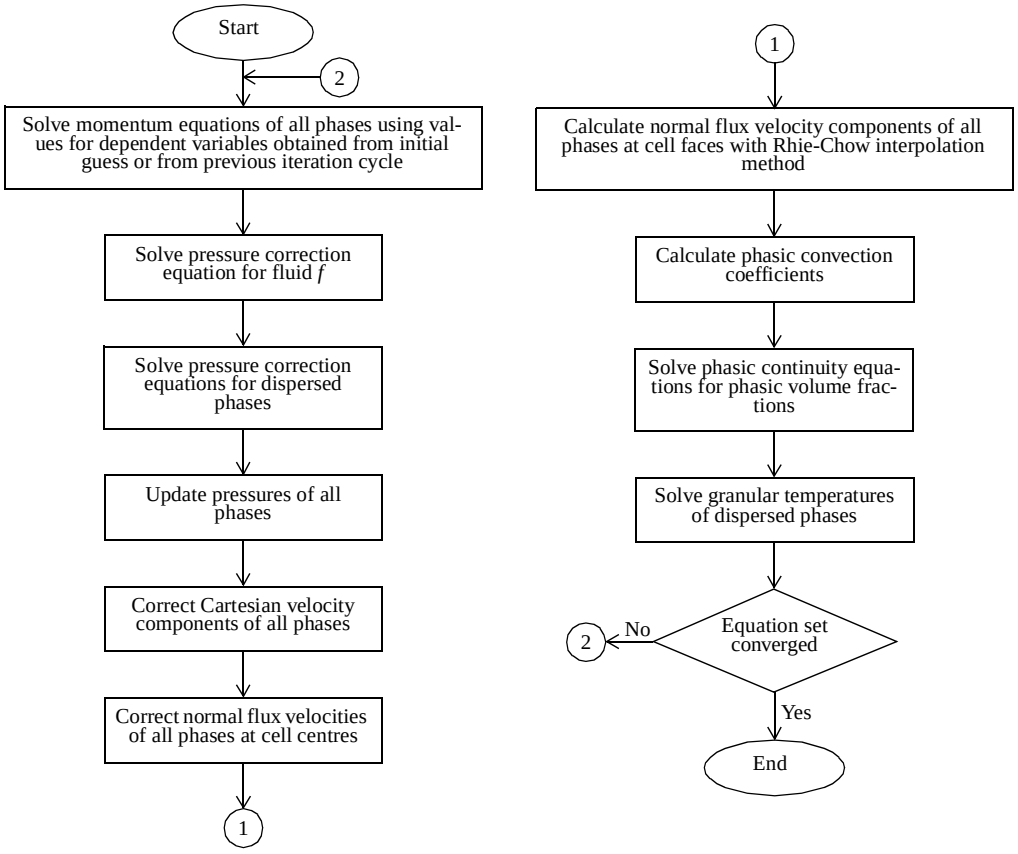

Figure 6. Computational flow chart of equation-sequential solution method.

where

$$a_{U_\alpha^k}\Big|_{\boldsymbol{P}} = \sum_{\boldsymbol{c}} a_{U_\alpha^k}\Big|_{\boldsymbol{c}} + \sum_{\beta=1}^{N_\mathrm{P}} \dot{m}_{\alpha\beta}\Big|_{\boldsymbol{P}} V_P + \sum_{\beta=1}^{N_\mathrm{P}} B_{\alpha\beta}\Big|_{\boldsymbol{P}} V_P - {}^{1}\boldsymbol{F}_\alpha^T\Big|_{\boldsymbol{P}} V_P + \frac{\varepsilon_\alpha\Big|_{\boldsymbol{P}} \rho_\alpha\Big|_{\boldsymbol{P}} V_P}{\Delta t} \quad \text{and} \tag{111}$$

$$s_{U_\alpha^k}^R = \left[\varepsilon_\alpha \eta_\alpha^{\mathrm{eff}} \frac{A_m^1 A_k^j}{|\boldsymbol{J}|} \frac{\partial U_\alpha^m}{\partial \xi^j}\right]_{\boldsymbol{d}} + \left[\varepsilon_\alpha \eta_\alpha^{\mathrm{eff}} \frac{A_m^2 A_k^j}{|\boldsymbol{J}|} \frac{\partial U_\alpha^m}{\partial \xi^j}\right]_{\boldsymbol{s}} + \left[\varepsilon_\alpha \eta_\alpha^{\mathrm{eff}} \frac{A_m^3 A_k^j}{|\boldsymbol{J}|} \frac{\partial U_\alpha^m}{\partial \xi^j}\right]_{\boldsymbol{w}} + \varepsilon_\alpha\Big|_{\boldsymbol{P}} \rho_\alpha\Big|_{\boldsymbol{P}} \boldsymbol{g}\, V_P + \sum_{\beta=1}^{N_\mathrm{P}} \dot{m}_{\beta\alpha}\Big|_{\boldsymbol{P}} U_\beta^k\Big|_{\boldsymbol{P}} V_P + \sum_{\beta=1}^{N_\mathrm{P}} B_{\alpha\beta}\Big|_{\boldsymbol{P}} U_\beta^k\Big|_{\boldsymbol{P}} V_P + {}^{0}\boldsymbol{F}_\alpha^T\Big|_{\boldsymbol{P}} V_P + S_{U_\alpha^k}^D + \left(\frac{\varepsilon_\alpha\Big|_{\boldsymbol{P}} \rho_\alpha\Big|_{\boldsymbol{P}} U_\alpha^k\Big|_{\boldsymbol{P}} V_P}{\Delta t}\right)\Bigg|_{\boldsymbol{t}}. \tag{112}$$

The treatment proceeds now in a fully analogous manner with the treatment of the fluid phase given in section 4.1.1 and in Appendix C, including the definitions of the new estimates (C2) and the approximation of values at the neighbouring cells (C3). As a result of this treatment, the corrections of the phasic Cartesian velocity components of the dispersed phase are related to the corrections of the fluid pressure and apparent pressure of the dispersed phase as

$$\delta U_\alpha^k\Big|_{\boldsymbol{P}} = -H_{\alpha k}^{i}\Big|_{\boldsymbol{P}}\left(\frac{\partial\,\delta P_\alpha^{\mathrm{a}}}{\partial \xi^i}\bigg|_{\boldsymbol{P}} + \varepsilon_\alpha\Big|_{\boldsymbol{P}}\frac{\partial\,\delta P_f}{\partial \xi^i}\bigg|_{\boldsymbol{P}}\right), \tag{113}$$

where $H_{\alpha k}^{i}\Big|_{\boldsymbol{P}}$ and $h_{\alpha}^{k}\Big|_{\boldsymbol{P}}$ are coefficients defined by equations (94) and (95), respectively. As previously, the corrections of the phasic normal flux velocity components of the dispersed phase are obtained by utilizing the associated definition (78). This results in

$$\delta \hat{U}_\alpha^{\,i}\Big|_{\boldsymbol{P}} = -\hat{H}_\alpha^{ij}\Big|_{\boldsymbol{P}}\left(\frac{\partial\,\delta P_\alpha^{\mathrm{a}}}{\partial \xi^j}\bigg|_{\boldsymbol{P}} + \varepsilon_\alpha\Big|_{\boldsymbol{P}}\frac{\partial\,\delta P_f}{\partial \xi^j}\bigg|_{\boldsymbol{P}}\right), \tag{114}$$

where the coefficient $\hat{H}_\alpha^{ij}\Big|_{\boldsymbol{P}}$ is defined by equation (97), in line with $H_{\alpha k}^{i}\Big|_{\boldsymbol{P}}$ and $h_{\alpha}^{k}\Big|_{\boldsymbol{P}}$.

4.2.1.1 Incompressible model for dispersed phases

As for the incompressible treatment of the dispersed phases with the FPS, the derivation of the apparent pressure correction equations with the EAP resembles closely to the derivation of the fluid pressure correction equations. By substituting the new estimates of the phasic convection coefficients (81) of the dispersed phase to the corresponding mass balance (61), and by utilizing equation (114), the apparent pressure correction equation of the EAP approach can be written as

$$\begin{aligned} a_{P_\alpha}\Big|_{\boldsymbol{P}}\delta P_\alpha^{\mathrm{a}}\Big|_{\boldsymbol{P}} + \sum_{\boldsymbol{c},\boldsymbol{C}}\varepsilon_\alpha\Big|_{\boldsymbol{c}} a_{P_\alpha}\Big|_{\boldsymbol{c}}\delta P_f\Big|_{\boldsymbol{P}} &= \sum_{\boldsymbol{c},\boldsymbol{C}} a_{P_\alpha}\Big|_{\boldsymbol{c}}\delta P_\alpha^{\mathrm{a}}\Big|_{\boldsymbol{C}} \\ &\quad + \sum_{\boldsymbol{c},\boldsymbol{C}}\varepsilon_\alpha\Big|_{\boldsymbol{c}} a_{P_\alpha}\Big|_{\boldsymbol{c}}\delta P_f\Big|_{\boldsymbol{C}} + S_{P_\alpha}^{D} + S_{P_{\alpha f}}^{D} - R_{m_\alpha}\ , \end{aligned} \tag{115}$$

where the coefficients $a_{P_\alpha}\Big|_{\boldsymbol{P}}$ and $a_{P_\alpha}\Big|_{\boldsymbol{c}}$ are given by equations (99). R_{m_α} stands for the dispersed phase mass residual (100), as before. Similar to the treatment of the fluid phase, the central difference approximation on the computational space has been assumed for the pressure correction gradients of both phases while deriving the apparent pressure correction equation (115). This equation can be rearranged

into the form

$$a_{P_\alpha}\big|_{\boldsymbol{P}}\,\delta P_\alpha^{\mathrm{a}}\big|_{\boldsymbol{P}} \;=\; \sum_{\boldsymbol{c},\,\boldsymbol{C}} a_{P_\alpha}\big|_{\boldsymbol{c}}\,\delta P_\alpha^{\mathrm{a}}\big|_{\boldsymbol{C}} + S_{\delta P_{\alpha f}} + S_{P_\alpha}^{D} + S_{P_{\alpha f}}^{D} - R_{m_\alpha}\,, \tag{116}$$

where the source term $S_{P_\alpha}^{D}$, related to the cross-derivatives of the apparent pressure correction, is given by equation (101).

The apparent pressure correction equation (116) reverts to the corresponding equation of the FPS approach with two additional source terms, $S_{\delta P_{\alpha f}}$ and $S_{P_{\alpha f}}^{D}$, originating from the fluid pressure gradient. These source terms are specified as

$$S_{\delta P_{\alpha f}} \;=\; \sum_{\boldsymbol{c},\,\boldsymbol{C}} \varepsilon_\alpha\big|_{\boldsymbol{c}}\, a_{P_\alpha}\big|_{\boldsymbol{c}}\,(\delta P_f\big|_{\boldsymbol{C}} - \delta P_f\big|_{\boldsymbol{P}}) \;\text{ and} \tag{117}$$

$$\begin{aligned} S_{P_{\alpha f}}^{D} \;=\; & \left[\varepsilon_\alpha E_{P_\alpha}^{12}\frac{\partial\,{}^{*}\delta P_f}{\partial\varsigma} + \varepsilon_\alpha E_{P_\alpha}^{13}\frac{\partial\,{}^{*}\delta P_f}{\partial\zeta}\right]_{\boldsymbol{d}} + \left[\varepsilon_\alpha E_{P_\alpha}^{21}\frac{\partial\,{}^{*}\delta P_f}{\partial\xi} + \varepsilon_\alpha E_{P_\alpha}^{23}\frac{\partial\,{}^{*}\delta P_f}{\partial\zeta}\right]_{\boldsymbol{s}} \\ & + \left[\varepsilon_\alpha E_{P_\alpha}^{31}\frac{\partial\,{}^{*}\delta P_f}{\partial\xi} + \varepsilon_\alpha E_{P_\alpha}^{32}\frac{\partial\,{}^{*}\delta P_f}{\partial\varsigma}\right]_{\boldsymbol{w}}\,. \end{aligned} \tag{118}$$

The origin of the source term $S_{P_{\alpha f}}^{D}$ is again in the cross-derivatives of the fluid pressure corrections. There the coefficient $E_{P_\alpha}^{ij}$ is the same that is found from the definition of $S_{P_\alpha}^{D}$ in the FPS approach (101), and which is defined by equation (102).

If the grid in the physical space is nearly orthogonal, in the computational space, the cross-derivatives included in the source terms $S_{P_\alpha}^{D}$ and $S_{P_{\alpha f}}^{D}$ are small compared to the components normal of the cell faces. Adaptation of this simplification, originally suggested by Rhie & Chow [49], the only difference between the FPS and the EAP approaches is in the source term $S_{\delta P_{\alpha f}}$.

4.2.1.2 Compressible model for dispersed phases

By following the same naming convention as with the FPS, the term compressibility here means that the $\varepsilon_\alpha(P_\alpha^{\mathrm{a}})$ dependency of the dispersed phases is handled similar to the $\rho_f(P_f)$ dependency in compressible single phase flows. Accordingly, the derivation of the apparent pressure correction equation is fully analogous with the treatment given for the compressible model with FPS. The only exception is that with the EAP model the corrections to the phasic normal flux velocity components are given by equation (114) instead of equation (96).

On these basis, the following apparent pressure correction equation, corre-

sponding to equation (107), is obtained

$$
\begin{aligned}
&\left.\frac{\left(c_\alpha\big|_{\boldsymbol{P}}\rho_\alpha\big|_{\boldsymbol{P}} V_P\,\delta P_\alpha^{\,a}\big|_{\boldsymbol{P}}\right)}{\Delta t}\right|_{\boldsymbol{t+\Delta t}} \\
&+\left[c_\alpha\rho_\alpha\hat{U}_\alpha^{\,1}\delta P_\alpha^{\,a}-\varepsilon_\alpha\rho_\alpha\hat{H}_\alpha^{1j}\left(\frac{\partial\,\delta P_\alpha^{\,a}}{\partial\xi^j}+\varepsilon_\alpha\frac{\partial\,\delta P_f}{\partial\xi^j}\right)\right]_{\boldsymbol{d}}^{\boldsymbol{u}} \\
&+\left[c_\alpha\rho_\alpha\hat{U}_\alpha^{\,2}\delta P_\alpha^{\,a}-\varepsilon_\alpha\rho_\alpha\hat{H}_\alpha^{2j}\left(\frac{\partial\,\delta P_\alpha^{\,a}}{\partial\xi^j}+\varepsilon_\alpha\frac{\partial\,\delta P_f}{\partial\xi^j}\right)\right]_{\boldsymbol{s}}^{\boldsymbol{n}} \\
&+\left[c_\alpha\rho_\alpha\hat{U}_\alpha^{\,3}\delta P_\alpha^{\,a}-\varepsilon_\alpha\rho_\alpha\hat{H}_\alpha^{3j}\left(\frac{\partial\,\delta P_\alpha^{\,a}}{\partial\xi^j}+\varepsilon_\alpha\frac{\partial\,\delta P_f}{\partial\xi^j}\right)\right]_{\boldsymbol{w}}^{\boldsymbol{e}}+R_{m_\alpha}\;=\;0\;\;.
\end{aligned}
\tag{119}
$$

In equation (119), c_α and R_{m_α} are defined by equations (106) and (100), respectively. By utilizing the definitions of the phasic pseudo convection and diffusion coefficients (108), equation (119) can be expanded to the form

$$
\begin{aligned}
&\left.\frac{\left(c_\alpha\big|_{\boldsymbol{P}}\rho_\alpha\big|_{\boldsymbol{P}} V_P\,\delta P_\alpha^{\,a}\big|_{\boldsymbol{P}}\right)}{\Delta t}\right|_{\boldsymbol{t+\Delta t}}+\left[C_{P_\alpha}^{1}\delta P_\alpha^{\,a}-D_{P_\alpha}^{1j}\frac{\partial\,\delta P_\alpha^{\,a}}{\partial\,\xi^j}\right]_{\boldsymbol{d}}^{\boldsymbol{u}} \\
&+\left[C_{P_\alpha}^{2}\delta P_\alpha^{\,a}-D_{P_\alpha}^{2j}\frac{\partial\,\delta P_\alpha^{\,a}}{\partial\xi^j}\right]_{\boldsymbol{s}}^{\boldsymbol{n}}+\left[C_{P_\alpha}^{3}\delta P_\alpha^{\,a}-D_{P_\alpha}^{3j}\frac{\partial\,\delta P_\alpha^{\,a}}{\partial\xi^j}\right]_{\boldsymbol{w}}^{\boldsymbol{e}} \\
&-\left[\varepsilon_\alpha D_{P_\alpha}^{1j}\frac{\partial\,\delta P_f}{\partial\xi^j}\right]_{\boldsymbol{d}}^{\boldsymbol{u}}-\left[\varepsilon_\alpha D_{P_\alpha}^{2j}\frac{\partial\,\delta P_f}{\partial\xi^j}\right]_{\boldsymbol{s}}^{\boldsymbol{n}}-\left[\varepsilon_\alpha D_{P_\alpha}^{3j}\frac{\partial\,\delta P_f}{\partial\xi^j}\right]_{\boldsymbol{w}}^{\boldsymbol{e}}+R_{m_\alpha}\;=\;0\;\;.
\end{aligned}
\tag{120}
$$

Again, by applying the central difference approximation on the computational space to the gradients of the fluid pressure, the apparent pressure correction equation (120) can be transformed into the form

$$
\begin{aligned}
&\left.\frac{\left(c_\alpha\big|_{\boldsymbol{P}}\rho_\alpha\big|_{\boldsymbol{P}} V_P\,\delta P_\alpha^{\,a}\big|_{\boldsymbol{P}}\right)}{\Delta t}\right|_{\boldsymbol{t+\Delta t}}+\left[C_{P_\alpha}^{1}\delta P_\alpha^{\,a}-D_{P_\alpha}^{1j}\frac{\partial\,\delta P_\alpha^{\,a}}{\partial\xi^j}\right]_{\boldsymbol{d}}^{\boldsymbol{u}} \\
&+\left[C_{P_\alpha}^{2}\delta P_\alpha^{\,a}-D_{P_\alpha}^{2j}\frac{\partial\,\delta P_\alpha^{\,a}}{\partial\xi^j}\right]_{\boldsymbol{s}}^{\boldsymbol{n}}+\left[C_{P_\alpha}^{3}\delta P_\alpha^{\,a}-D_{P_\alpha}^{3j}\frac{\partial\,\delta P_\alpha^{\,a}}{\partial\xi^j}\right]_{\boldsymbol{w}}^{\boldsymbol{e}} \\
&-S_{\delta P_{\alpha f}}-S_{P_{\alpha f}}^{D}+R_{m_\alpha}\;=\;0\;\;,
\end{aligned}
\tag{121}
$$

where $S_{\delta P_{\alpha f}}$ and $S_{P_{\alpha f}}^{D}$ are the source terms related to the gradients of the fluid pressure corrections, given by equations (117) and (118), respectively.

The same remarks about the differences between the FPS and the EAP approaches as with the incompressible model are also valid for the compressible model. Clearly, under the approximation of Rhie & Chow [49] for the nearly orthogonal grid, the only difference is found to be the source term $S_{\delta P_{\alpha f}}$.

5 MOMENTUM INTERPOLATION

The principal difficulty, related to the otherwise beneficial collocated arrangement of computational elements, is the need to interpolate the phasic Cartesian velocity components from cell centres to cell faces, in order to calculate the phasic convection coefficients (50). A simple weighted linear interpolation scheme [34] would lead to the chequer-board oscillations in the phasic pressure field, a consequence of the discretization approximation used for the pressure gradients. To avoid this decoupling of adjacent cells, the Rhie-Chow momentum interpolation scheme [49] imitating the staggered grid solution (Figure 7) is used.

5.1 EXTENDED MOMENTUM INTERPOLATION SCHEME

The Rhie-Chow momentum interpolation scheme has originally been introduced for single phase flow, but a straightforward application to the multi-fluid model equations can be achieved based on the shared pressure concept, described in section 2.2. To achieve the same level of accuracy for both pressure gradient terms in the momentum equations of the dispersed phases, the Rhie-Chow interpolation scheme has to be extended by applying an analogous fourth order smoothing scheme for the apparent pressure as for the hydrodynamic pressure. Thus, the momentum balance of the dispersed phase is written in the form

$$U_\alpha^k\Big|_{\boldsymbol{P}} + N_{\alpha k}^{\ i}\Big|_{\boldsymbol{P}} \left.\frac{\partial P_\alpha^{\mathrm{a}}}{\partial \xi^i}\right|_{\boldsymbol{P}} + \varepsilon_\alpha\Big|_{\boldsymbol{P}} N_{\alpha k}^{\ i}\Big|_{\boldsymbol{P}} \left.\frac{\partial P_f}{\partial \xi^i}\right|_{\boldsymbol{P}} = M_\alpha\Big|_{\boldsymbol{P}}, \text{ where} \tag{122}$$

$$M_\alpha\Big|_{\boldsymbol{P}} = \left(\sum_{\boldsymbol{c},\,\boldsymbol{C}} a_{U_\alpha^k}\Big|_{\boldsymbol{c}} U_\alpha^k\Big|_{\boldsymbol{C}} + s_{U_\alpha^k}^R \right) \Big/ a_{U_\alpha^k}\Big|_{\boldsymbol{P}} \text{ and} \tag{123}$$

$$N_{\alpha k}^{\ i}\Big|_{\boldsymbol{P}} = \frac{A_k^i\Big|_{\boldsymbol{P}}}{a_{U_\alpha^k}\Big|_{\boldsymbol{P}}}. \tag{124}$$

The phasic Cartesian velocity components at the cell faces, i.e., the pseudo staggered grid velocities, are found by interpolation of equation (122) from the adjacent cell centres to the staggered grid location as illustrated in Figure 7.

In the Rhie-Chow interpolation scheme, weighted linear interpolation is applied to the source-like term M_α. This allows the left side of equation (122) to be approximated with the same scheme. Accordingly, the momentum balance for the imaginary staggered cell can be expressed as

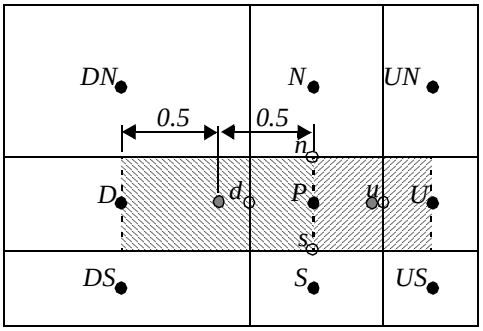

Figure 7. Staggered cell locations for x-component (DU) velocity for a regular non-uniform mesh. Grey circles denote staggered cell centres.

$$U_\alpha^k\Big|_{\boldsymbol{c}} + N_{\alpha k}^{\,i}\Big|_{\boldsymbol{c}} \frac{\partial P_\alpha^{\mathrm{a}}}{\partial \xi^i}\bigg|_{\boldsymbol{c}} + \varepsilon_\alpha\Big|_{\boldsymbol{c}} N_{\alpha k}^{\,i}\Big|_{\boldsymbol{c}} \frac{\partial P_f}{\partial \xi^i}\bigg|_{\boldsymbol{c}}$$

$$= \left\{ U_\alpha^k\Big|_H + N_{\alpha k}^{\,i}\Big|_H \frac{\partial P_\alpha^{\mathrm{a}}}{\partial \xi^i}\bigg|_{\boldsymbol{P}} + \varepsilon_\alpha\Big|_H N_{\alpha k}^{\,i}\Big|_H \frac{\partial P_f}{\partial \xi^i}\bigg|_H \right\}_{\boldsymbol{C}}^{\boldsymbol{P}}, \tag{125}$$

where the notation $\{\ |_H\ \}_C^P$ stands for the weighted linear interpolation between the cell centres $H = P$ and C. If it is assumed that

$$\left\{ N_{\alpha k}^{\,i}\Big|_H \frac{\partial P_\alpha^{\mathrm{a}}}{\partial \xi^i}\bigg|_H \right\}_C^P = \left\{ N_{\alpha k}^{\,i}\Big|_H \right\}_C^P \left\{ \frac{\partial P_\alpha^{\mathrm{a}}}{\partial \xi^i}\bigg|_H \right\}_C^P, \tag{126}$$

$$\left\{ \varepsilon_\alpha\Big|_H N_{\alpha k}^{\,i}\Big|_H \frac{\partial P_f}{\partial \xi^i}\bigg|_H \right\}_C^P = \{\ \varepsilon_\alpha\Big|_H\ \}_C^P \left\{ N_{\alpha k}^{\,i}\Big|_H \right\}_C^P \left\{ \frac{\partial P_f}{\partial \xi^i}\bigg|_H \right\}_C^P, \tag{127}$$

$$\varepsilon_\alpha\Big|_{\boldsymbol{c}} = \{\ \varepsilon_\alpha\Big|_H\ \}_C^P \quad \text{and} \quad N_{\alpha k}^{\,i}\Big|_{\boldsymbol{c}} = \left\{ N_{\alpha k}^{\,i}\Big|_H \right\}_C^P, \tag{128}$$

equation (125) can be simplified to the form

$$U_\alpha^k\Big|_{\boldsymbol{c}} = \left\{ U_\alpha^k\Big|_H \right\}_C^P + \left\{ N_{\alpha k}^{\ i}\Big|_H \right\}_C^P \left(\left\{ \frac{\partial P_\alpha^{\,a}}{\partial \xi^i}\Big|_H \right\}_C^P - \frac{\partial P_\alpha^{\,a}}{\partial \xi^i}\Big|_{\boldsymbol{c}} \right) + \{ \varepsilon_\alpha|_H \}_C^P \left\{ N_{\alpha k}^{\ i}\Big|_H \right\}_C^P \left(\left\{ \frac{\partial P_f}{\partial \xi^i}\Big|_H \right\}_C^P - \frac{\partial P_f}{\partial \xi^i}\Big|_{\boldsymbol{c}} \right) . \tag{129}$$

As the pressure gradients in the pressure correction equation are calculated by central differences, it is essential for the conservation of mass that the interpolations of cell centre pressure gradients to the cell faces in equation (129) are calculated with the weight factor equal to one half. In contrast, the pressure gradients at the cell faces are approximated, as in the staggered solution method, with the difference between the pressures on cell centres of adjacent control volumes.

The required phasic normal flux velocity components of the dispersed phases are found with the help of the associated definition. This results in the following expression

$$\hat{U}_\alpha^{\ i}\Big|_{\boldsymbol{c}} = \left\{ \hat{U}_\alpha^{\ i}\Big|_H \right\}_C^P + \left\{ \hat{N}_\alpha^{\ ii}\Big|_H \right\}_C^P \left(\left\{ \frac{\partial P_\alpha^{\,a}}{\partial \xi^i}\Big|_H \right\}_C^P - \frac{\partial P_\alpha^{\,a}}{\partial \xi^i}\Big|_{\boldsymbol{c}} \right) + \{ \varepsilon_\alpha|_H \}_C^P \left\{ \hat{N}_\alpha^{\ ii}\Big|_H \right\}_C^P \left(\left\{ \frac{\partial P_f}{\partial \xi^i}\Big|_H \right\}_C^P - \frac{\partial P_f}{\partial \xi^i}\Big|_{\boldsymbol{c}} \right) , \tag{130}$$

where the coefficients $\hat{N}_\alpha^{\ ii}$ are defined as

$$\hat{N}_\alpha^{\ ij}\Big|_{\boldsymbol{P}} = A_k^i\Big|_{\boldsymbol{P}} N_{\alpha k}^{\ j}\Big|_{\boldsymbol{P}} = \frac{A_k^i\Big|_{\boldsymbol{P}} A_k^j\Big|_P}{a_{U_\alpha^k}\Big|_{\boldsymbol{P}}} . \tag{131}$$

As seen from the interpolation equation (130), only the diagonal components of the pressure gradient terms are retained. This simplification is valid because the cross-derivative terms cancel out when all the pressure gradients are calculated with the central difference approximation.

In case of rapidly changing source terms, e.g., the buoyancy force on different sides of a sharp interface, the weighted linear interpolation applied to source terms while carrying out the Rhie-Chow momentum interpolation may not be accurate enough resulting in mass imbalance in cells adjacent to the interface. This difficulty can be relieved with a so-called *improved* Rhie-Chow momentum interpolation method described in Appendix D. The *extended* Rhie-Chow momentum interpolation derived above can be used instead of or in combination with the *improved* Rhie-Chow interpolation.

6 CONCLUSIONS

This thesis work concentrated on the problems encountered while solving dispersed multi-phase problems numerically with a collocated Control Volume Method (CVM). The essential aspects were considered to be the treatment and efficiency of inter-phase coupling terms in sequential solution, exceeding the bounds of validity of the shared pressure concept in cases of high dispersed phase pressure and the conservation of mass in momentum interpolation for rapidly changing source terms. These aspects were studied only a special application in mind, i.e., a fluidized gas-particle bed or a liquid-particle bed.

It would be intuitively expected that to have a sequential iterative solver converge, the inter-phase coupling terms have to be treated fully implicitly when the interfacial transfer coefficient becomes large. This has also been confirmed by Oliveira and Issa [42]. The requirement of implicit treatment is connected to the very short characteristic times of the interfacial transfer in these conditions and to the nature of the iterative solution method itself. In typical fluidized bed conditions, represented here by air-glass particle and water-glass particle flows, the characteristic times of interfacial momentum transport by hydrodynamic phenomena in most of the bed sections are not as small. However, there always exist conditions, e.g., start-up of the bed, and locations in the bed, e.g., heat transfer surfaces, pipe bundles and corners, where the inter-phase coupling between dispersed phases is tight and the dispersed phase pressure is significant. Thus, the benefits of treating inter-phase coupling terms in a partially implicit, semi-implicit or fully implicit way and of including inter-phase coupling terms into the pressure correction scheme were studied in these conditions.

In both flow configurations A and B the semi-implicit SINCE method resulted in about 5% and the fully implicit PEA method about 35% higher convergence rate of phasic momentum equations, respectively. The most important reason for the improvement can be found in the correctness of the few first approximates when a new time step is entered. The effect of including inter-phase coupling terms into the pressure correction scheme, the essence of the IPSA–C, is limited to the first few time steps, and there is practically no improvement of the overall convergence rate. This can be attributed to the generally poor performance of the pressure correction step.

When the time step of simulation is kept well below the characteristic time scale of interfacial transfer processes, the partially implicit treatment of coupling terms in combination with the IPSA solution algorithm provides the most efficient approach. This result is totally based on the smaller number of computational operations required by these simpler schemes. When a longer time step is required or there is a region in the solution domain involved with very small characteristic time scales of interfacial coupling, the semi-implicit or fully implicit treatment of coupling terms becomes necessary. Then the PEA method provides the best efficiency for two-phase flows, providing a considerably better convergence with momentum equations but being only slightly more laborious computationally than the partially implicit treatment. In multi-phase flows the SINCE method provides the only option for the partially implicit treatment. Its convergence rate with momentum equations is only slightly better than with the partially implicit method though it is computationally more involved. However, a slight improvement of efficiency can

be obtained by calculating new source terms at every inner iteration. The IPSA–C method is arguably the preferred solution method for conditions where the interfacial coupling is tighter than in the flow configurations studied, e.g., in bubbly air-water flows, or if the pressure correction algorithm can be enhanced to give better approximations in general.

To overcome the poor performance of the pressure correction step, the concept of multi-pressure algorithms was introduced in chapter 4. Their usefulness should be obvious but no test of their real functionality has been included. Especially tempting are the compressible versions of the FPS and the EAP, as despite of considering the volume fraction also as a variable during the pressure correction step they still reduce to the same treatment as in compressible single-phase flows.

A very crucial operation for the success of a collocated CVM utilizing iterative solution is the conservation of mass in momentum interpolation, a part of the pressure-correction step. The improved Rhie-Chow interpolation scheme presented in Appendix D is known to be efficient in reducing the error in interpolation (CFDS-FLOW3D). If the shared pressure concept is abandoned and a proper treatment is given for the dispersed phase pressure both the customary and the improved Rhie-Chow interpolation method must be expanded. Thus an approach, referred to as the extended Rhie-Chow interpolation, applicable to both momentum interpolation schemes is presented.

Thus far the majority of the studies concerning numerical solution of multi-fluid equations have concentrated on the special difficulties of these flows, i.e., the interphase couplings, moving interfaces, strong non-linearity and the large number of dependent variables. However, the development of constitutive models for dispersed multi-phase flows has revealed that in contrary to single phase flows the primary transfer mechanism of information does not operate only from large to small flow scales but also in opposite direction. This is especially true in the case of fluidized beds. The consequence of the opposite transfer of information is that the small scale phenomena are important in creation of the macro-scale structures and, accordingly, they should be modelled and solved to adequate accuracy. Therefore, reasonably accurate and predictive simulations will be computationally very intensive and all progress in solution efficiency will be highly useful. Approaches such as special multi-grid solution cycles, being efficient to transport information over the spectrum of flow scales, should be utilized.

Another way to improve the transfer of information between different scales of flow can be achieved by solving separate conservation equations for a selected ranges of scales. In this approach, an additional difficulty in constituting the conservation equations as well as describing there mutual interactions will be faced.

REFERENCES

1. Agee, L., Banerjee, S., Duffey, R. B. and Hughes, E. D. Some aspects of two-fluid models for two-phase flow and their numerical solution. In: Reocreux, M. and Katz, G. (eds.) *Proc. of the 2nd CSNI Specialists' Meeting on Transient Two-Phase Flow,* Vol. 1. Paris, 1978. Pp. 59–82.

2. Aidun, C. K. and Lu, Y. Lattice Boltzmann Simulation of Solid Particles Suspended in Fluid. *Journal of Statistical Physics,* 1995. Vol. 81, pp. 49–61.

3. Aidun, C. K., Lu, Y. and Ding, E.-J. Dynamic simulation of particles suspended in fluid. The 1997 *ASME Fluids Engineering Division Summer Meeting,* FEDSM97–3181, June 22–26, 1997.

4. Anderson, T. B. and Jackson, R. A fluid mechanical description of fluidized beds. *Indust. Eng. Chem. Fundamentals,* 1967. Vol. 6, pp. 527–534.

5. Andrews, M. J. and O'Rourke, P. J. The multiphase particle-in-cell (MP-PIC) method for dense particulate flows. *Int. J. Multiphase Flow,* 1996. Vol. 22, pp. 379–402.

6. Balzer, G. and Simonin, O. Extension of Eulerian Gas-Solid Flow Modelling to Dense Fluidized Bed. *Proc. 5th Int. Symp. on Refined Flow Modelling and Turbulence Measurements,* Ed. L. Viollet, Paris, 1993. Pp. 417–424.

7. Batchelor, G. K. The stress system in a suspension of force-free particles. *J. Fluid Mech.,* 1970. Vol. 41, pp. 545–570.

8. Berlemont, A., Desjonqueres, P. and Gouesbet, G. Particle Lagrangian simulation in turbulent flows. *Int. J. Multiphase Flow,* 1990. Vol. 16, pp. 19–34.

9. Bouillard, J. X., Lyczkowski, R. W. and Gidaspow, D. Porosity distributions in a fluidized bed with an immersed obstacle. *AIChE J.,* 1989. Vol. 35, pp. 908–922.

10. Burns, A. D. Personal communication. 1995.

11. Buyevich, Y. A. Statistical hydromechanics of disperse systems. Part 1. Physical background and general equations. *J. Fluid Mech.,* 1971. Vol. 49, part 3, pp. 489–507.

12. Buyevich, Y. A. and Shchelchkova, I. N. Flow of dense suspensions. *Prog. Aerospace Sci,* 1978. Vol. 18, pp. 121–150.

13. Campbell, C. S. and Wang, D. G. Particle pressures in gas-fluidized beds. *J. Fluid Mech.,* 1991. Vol. 227, pp. 495–508.

14. CFX 4.1 Flow Solver User Guide. Computational Fluid Dynamics Services, Oxfordshire, 1995.

15. Chapman, S. and Cowling, T. G. *The Mathematical Theory of Non-Uniform Gases*. 3rd Ed., Cambridge University Press, Cambridge, 1970.

16. Crowe, C. T. REVIEW – Numerical Models for Dilute Gas-Particle Flows. *Journal of Fluids Engineering*, 1982. Vol. 104, pp. 297–303.

17. Ding, J. and Gidaspow, D. A Bubbling Fluidization Model Using Kinetic Theory of Granular Flow. *AIChE Journal*, 1990. Vol. 36, pp. 523–538.

18. Van Doormal, J. P. and Raithby, G. D. Enhancements of the SIMPLE method for predicting incompressible fluid flows. *Num. Heat Transfer*, 1984. Vol. 7, pp. 147–163.

19. Drew, D. A. Averaged Field Equations for Two-Phase Media. *Studies in Applied Mathematics*, 1971. Vol. L No. 2, pp. 133–166.

20. Drew, D. A. Mathematical modeling of two-phase flow. *Ann. Rev. Fluid Mech.*, 1983. Vol. 15, pp. 261–291.

21. Drew, D. A. and Lahey Jr., R. T. Application of general constitutive principles to the derivation of multidimensional two-phase flow equations. *Int. J. Multiphase Flow*, 1979. Vol. 5, pp. 243–264.

22. Drew, D. A. and Segel, L. A. Analysis of Fluidized Beds and Foams Using Averaged Equations. *Studies in Applied Mathematics*, 1971. Vol. L No. 3, pp. 233–257.

23. Faeth, G. M. Recent advances in modeling particle transport properties and dispersion in turbulent flow. *Proc. ASME-JSME Thermal Engineering Conference*, Vol. 2, pp. 517–534, 1983.

24. FLUENT; User's Guide, Version 4.3. Fluent Inc.

25. Gosman, A. D. and Ioannides, E. Aspects of computer simulation of liquid-fuelled combustors. Paper AIAA-81–0323, presented at *AIAA 19th Aerospace Sciences Meeting*, St. Louis, MO, 1981.

26. Harlow, F. H. and Amsden A. A. Numerical calculation of multiphase fluid flow. *J. Comput. Phys.*, 1975. Vol. 17, pp. 19–52.

27. He, J. and Simonin, O. Non-equilibrium prediction of the particle-phase stress tensor in vertical pneumatic conveying. *ASME Gas Solid Flows*, 1993. Vol. 166, pp. 253–263.

28. Hiltunen, K. A Stabilized Finite Element Method for Particulate Two-phase Flow Equations: Laminar isothermal flow. *Comput. Methods Appl. Mech. Engrg*, 1997. Vol. 147, pp. 387–399.

29. Hwang, G. J. and Shen, H. H. Modeling the solid phase stress in a fluid-solid mixture. *Int. J. Multiphase Flow*, 1989. Vol. 15, pp. 257–268.

30. Hwang, G. J. and Shen, H. H. Modeling the phase interaction in the momentum equations of a fluid-solid mixture. *Int. J. Multiphase Flow*, 1991. Vol. 17, pp. 45–57.

31. Ishii, M. *Thermo-fluid dynamic theory of two-phase flow.* Direction des Etudes et Recherches d'Electricite de France, Paris: Eyrolles, 1975. 248 p.

32. Jenkins, J. T. and Savage, S. B. A theory for the rapid flow of identical, smooth, nearly elastic, spherical particles. *J. Fluid Mech*., 1983. Vol. 130, pp. 187–202.

33. Joseph, D. D., Lundgren, T. S., Jackson, R. and Saville, D. A. Ensemble averaged and mixture theory equations for incompressible fluid-particle suspensions. *Int. J. Multiphase Flow*, 1990. Vol. 16, pp. 35–42.

34. Karema, H. and Lo, S. Efficiency of interphase coupling algorithms in fluidized bed conditions. *Computers & Fluids*, 1999. Vol. 28, pp. 323–360.

35. Lectures on PHOENICS; Two-Phase Flows. CHAM Ltd.

36. Lien, F. S. and Leschziner, M. A. A general non-orthogonal collocated finite volume algorithm for turbulent flow at all speeds incorporating second-moment turbulence-transport closure, Part 1: Computational implementation. *Comput. Methods Appl. Mech. Engrg.*, 1994. Vol. 114, pp. 123–148.

37. Lo, S. M. *Mathematical basis of a multi-phase flow model*. United Kingdom Atomic Energy Authority, Computational Fluid Dynamics Section, Report AERE R 13432, 1989.

38. Lo, S. M. *Multiphase flow model in the Harwell-FLOW3D computer code*. AEA Industrial Technology, Report AEA-InTech-0062, 1990.

39. Lun, C. K. K., Savage, S. B., Jeffrey, D. J. and Chepurniy, N. Kinetic theories for granular flow: inelastic particles in Couette flow and slightly inelastic particles in a general flowfield. *J. Fluid Mech.*, 1984. Vol. 140, pp. 223–256.

40. Masson C. and Baliga, B. R. A control-volume finite element method for dilute gas-solid particle flows. *Computers and Fluids*, 1994. Vol. 23, pp. 1073–1096.

41. Maxey, M. R. and Riley, J. J. Equation of motion for a small rigid sphere in a nonuniform flow. *Phys. Fluids*, 1983. Vol. 26, pp. 883–889.

42. Oliveira, P. J. and Issa, R. I. On the numerical treatment of interphase forces in two-phase flow. *Numerical Methods in Multiphase Flows*, 1994. ASME FED-Vol. 185, pp. 131–140.

43. Patankar, S. V. *Numerical Heat Transfer and Fluid Flow.* New York: Hemisphere, 1980. 197 p.

44. Patankar, S. V. and Spalding, D. B. A calculation procedure for heat, mass and momentum transfer in parabolic flows. *Int. J. Heat Mass Transfer,* 1972. Vol. 15, pp. 1787–1806.

45. Pita, J. A. and Sundaresan, S. Gas-solid flow in vertical tubes. *AIChE Journal*, 1991. Vol. 37, No. 7, pp. 1009–1018.

46. Prosperetti, A. and Jones, A. V. Pressure forces in disperse two-phase flow. *Int. J. Multiphase Flow,* 1984. Vol. 10, pp. 425–440.

47. Reeks, M. W. On a kinetic equation for the transport of particles in turbulent flows. *Phys. Fluids A*, 1991. Vol. 3, pp. 446–456.

48. Reeks, M. W. On the continuum equations for dispersed particles in nonuniform flows. *Phys. Fluids A*, 1992. Vol. 4, pp. 1290–1303.

49. Rhie, C. M. and Chow, W. L. Numerical Study of the Turbulent Flow Past an Airfoil with Trailing Edge Separation. *AIAA Journal,* 1983. Vol. 21, pp. 1525–1532.

50. Sinclair, J. L. and Jackson, R. Gas-particle flow in a vertical pipe with particle-particle interactions. *AIChE Journal,* 1989. Vol. 35, No. 9, pp. 1473–1486.

51. Spalding, D. B. The calculation of free-convection phenomena in gas-liquid mixtures. In: Spalding, D. B. & Afgan, N. (eds.) *Heat transfer and turbulent buoyant convection Studies and Applications for Natural Environment, Buildings and Engineering Systems,* Vol. II. Hemisphere, 1976. Pp. 569–586.

52. Spalding, D. B. Numerical computation of multi-phase fluid flow and heat transfer. In: Taylor, C. & Morgan, K. (eds.) *Recent Advances in Numerical Methods in Fluids,* Vol. 1. Pineridge Press, 1980. Pp. 139–168.

53. Spalding, D. B. Developments in the IPSA Procedure for Numerical Computation of Multiphase-Flow Phenomena with Interphase Slip, Unequal Temperatures, Etc. In: Shih, T. M. (ed.) *Numerical Methodologies in Heat Transfer,* Proceedings of the Second National Symposium. Hemisphere, 1983. Pp. 421–436.

54. Soo, S. L. *Multiphase Fluid Dynamics*. Beijing: Science Press, 1990. 691 p.

55. Stewart, H. B. and Wendroff, B. Two-phase flow: models and methods. *J. Comp. Phys.*, 1984. Vol. 56, pp. 363–409.

56. Weber, R., Boysan, F., Ayers, W. H. and Swithenbank, J. Simulation of dispersion of heavy particles in confined turbulent flows. *AIChE Journal*, 1984. Vol. 30, pp. 490–493.

APPENDIX A

Interfacial Mean Pressure model, IMP

Equation (5) together with the definitions (14) and (15) produce the following balance equation of momentum

$$\frac{\partial}{\partial t}(\varepsilon_\alpha \bar{\rho}_\alpha \tilde{\boldsymbol{U}}_\alpha) + \nabla \bullet (\varepsilon_\alpha \bar{\rho}_\alpha \tilde{\boldsymbol{U}}_\alpha \otimes \tilde{\boldsymbol{U}}_\alpha) = \nabla \bullet (\varepsilon_\alpha \bar{\boldsymbol{T}}_\alpha) + \varepsilon_\alpha \bar{\rho}_\alpha \boldsymbol{g} + M_\alpha^I \boldsymbol{U}_\alpha^I + P_\alpha^I \nabla \varepsilon_\alpha + \boldsymbol{F}_\alpha^D + \boldsymbol{F}_\alpha^S \quad . \tag{A1}$$

By extracting the pressure contribution from the first term on the right side of equation (A1), on the basis of the definition (11), and combining it with the fourth term results in

$$-\nabla(\varepsilon_\alpha \bar{P}_\alpha) + P_\alpha^I \nabla \varepsilon_\alpha = -\varepsilon_\alpha \nabla \bar{P}_\alpha + (P_\alpha^I - \bar{P}_\alpha) \nabla \varepsilon_\alpha \, . \tag{A2}$$

For problems involved with the surface tension the relation between the interfacial mean pressures can be written as

$$P_d^I - P_f^I = \sigma \kappa \, , \tag{A3}$$

where σ is the surface tension coefficient and κ is the average mean curvature. Further discussion on pressure approximations can be found, e.g., in [1]. Thus, by taking into account the definitions of stresses (12) and (13), for particulate flows, the momentum equations of fluid and dispersed phases can be written as given in (19) and (20).

Direct Interfacial Force model, DIF

By combining equations (14) and (18) with equation (5) results in the momentum equations for the fluid and dispersed phases of the form

$$\frac{\sigma}{\partial t}(\varepsilon_f \bar{\rho}_f \tilde{\boldsymbol{U}}_f) + \nabla \bullet (\varepsilon_f \bar{\rho}_f \tilde{\boldsymbol{U}}_f \otimes \tilde{\boldsymbol{U}}_f) = \nabla \bullet (\varepsilon_f \bar{\boldsymbol{T}}_f) + \varepsilon_f \bar{\rho}_f \boldsymbol{g} + M_f^I \boldsymbol{U}_f^I + \boldsymbol{F}_T^I - \sum_{\beta=1}^{N_d} (\varepsilon_\beta \nabla \bullet \bar{\boldsymbol{T}}_f^{\,v} + \boldsymbol{F}_\beta^D - \nabla \bullet (\varepsilon_\beta \bar{\boldsymbol{T}}_\beta^{\,p})) + \boldsymbol{F}_f^S \quad \text{and} \tag{A4}$$

$$\frac{\partial}{\partial t}(\varepsilon_d \bar{\rho}_d \tilde{\boldsymbol{U}}_d) + \nabla \bullet (\varepsilon_d \bar{\rho}_d \tilde{\boldsymbol{U}}_d \otimes \tilde{\boldsymbol{U}}_d) = \nabla \bullet (\varepsilon_d \bar{\boldsymbol{T}}_d) + \varepsilon_d \bar{\rho}_d \boldsymbol{g} + M_d^I \boldsymbol{U}_d^I + \varepsilon_d \nabla \bullet \bar{\boldsymbol{T}}_f^{\,v} + \boldsymbol{F}_d^D - \nabla \bullet (\varepsilon_d \bar{\boldsymbol{T}}_d^{\,p}) + \boldsymbol{F}_d^S \quad . \tag{A5}$$

By utilizing the definition (12) the viscous stress parts of the first term on the right side and of the interfacial momentum source in equation (A4) can be expanded and then subsequently simplified as

$$\begin{aligned}
&\nabla \bullet (\varepsilon_f \boldsymbol{T}_f^{\nu}) - \sum_{\beta=1} (\varepsilon_\beta \nabla \bullet \boldsymbol{T}_f^{\nu}) \\
&\quad = \varepsilon_f \nabla \bullet \bar{\boldsymbol{T}}_f^{\mathrm{V}} + \bar{\boldsymbol{T}}_f^{\mathrm{V}} \nabla \varepsilon_f - \sum_{\beta=1}^{N_d} (\nabla \bullet (\varepsilon_\beta \bar{\boldsymbol{T}}_f^{\mathrm{V}}) - \bar{\boldsymbol{T}}_f^{\mathrm{V}} \nabla \varepsilon_\beta) \\
&\quad = \varepsilon_f \nabla \bullet \bar{\boldsymbol{T}}_f^{\mathrm{V}} - \sum_{\beta=1}^{N_d} (\nabla \bullet (\varepsilon_\beta \bar{\boldsymbol{T}}_f^{\mathrm{V}})) + \bar{\boldsymbol{T}}_f^{\mathrm{V}} \nabla \left(\varepsilon_f + \sum_{\beta=1}^{N_d} \varepsilon_\beta \right) \\
&\quad = \varepsilon_f \nabla \bullet \bar{\boldsymbol{T}}_f^{\mathrm{V}} - \sum_{\beta=1}^{N_d} (\nabla \bullet (\varepsilon_\beta \bar{\boldsymbol{T}}_f^{\mathrm{V}})) \quad .
\end{aligned} \tag{A6}$$

With the result (A6) and with the definitions (12) and (13) the momentum balances (A4) and (A5) can be written into the form of (21) and (22).

1. Drew, D. A. Mathematical modeling of two-phase flow. *Ann. Rev. Fluid Mech.*, 1983. Vol. 15, pp. 261–291.

APPENDIX B

The non-singular coordinate transformation mapping from a right-handed Cartesian frame in the physical space $x^i = (x, y, z)$ to a right-handed curvilinear frame in the computational space $\xi^i = (\xi, \varsigma, \zeta)$ is determined by specifying the Jacobian matrix of this transformation

$$\boldsymbol{J}_j^i = \frac{\partial x^i}{\partial \xi^j}. \tag{B1}$$

Additional useful mathematical concepts in this context are the inverse Jacobian matrix $\boldsymbol{J}_j^i$, the Jacobian determinant $|\boldsymbol{J}|$ and the adjugate Jacobian matrix A_j^i

$$\bar{\boldsymbol{J}}_j^i = \frac{\partial \xi^i}{\partial x^j}, \tag{B2}$$

$$|\boldsymbol{J}| = \det(\boldsymbol{J}_j^i) \quad \text{and} \tag{B3}$$

$$A_j^i = |\boldsymbol{J}| \bar{\boldsymbol{J}}_j^i. \tag{B4}$$

Every curvilinear frame $\xi^i(x^j)$ can be associated with two distinct frames of basis vectors of which the first one is tangential to the coordinate curves $\boldsymbol{e}_{(i)}$ and the other one is normal to the coordinate surfaces $\boldsymbol{e}^{(i)}$. Their Cartesian components are given by

$$\boldsymbol{e}_{(i)k} = \boldsymbol{J}_i^k \quad \text{and} \quad \boldsymbol{e}_{(i)}^k = \bar{\boldsymbol{J}}_k^i. \tag{B5}$$

The area vectors of the surfaces of an elementary grid cell (Figure 1(a)) $\boldsymbol{A}^{(i)}$, i.e., the vectors pointing to the outward normal direction of a cell face with magnitude equal to the area of the face, are obtained as

$$\boldsymbol{A}^{(1)} = \boldsymbol{e}_{(2)} \times \boldsymbol{e}_{(3)}, \quad \boldsymbol{A}^{(2)} = \boldsymbol{e}_{(3)} \times \boldsymbol{e}_{(1)} \quad \text{and} \quad \boldsymbol{A}^{(3)} = \boldsymbol{e}_{(1)} \times \boldsymbol{e}_{(2)}. \tag{B6}$$

With the help of these area vectors the volume of an elementary grid cell V_P is then related to the Jacobian determinant as

$$\boldsymbol{A}^{(i)} \bullet \boldsymbol{e}_{(j)} = \boldsymbol{e}_{(1)} \bullet \boldsymbol{e}_{(2)} \times \boldsymbol{e}_{(3)} \delta_j^i = V_P \delta_j^i = |\boldsymbol{J}| \delta_j^i. \tag{B7}$$

Because the two frames of basis vectors defined by (B5) are dual to each other $\boldsymbol{e}^{(i)} \bullet \boldsymbol{e}_{(j)} = \delta_j^i$, equation (B7) can be written in the form

$$\boldsymbol{A}^{(i)} \bullet \boldsymbol{e}_{(j)} = |\boldsymbol{J}| \, \boldsymbol{e}^{(i)} \bullet \boldsymbol{e}_{(j)}. \tag{B8}$$

In this way the contravariant frame of basis vectors $\boldsymbol{e}^{(i)}$ is related to the area vectors $\boldsymbol{A}^{(i)}$, which in turn are dependent on the covariant frame of basis vectors $\boldsymbol{e}_{(i)}$

$$\boldsymbol{e}^{(i)} = \frac{\boldsymbol{A}^{(i)}}{|\boldsymbol{J}|} = \frac{\frac{1}{2}\varepsilon^{ijk}\boldsymbol{e}_{(j)} \times \boldsymbol{e}_{(k)}}{|\boldsymbol{J}|}. \tag{B9}$$

Thus the Cartesian components of area vectors $\boldsymbol{A}_k^{(i)}$ are determined by the adjugate Jacobian matrix A_k^i as

$$\boldsymbol{A}_k^{(i)} = |\boldsymbol{J}|\, \bar{\boldsymbol{J}}_k^i = A_k^i. \tag{B10}$$

As evident in the subsequent treatment, the necessary information to perform the coordinate transformation includes only volumes and Cartesian components of the area vectors of grid cells in the physical space. This information is completed by calculating the Jacobian determinant $|\boldsymbol{J}|$ and the adjugate Jacobian matrix A_k^i of the transformation.

Since separate balance equations for velocity components in the physical space are used, these components are treated in essence like any other scalar dependent variable Φ. Thus it is only necessary to transform the prototype equation (34) in order to describe the method. Using tensorial notation, equation (34) in the physical space coordinates can be written as

$$\begin{aligned} &\frac{\partial}{\partial t}(\varepsilon_\alpha \rho_\alpha \Phi_\alpha) + \frac{\partial}{\partial x^i}\left(\varepsilon_\alpha\left(\rho_\alpha U_\alpha^i \Phi_\alpha - \Gamma_\alpha \frac{\partial \Phi_\alpha}{\partial x^i}\right)\right) \\ &= \sum_{\beta=1}^{N_P} (\dot{m}_{\beta\alpha}\Phi_\beta - \dot{m}_{\alpha\beta}\Phi_\alpha) + \sum_{\beta=1}^{N_P} B_{\alpha\beta}^I (\Phi_\beta - \Phi_\alpha) + S_\alpha. \end{aligned} \tag{B11}$$

Equation (B11) can be simply rewritten as

$$\frac{\partial}{\partial t}(\varepsilon_\alpha \rho_\alpha \Phi_\alpha) + \frac{\partial}{\partial x^i}(I_{\Phi_\alpha}^i) = S_\alpha^T \tag{B12}$$

by defining the total phasic flux $I_{\Phi_\alpha}^i$ and the total phasic source S_α^T to be

$$I_{\Phi_\alpha}^i = \varepsilon_\alpha\left(\rho_\alpha U_\alpha^i \Phi_\alpha - \Gamma_\alpha \frac{\partial \Phi_\alpha}{\partial x^i}\right) \quad \text{and} \tag{B13}$$

$$S_\alpha^T = \sum_{\beta=1}^{N_P} (\dot{m}_{\beta\alpha}\Phi_\beta - \dot{m}_{\alpha\beta}\Phi_\alpha) + \sum_{\beta=1}^{N_P} B_{\alpha\beta}^I (\Phi_\beta - \Phi_\alpha) + S_\alpha. \tag{B14}$$

On the basis of the Gauss law, equation (B12) is equivalent to the conservation law

$$\int_{V_P} \varepsilon_\alpha \rho_\alpha \Phi_\alpha \, dV_P + \int_{A_P} \boldsymbol{I}_{\Phi_\alpha} \bullet \boldsymbol{n} \, dA_P = \int_{V_P} S_\alpha^T dV_P \,, \tag{B15}$$

where V_P is the volume of any physical space domain and A_P its surface.

According to tensor calculus, the covariant divergence of a vector is defined as

$$\nabla \bullet \boldsymbol{V} = \frac{1}{|\boldsymbol{J}|} \frac{\partial}{\partial \xi^i} (|\boldsymbol{J}| V^i) \,, \tag{B16}$$

in which $\boldsymbol{V}$ is a generic vector and V^i its contravariant component. Instead of using the contravariant component of a vector, it is more beneficial to utilize the normal flux component $\hat{V}^i$ defined as

$$\hat{V}^i = |\boldsymbol{J}| V^i = |\boldsymbol{J}| \bar{\boldsymbol{J}}_j^i V^j = A_j^i V^j = \boldsymbol{A}^{(i)} \bullet \boldsymbol{V} \,. \tag{B17}$$

With definitions (B16) and (B17), and on the basis of the information in equation (B15), the balance equation (B12) can be transformed to the computational space coordinates

$$\frac{\partial}{\partial t} (|\boldsymbol{J}| \varepsilon_\alpha \rho_\alpha \Phi_\alpha) + \frac{\partial}{\partial \xi^i} (\hat{I}_{\Phi_\alpha}^i) = |\boldsymbol{J}| S_\alpha^T, \tag{B18}$$

in which $\hat{I}_{\Phi_\alpha}^i$ is the total normal phasic flux

$$\begin{aligned} \hat{I}_{\Phi_\alpha}^i &= |\boldsymbol{J}| I_{\Phi_\alpha}^i = |\boldsymbol{J}| \varepsilon_\alpha \left(\rho_\alpha U_\alpha^i \Phi_\alpha - \Gamma_\alpha g^{ij} \frac{\partial \Phi_\alpha}{\partial \xi^j} \right) \\ &= \varepsilon_\alpha \left(\rho_\alpha \hat{U}_\alpha^i \Phi_\alpha - \Gamma_\alpha |\boldsymbol{J}| g^{ij} \frac{\partial \Phi_\alpha}{\partial \xi^j} \right) \,. \end{aligned} \tag{B19}$$

For mass balances and fluxes the dependent variable Φ_α should be set equal to one.

In equation (B19) g^{ij} is the inverse metric tensor

$$g^{ij} = \boldsymbol{e}^{(i)} \bullet \boldsymbol{e}^{(j)} = \frac{\boldsymbol{A}^{(i)} \bullet \boldsymbol{A}^{(j)}}{|\boldsymbol{J}|^2} = \frac{A_m^i A_m^j}{|\boldsymbol{J}|^2} \,, \tag{B20}$$

which is used to raise the index of the covariant vector $\partial \Phi_\alpha / \partial \xi^i$ and $\hat{U}_\alpha^i$ is the normal flux velocity component

$$\hat{U}_\alpha^i = |\boldsymbol{J}| U_\alpha^i = \boldsymbol{A}^{(i)} \bullet \boldsymbol{U}_\alpha \,. \tag{B21}$$

The prototype conservation equation in the computational space (B18) has in effect the same structure as the one in the physical space, equation (B12), with the exception that the diffusivity Γ_α has been replaced by the diffusivity tensor

$$\Gamma_\alpha^{ij} = |\boldsymbol{J}| g^{ij} \Gamma_\alpha = \frac{A_m^i A_m^j}{|\boldsymbol{J}|} \Gamma_\alpha = G^{ij} \Gamma_\alpha . \tag{B22}$$

The multiplier G^{ij} in equation (B22) containing only geometric information is referred to as the geometric diffusion coefficient.

Following the structure of the prototype equation (B11), the macroscopic momentum balance (32) is expressed in a tensorial form as

$$\begin{aligned} &\frac{\partial}{\partial t}(\varepsilon_\alpha \rho_\alpha U_\alpha^k) + \frac{\partial}{\partial x^i}\left(\varepsilon_\alpha\left(\rho_\alpha U_\alpha^i U_\alpha^k - \eta_\alpha \frac{\partial U_\alpha^k}{\partial x^i}\right)\right) \\ &= -\varepsilon_\alpha \frac{\partial P_\alpha}{\partial x^k} + \frac{\partial}{\partial x^i}\left(\varepsilon_\alpha \eta_\alpha \frac{\partial U_\alpha^i}{\partial x^k}\right) + \frac{\partial}{\partial x^k}(\varepsilon_\alpha \bar{P}_\alpha^{\,e}) + \varepsilon_\alpha \bar{\rho}_\alpha \boldsymbol{g} \\ &+ \sum_{\beta=1}^{N_P} (\dot{m}_{\beta\alpha} U_\beta^k - \dot{m}_{\alpha\beta} U_\alpha^k) + \sum_{\beta=1}^{N_P} B_{\alpha\beta}(U_\beta^k - U_\alpha^k) + \boldsymbol{F}_\alpha^T . \end{aligned} \tag{B23}$$

Accordingly, the first three terms on the right-hand side of equation (B23) are also treated as source terms. Utilizing the Gauss law on a volume of the physical space V_P , the pressure gradient term can be put into the following form

$$-\int_{A_P} \varepsilon_\alpha \nabla P_\alpha \bullet \boldsymbol{n}\, dA_P = -\int_{V_P} \varepsilon_\alpha \nabla P_\alpha \, dV_P . \tag{B24}$$

Associating the volume V_P with a differential control volume, the coordinate transformation of the pressure gradient term can be given as

$$-|\boldsymbol{J}| \varepsilon_\alpha \frac{\partial P_\alpha}{\partial x^k} = -|\boldsymbol{J}| \varepsilon_\alpha \bar{\boldsymbol{J}}_k^{\,i} \frac{\partial P_\alpha}{\partial \xi^i} = -\varepsilon_\alpha A_k^i \frac{\partial P_\alpha}{\partial \xi^i} . \tag{B25}$$

The chain rule can be used to relate the derivatives in the physical space to the derivatives in the computational space

$$\frac{\partial \Phi_\alpha}{\partial x^i} = \frac{\partial \xi^j}{\partial x^i} \frac{\partial \Phi_\alpha}{\partial \xi^j} = \bar{\boldsymbol{J}}_i^{\,j} \frac{\partial \Phi_\alpha}{\partial \xi^j} . \tag{B26}$$

This relation can be utilized to transform the second term on the right-hand side of equation (B23) as follows

$$\frac{\partial}{\partial x^i}\left(\varepsilon_\alpha \eta_\alpha \frac{\partial U_\alpha^i}{\partial x^k}\right) = \bar{J}_m^{\,i}\frac{\partial}{\partial \xi^i}\left(\varepsilon_\alpha \eta_\alpha \bar{J}_k^{\,j}\frac{\partial U_\alpha^m}{\partial \xi^j}\right)$$
$$= \frac{\partial}{\partial \xi^i}\left(\varepsilon_\alpha \eta_\alpha \frac{A_m^i A_k^j}{|J|^2}\frac{\partial U_\alpha^m}{\partial \xi^j}\right) . \qquad \text{(B27)}$$

APPENDIX C

In order to obtain the pressure correction equation for the fluid phase in the frame of the phase-sequential solution method, the momentum equation of the fluid is written in the form

$$a_{U_f^k}\Big|_{\boldsymbol{P}} U_f^k\Big|_{\boldsymbol{P}} = \sum_{\boldsymbol{c},\,\boldsymbol{C}} a_{U_f^k}\Big|_{\boldsymbol{c}} U_f^k\Big|_{\boldsymbol{C}} - \varepsilon_f\Big|_{\boldsymbol{P}} A_k^i\Big|_{\boldsymbol{P}} \frac{\partial P_f}{\partial \xi^i}\Big|_{\boldsymbol{P}} + s_{U_f^k}^R . \tag{C1}$$

Such corrections to the fluid pressure δP_f are then introduced which produce new estimates of the phasic velocities $U_f^k\Big|^*$ obeying the fluid mass balance. These new estimates are defined as a sum of the current value and the correction as

$$U_f^k\Big|^* = U_f^k + \delta U_f^k \quad \text{and} \quad P_f\Big|^* = P_f + \delta P_f . \tag{C2}$$

In order to limit the interdependency of the cells in equation (C1), the velocity corrections to the neighbours of the cell under consideration are discarded. Accordingly, the velocities in the neighbouring cells are approximated as

$$U_f^k\Big|_{\boldsymbol{C}}^* = U_f^k\Big|_{\boldsymbol{C}} + W_{pc}\left(U_f^k\Big|_{\boldsymbol{P}}^* - U_f^k\Big|_{\boldsymbol{P}}\right), \tag{C3}$$

where the weight factor $W_{pc} = 0$ for the SIMPLE algorithm and $W_{pc} = 1$ for the SIMPLEC algorithm [1]. Substitution of equations (C2) and (C3) to equation (C1) results in

$$\begin{aligned} a_{U_f^k}\Big|_{\boldsymbol{P}} U_f^k\Big|_{\boldsymbol{P}}^* = {} & \sum_{\boldsymbol{c},\,\boldsymbol{C}} a_{U_f^k}\Big|_{\boldsymbol{c}} \left(U_f^k\Big|_{\boldsymbol{C}} + W_{pc}\left(U_f^k\Big|_{\boldsymbol{P}}^* - U_f^k\Big|_{\boldsymbol{P}}\right)\right) \\ & - \varepsilon_f\Big|_{\boldsymbol{P}} A_k^i\Big|_{\boldsymbol{P}} \frac{\partial P_f}{\partial \xi^i}\Big|_{\boldsymbol{P}} - \varepsilon_f\Big|_{\boldsymbol{P}} A_k^i\Big|_{\boldsymbol{P}} \frac{\partial\, \delta P_f}{\partial \xi^i}\Big|_{\boldsymbol{P}} + s_{U_f^k}^R . \end{aligned} \tag{C4}$$

By expanding the terms on the right side, equation (C4) can be arranged into the form

$$\begin{aligned} \left(a_{U_f^k}\Big|_{\boldsymbol{P}} - W_{pc}\sum_{\boldsymbol{c},\,\boldsymbol{C}} a_{U_f^k}\Big|_{\boldsymbol{c}}\right) U_f^k\Big|_{\boldsymbol{P}}^* = {} & \sum_{\boldsymbol{c},\,\boldsymbol{C}} a_{U_f^k}\Big|_{\boldsymbol{c}} U_f^k\Big|_{\boldsymbol{C}} - \varepsilon_f\Big|_{\boldsymbol{P}} A_k^i\Big|_{\boldsymbol{P}} \frac{\partial P_f}{\partial \xi^i}\Big|_{\boldsymbol{P}} \\ & + s_{U_f^k}^R - W_{pc}\sum_{\boldsymbol{c},\,\boldsymbol{C}} a_{U_f^k}\Big|_{\boldsymbol{c}} U_f^k\Big|_{\boldsymbol{P}} - \varepsilon_f\Big|_{\boldsymbol{P}} A_k^i\Big|_{\boldsymbol{P}} \frac{\partial\, \delta P_f}{\partial \xi^i}\Big|_{\boldsymbol{P}} . \end{aligned} \tag{C5}$$

The first three terms on the right side equal to the corresponding side of equation (C1) calculated with the current values of the fluid mean velocity. Substitution of

that equation into equation (C5) gives

$$\left(a_{U_f^k}\Big|_{\boldsymbol{P}} - W_{pc} \sum_{\boldsymbol{c},\,\boldsymbol{C}} a_{U_f^k}\Big|_{\boldsymbol{c}} \right) U_f^k\Big|_{\boldsymbol{P}}^{*} = a_{U_f^k}\Big|_{\boldsymbol{P}} U_f^k\Big|_{\boldsymbol{P}} - W_{pc} \sum_{\boldsymbol{c},\,\boldsymbol{C}} a_{U_f^k}\Big|_{\boldsymbol{c}} U_f^k\Big|_{\boldsymbol{P}} - \varepsilon_f\Big|_{\boldsymbol{P}} A_k^i\Big|_{\boldsymbol{P}} \frac{\partial\, \delta P_f}{\partial \xi^i}\Big|_{\boldsymbol{P}} \quad . \tag{C6}$$

With the help of the definition (C2) equation (C6) can be solved for the unknown corrections to the phasic Cartesian velocity components of the fluid phase

$$\delta U_f^k\Big|_{\boldsymbol{P}} = - H_{fk}^i\Big|_{\boldsymbol{P}} \frac{\partial\, \delta P_f}{\partial \xi^i}\Big|_{\boldsymbol{P}} \text{, where} \tag{C7}$$

$$H_{fk}^i\Big|_{\boldsymbol{P}} = \frac{\varepsilon_f\Big|_{\boldsymbol{P}} A_k^i\Big|_{\boldsymbol{P}}}{V_P}\, h_f^k\Big|_{\boldsymbol{P}} \quad \text{and} \tag{C8}$$

$$h_f^k\Big|_{\boldsymbol{P}} = \frac{V_P}{a_{U_f^k}\Big|_{\boldsymbol{P}} - W_{pc} \sum_{\boldsymbol{c},\,\boldsymbol{C}} a_{U_f^k}\Big|_{\boldsymbol{c}}} . \tag{C9}$$

Equation (C7) provides now the desired relation between the fluid pressure corrections and the phasic Cartesian velocity components of the fluid.

1. Van Doormal, J. P. and Raithby, G. D. Enhancements of the SIMPLE method for predicting incompressible fluid flows. *Numerical Heat Transfer*, 1984. Vol. 7, pp. 147–163.

APPENDIX D

The essential idea in the improved Rhie-Chow momentum interpolation scheme is that after proper treatment the source term is immersed in the pressure gradient term, partly or completely. The advantage of this treatment is the smoother behaviour of this combined term as the source term alone. Although both the pressure gradient term and the source term are multiplied by the volume fraction, they are kept in this form as the volume fraction diminishes the strong variations of source term.

At first, the part of the source term having rapid changes in it's value is separated from the rest

$$\mathbf{S}_{U_\alpha}^{R} = \mathbf{S}_{U_\alpha}^{R,\,Imp} + \mathbf{S}_{U_\alpha}^{R,\,Base}, \tag{D1}$$

where $\mathbf{S}_{U_\alpha}^{R,\,Imp}$ and $\mathbf{S}_{U_\alpha}^{R,\,Base}$ are the part for improved treatment and the remaining part of a customary source term. As in the discretized balance equation the source term is in a linearized form, these terms include only the zero order terms whereas the first order terms are combined to the current point coefficient $a_{U_\alpha^k}\big|_{\boldsymbol{P}}$. Next, all the extracted source terms, defined at cell centres, are interpolated to cell faces by a weighted linear interpolation with a weight factor of one half. The covariant components of these interpolated source terms are then calculated

$$\hat{\boldsymbol{S}}_{U_\alpha}^{R,\,Imp}\Big|_{\boldsymbol{c}} = \left\{ \boldsymbol{S}_{U_\alpha}^{R,\,Imp}\Big|_{H} \right\}_{C}^{P} \bullet \frac{\boldsymbol{A}}{|\boldsymbol{A}|}\Big|_{\boldsymbol{c}}. \tag{D2}$$

In equation (D2) the notation $\{\ |_H\ \}_C^P$ stands for the weighted linear interpolation between the cell centres $H = P$ and C and $\boldsymbol{A}/|\boldsymbol{A}|$ is a unit area vector of the cell face between the current and neighbour cells. To obey the conservation laws these cell face covariant components are used to define new cell centre source terms with the help of the generalized Gauss law

$$\bar{\mathbf{S}}_{U_\alpha}^{R,\,Imp}\Big|_{\boldsymbol{P}} = \sum_{\boldsymbol{c}} W_{\boldsymbol{c}} \frac{\boldsymbol{A}^{(i)}\big|_{\boldsymbol{c}}}{|\boldsymbol{J}|}\, \hat{\mathbf{S}}_{U_\alpha}^{R,\,Imp}\Big|_{\boldsymbol{c}}, \tag{D3}$$

in which $W_{\boldsymbol{c}}$ is the weight factor from cells face $\boldsymbol{c}$ to current cell centre $\boldsymbol{P}$. In the improved procedure the cell face source terms (D2) are combined to shared pressure gradients at cell faces and the cell centre source terms (D3) are immersed to cell centre pressure gradients. The momentum balance is now written in the form

$$U_\alpha^k\big|_{\boldsymbol{P}} + \frac{1}{a_{U_\alpha^k}\big|_{\boldsymbol{P}}}\left(\varepsilon_\alpha\big|_{\boldsymbol{P}} A_k^i\big|_{\boldsymbol{P}} \frac{\partial P_f}{\partial \xi^i}\Big|_{\boldsymbol{P}} - s_{U_\alpha^k}^{R,\,Imp}\Big|_{\boldsymbol{P}} \right) = M_\alpha\big|_{\boldsymbol{P}}, \text{ where} \tag{D4}$$

$$M_\alpha\big|_{\boldsymbol{P}} = \left(\sum_{\boldsymbol{c},\boldsymbol{C}} a_{U_\alpha^k}\big|_{\boldsymbol{c}}\, U_\alpha^k\big|_{\boldsymbol{C}} + s_{U_\alpha^k}^{R,\,Base}\Big|_{\boldsymbol{P}} \right) \Big/ a_{U_\alpha^k}\big|_{\boldsymbol{P}} . \tag{D5}$$

By following the treatment in section 5.1 the momentum balance (D4) is interpolated for the imaginary staggered cell resulting to

$$\begin{aligned} & U_\alpha^k\big|_{\boldsymbol{c}} + \frac{1}{a_{U_\alpha^k}\big|_{\boldsymbol{c}}} \left(\varepsilon_\alpha\big|_{\boldsymbol{c}} A_k^i\big|_{\boldsymbol{c}} \frac{\partial P_f}{\partial \xi^i}\bigg|_{\boldsymbol{c}} - \hat{s}_{U_\alpha^k}^{R,\,Imp}\Big|_{\boldsymbol{c}} \right) \\ = & \left\{ U_\alpha^k\big|_H + \frac{1}{a_{U_\alpha^k}\big|_H} \left(\varepsilon_\alpha\big|_H A_k^i\big|_H \frac{\partial P_f}{\partial \xi^i}\bigg|_H - \bar{s}_{U_\alpha^k}^{R,\,Imp}\Big|_H \right) \right\}_{\boldsymbol{C}}^{\boldsymbol{P}} . \end{aligned} \tag{D6}$$

By defining the coefficient of pressure gradient term as for the extended Rhie-Chow method, i.e., $N_{\alpha k}^{\ i}$ by the equation (124), and with assumptions (127) and (128) the improved Rhie-Chow momentum interpolation scheme can be stated as

$$\begin{aligned} U_\alpha^k\big|_{\boldsymbol{c}} = & \left\{ U_\alpha^k\big|_H \right\}_C^P + \left\{ \varepsilon_\alpha\big|_H \right\}_C^P \left\{ N_{\alpha k}^{\ i}\big|_H \right\}_C^P \left(\left\{ \frac{\partial P_f}{\partial \xi^i}\bigg|_H \right\}_C^P - \frac{\partial P_f}{\partial \xi^i}\bigg|_{\boldsymbol{c}} \right) \\ & - \left\{ 1 / a_{U_\alpha^k}\big|_H \right\}_C^P \left(\left\{ \bar{s}_{U_\alpha^k}^{R,\,Imp}\Big|_H \right\}_C^P - \hat{s}_{U_\alpha^k}^{R,\,Imp}\Big|_{\boldsymbol{c}} \right) \end{aligned} \tag{D7}$$

$$N_{\alpha k}^{\ i}\big|_H = \frac{A_k^i\big|_H}{a_{U_\alpha^k}\big|_H} . \tag{D8}$$

As before, the interpolation scheme for phasic normal flux velocity components is obtained by applying the definition (B21)

$$\begin{aligned} \hat{U}_\alpha^{\ i}\big|_{\boldsymbol{c}} = & \left\{ \hat{U}_\alpha^{\ i}\big|_H \right\}_C^P + \left\{ \varepsilon_\alpha\big|_H \right\}_C^P \left\{ \hat{N}_\alpha^{\ ii}\big|_H \right\}_C^P \left(\left\{ \frac{\partial P_f}{\partial \xi^i}\bigg|_H \right\}_C^P - \frac{\partial P_f}{\partial \xi^i}\bigg|_{\boldsymbol{c}} \right) \\ & - \left\{ N_{\alpha k}^{\ i}\big|_H \right\}_C^P \left(\left\{ \bar{s}_{U_\alpha^k}^{R,\,Imp}\Big|_H \right\}_C^P - \hat{s}_{U_\alpha^k}^{R,\,Imp}\Big|_{\boldsymbol{c}} \right) \quad \text{and} \end{aligned} \tag{D9}$$

$$\hat{N}_\alpha^{\ ij}\big|_{\boldsymbol{P}} = A_k^i\big|_{\boldsymbol{P}} N_{\alpha k}^{\ j}\big|_{\boldsymbol{P}} = \frac{A_k^i\big|_{\boldsymbol{P}} A_k^j\big|_P}{a_{U_\alpha^k}\big|_{\boldsymbol{P}}} . \tag{D10}$$

Appendix E of this publication is not included in the PDF version.

Please order the printed version to get the complete publication

(http://otatrip.hut.fi/vtt/jure/index.html)

Published by

Vuorimiehentie 5, P.O.Box 2000, FIN–02044 VTT, Finland
Phone internat. +358 9 4561
Fax +358 9 456 4374

Series title, number and report code of publication

VTT Publications 458
VTT–PUBS–458

Author(s)
Karema, Hannu

Title

Numerical treatment of inter-phase coupling and phasic pressures in multi-fluid modelling

Abstract

This thesis work concentrates on the area of dispersed multi-phase flows and, especially, to the problems encountered while solving their governing equations numerically with a collocated Control Volume Method (CVM). To allow flexible description of geometry all treatment is expressed in a form suitable for local Body Fitted Coordinates (BFC) in a multi-block structure. All work is related to conditions found in a simplified fluidized bed reactor. The problems covered are the treatment and efficiency of inter-phase coupling terms in sequential solution, the exceeding of the bounds of validity of the shared pressure concept in cases of high dispersed phase pressure and the conservation of mass in momentum interpolation for rapidly changing source terms.

The efficiency of different inter-phase coupling algorithms is studied in typical fluidized bed conditions, where the coupling of momentum equations is moderate in most sections of the bed and where several alternatives of different complexity exist. The interphase coupling algorithms studied are the partially implicit treatment, the Partial Elimination Algorithm (PEA) and the SImultaneous solution of Non-linearly Coupled Equations (SINCE). In addition to these special treatments of linearized coupling terms, the fundamental ideas of the SINCE are applied also to the SIMPLE(C) type pressure correction equation in the framework of the Inter- Phase Slip Algorithm (IPSA). The resulting solution algorithm referred to as the InterPhase Slip Algorithm – Coupled (IPSA–C) then incorporates interface couplings also into the mass balancing shared pressure correction step of the solution.

It is shown that these advanced methods to treat interphase coupling terms result in a faster convergence of momentum equations despite of the increased number of computational operations required by the algorithms. When solving the entire equation set, however, this improved solution efficiency is mostly lost due to the poorly performing pressure correction step in which volume fractions are assumed constant and the global mass balancing is based on shared pressure. Improved pressure correction algorithms utilizing separate fluid and dispersed phase pressures, the Fluid Pressure in Source term (FPS) and the Equivalent Approximation of Pressures (EAP), are then introduced. Further, an expanded Rhie-Chow momentum interpolation scheme is derived which allows equal treatment for all pressures. All the computations are carried out in the context of a collocated multi-block control volume solver CFDS-FLOW3D.

Keywords

multi-phase flow, multi-fluid modelling, inter-phase coupling, phasic pressures, numerical methods, Control Volume Method, Body Fitted Coordinates, fluidized beds, chemical reactors

Activity unit

VTT Processes, Koivurannantie 1, P.O.Box 1603, FIN–40101 JYVÄSKYLÄ, Finland

ISBN			Project number
951–38–5969–X (soft back ed.) 951–38–5970–3 (URL:http://www.inf.vtt.fi/pdf/)			
Date	Language	Pages	Price
February 2002	English	62 p. + app. 51 p.	C
Name of project		Commissioned by	
Series title and ISSN VTT Publications 1235–0621 (soft back ed.) 1455–0849 (URL: http://www.inf.vtt.fi/pdf/)		Sold by VTT Information Service P.O.Box 2000, FIN–02044 VTT, Finland Phone internat. +358 9 456 4404 Fax +358 9 456 4374	